STUDY ON FRAGMENTED ROCKS INDUCED BY BENCH BLASTING AND THEIR FLIGHT CHARACTERISTICS IN OPEN PIT MINE

髙橋, 良尭

STUDY ON FRAGMENTED ROCKS INDUCED BY BENCH BLASTING AND THEIR FLIGHT CHARACTERISTICS IN OPEN PIT MINE

A DOCTORAL THESIS

By
Yoshiaki TAKAHASHI

DEPARTMENT OF EARTH RESOURCES ENGINEERING
GRADUATE SCHOOL OF ENGINEERING
KYUSHU UNIVERSITY
JAPAN
2019

STUDY ON FRAGMENTED ROCKS INDUCED BY BENCH BLASTING AND THEIR FLIGHT CHARACTERISTICS IN OPENPIT MINE

A DOCTORAL THESIS

Submitted to the Department of Earth Resources Engineering,
Graduate School of Engineering, Kyushu University,
as a partial fulfillment of the requirements of the degree of
Doctor of Engineering

By:
Yoshiaki TAKAHASHI

M.T., Department of Earth Resources Engineering, Kyushu University,
2016

Supervised by:
Prof. Dr. Eng. Takashi SASAOKA

Department of Earth Resources Engineering
Graduate School of Engineering
Kyushu University
JAPAN
2019

Table of Content

1. INTRODUCTION

1.1. Importance of rock blasting in mining operation

In modern mining industry, rock blasting is the most commonly used method for rock mass breakage [1] and it has been adopted for not only mining but also civil engineering such as tunnels, highways and dams. This technique is one of the essential part of working cycle in the open-pit mining excavation [2]. Typical productions of mining industries such as coal and metal are key materials for other industries; therefore, to minimize the operation costs of mine is extremely important issues for the development of our society with the recent decrease of the amount of such resources. Especially, in Japan, there are approximately 500 mines or quarries and half of them are limestone quarry as listed in Table 1.1 [3]. It is only self-sufficient natural resource in Japan and its annual production in Japan is around 1.7 billion ton. Moreover, it is used for cement, concrete aggregate or smelting of iron which are fundamental materials for the infrastructure or building. For this reason, although the production value itself is just about 1,000 billion yen, it is said that the economic ripple effect is as much as a few trillion yen. Hence, mining is still one of the important industry in Japan.

However, the unit price of limestone is considerably cheap that is less than 8 USD/t [4]. Although a number of heavy machinery for excavation such as backhoe have been developed in recent years, it takes much time and cost to excavate by only such machinery. Rock blasting one of the effective way to excavate the rock mass. It can promptly and efficiently break and crush the objective with explosives and detonators in comparison to excavation by only current heavy machinery. This rock blasting technique have been dramatically developed with the growth of the mining industry, resulting in efficient and economic mining operation. There are a number of advantages of rock blasting in open-pit mining excavation.

On the other hand, in the case of actual blasting operations, however, some serious accidents such as flyrock, ground vibration, noise and dust are sometimes caused by this technique due to the use of a huge amount of explosives [5]. Since these phenomena directly or indirectly damage surrounding structures or inhabitants, the application of rock blasting technique in mining is strictly regulated by laws. Hence, the rock blasting have to be carefully performed in order to prevent such negative impacts on surrounding environment. The mining accidents induced by blasting can be generally controlled by blasting designs such as charge explosive (or powder factor), burden, delay time, hole spacing and so on [6]. In addition, these accidents are strongly depending upon the rock and/or geological conditions for example strength of rock mass, cracks or faults [7]; therefore, blasting designs have to be carefully determined by

considering complex rock mass conditions of the blasting face. Moreover, besides the safety issues, productivity such as the size of blast-induced fragmented rocks are also important aspects for the mining operation. Rock blasting in open-pit mining excavation have to be performed by considering both safe and productivity aspects at the same time. These issues make the blasting operation more difficult and complicate.

In order to overcome difficulties described above, a considerable number of researches on rock blasting have already conducted so far. Although a perfect theory has not been established yet, several theories of rock fracture mechanism induced by blasting have been proposed based on the results of numerical simulations and/or laboratory experiments. In addition, the most common research is the ones that focused on the safe operation of mine such as ground vibration and flyrock, and a number of prediction equations and/or prevention methods for them have been proposed from the aspects of actual operations. With the growth of the technologies, especially soft computing technique, the researches on rock blasting have dramatically developed and they have achieved many meaningful progresses.

However, the conditions of blasting face are extremely complicate and different from each blasting face. Moreover, more effective rock blasting methods are required with the decrease of natural resources. Generally speaking, 20% to 30% of the energy from the blast is spent on crushing the rock mass and the rest of blast energy causes unwanted results such as flyrock, ground vibrations and air blast, back break, and undesirable movement of muck pile [8]. Hence, further researches on this technique is urgent issue for continuous mining operation in the future for safe and efficient rock blasting. For this reason, the purpose of this study is to develop rock fracture mechanism induced by blasting and establish the guidelines for safe and efficient rock blasting in open-pit mine considering rock mass conditions.

Table 1.1 The number of mines in Japan (2015) [3]

	Metal & Non-metal	Limestone	Coal	Oil Natural gas	Total
The number of mines in Japan	164	245	15	59	483

1.2. Fracture mechanism induced by blasting

As a fundamental study, to comprehend the rock fracture mechanism induced by

blasting is extremely important to discuss the effect of rock blasting and establish the guidelines for effective and safe blasting designs. A large number of recent researches on rock blasting are mainly focused on the practical aspects such as controlling methods of the particle size of fragmentation rocks or prevention and prediction method of flyrock and/or blast-induced ground vibrations rather than the mechanism. However, to understand the fracture mechanism leads to improve such practical aspects. Until now, several fracture theories induced by blasting have been proposed by many researchers. In this section, four proposed rock fracture mechanism theories, shear failure theory, principle tensile failure theory, shock wave failure theory and the theory proposed by Ito and Sasa are introduced.

1.2.1. Shear failure theory [9]

One of the oldest theory of rock fracture induced by blasting is shear failure theory. A. W. Daw et al. reported that rock failure induced by blasting mainly caused by shear failure.

1.2.2. Principal tensile failure theory

Murata et al. concluded that rock failure induced by rock blasting mainly caused by gas pressure rather than energy of shock wave caused by the detonation [10]. This theory explained that only the circumstance of borehole is enlarged by the shock energy and then the uniform gas pressure induced by the detonation propagate in the room. Rock is broken by tensile stress caused by the gas; therefore, from the rock mechanics point of view, crack direction is parallel with the major principal stress. As the typical research example on a basis of this theory, Ito et al. simulated by finite element method (FEM) and evaluate the effect of gas pressure on rock fracture [11]. Their results suggested that the pressure of gas generally contribute to the generation of cracks in the case of smooth blasting.

1.2.3. Shock wave failure theory [12]

Stress waves propagate in the rock mass after the explosives is detonated in the blastholes. This pressure stress waves caused by shock wave reach the free face, and then the waves reflected at the free face. Because of this reflection, the pressure stress waves change to tensile stress waves (Hopkinson effect). The compressive strength of rock mass is generally 10 to 20 times as large as that of tensile strength, resulting in breaking from the free face. Hino et al. reported that rock fracture induced by blasting is mainly caused by theory listed above. Although the rock around the blasthole is crushed by shock wave, the area is relatively small and shock waves 3-daimentionally propagate outside of the crushed area in the rock mass. That is, this theory suggested

that the rock mass is broken by the action of the shock wave. Based on this theory, several numerical simulations have been conducted. Moreover, on a basis of this theory, S. Kubota et al. or S. H. Cho et al. performed Hopkinson pressure bar testing in order to discuss the effect of shock wave without gas pressure [13, 14] in order to estimate the dynamic tensile strength of rock.

1.2.4. The theory suggested by Ito and Sasa [15]

Principal tensile failure theory indicates that the main factor of rock failure is gas pressure, static stress. On the other hand, shock wave failure theory suggested that rock failure is mainly caused by shock wave, dynamic stress. Ito and Sasa discussed the rock failure induced by rock blasting from both the aspects; dynamic stress state which changes with distance and time elapses, and the static stress state which is constant as long as the volume of blasthole does not change. They approximately consider the stress waves as elastic stress waves since shock wave appreciably attenuated in detonation. Their results showed that resultant force of longitudinal wave from detonation source and reflected longitudinal and lateral waves from the free face works around the free face. The direction of these principle stress waves become parallel to the free face with increasing the distance from the detonation source. In addition, the maximum value of stress wave increased near the free face. All principle stresses become tensile stress wave near the free face, leading to breakage by Hopkinson effect.

Moreover, they also numerically simulated that the impacts of the decoupling on propagation behavior of the stress wave, the effect of characteristics of rock mass on the stress and strain, and wave form of the detonation wave. The results suggested that the stress induced by blasting is summation of the members with first, second and third power of the distance from the detonation source and the member with the first power strongly works with increasing the distance. Furthermore, they also made clear that the ratio between pressure stress and tensile one is strongly depending upon the wave form. When working time of detonation pressure is long, the tensile stress in circular direction is significantly large. Based on these results of a series of the simulations, they concluded that although existing rock fracture theories are reasonable from the each point of view, it is also affected by a number of complicated conditions such as cracks or characteristics of rock mass. They also suggested that the action induced by detonation can be divided into two types; one is the shock action, the other one is the gas action. From these point of views, cracks are generally generated in rock mass by the action of shock wave, and then the gas pressure help grow the cracks. In addition, the tensile failure started from the free face [16]. However, to establish a comprehensive fracture theory of rock blasting is significantly difficult since the outcome of blasting is influenced by a considerable number of factors for example the type of explosives,

usage of them and the type and characteristic of the rock.

1.3. Practical aspects of rock blasting

The proposed fundamental fracture theories of rock blasting are introduced in previous sections. On a basis of these theories, the guidelines for the rock blasting have been proposed so far. However, once mining operation started, the blasting designs are determined based on the experience of engineers in many cases especially in Japan, resulting in serious accidents or inefficient operation. For this reason, practical aspects such as prevention and prediction methods of accidents or controlling technique of size of fragmented rocks are also extremely important in the mining operation. Hence, from the aspect of safety; flyrock and ground vibrations, and productivity aspect; the controlling methods of size of fragmentation rocks are summarized in this section.

1.3.1. Blast-Induced Ground Vibration

Blast-induced ground vibration can cause the indirect damage to the surrounding facilities and buildings [17, 18]. It is a wave motion, spreading outward from the blast like ripples spreading outwards due to impact of a stone dropped into a pond of water [19]. After explosives are detonated in the borehole, 20 to 30% of the energy contribute to the fragmentation, and a part of the energy causes the ground vibration. It widely propagates and influence in comparison to the flyrock accidents. In addition, Monjezi et al. reported that high ground vibration affects the structural integrity, groundwater, and ecology of the nearby area [20]; therefore, mining companies have to carefully control the blast-induced ground vibration in order to minimize or eliminate the damage to nearby environment, and to reduce complaints from neighbors [20]. The ground vibration is strongly influenced by many factors as follow [19];

[1] Characteristics of explosives

The ground vibration is generated by the detonation of explosive; therefore, the ground vibration is strongly depends on the detonation velocity of the explosive.

[2] The amount of explosive

The part of detonation energy is consumed by ground vibration. The vibration becomes large with increasing the amount of explosive.

[3] Delay time

Delay time is the initiation time difference of each hole. In the simultaneous blasting, the energy from each hole contribute to the ground vibrations at the same time. On the other hand, delay blasting can separate the energy from each hole, leading to decrease the level of ground vibrations.

[4] The number of free face

Blast-induced ground vibrations generally increase with the decrease of the number of free faces. In addition, the vibrations become large with increase the distance between blastholes and free faces. The detonation energy is more likely to contribute to ground vibration since the energy is difficult to release at free face due to the large distance to the free face.

[5] The distance from the blast hole

The detonation energy attenuated with distance. The attenuation level is generally proportional to the inverse square of distance.

[6] The geological conditions

Blast-induced ground vibrations propagate in the rock mass; therefore, the characteristics of rock mass, fault, the water under the ground and so on significantly influence on the propagation behavior of the vibrations.

Since the blast-induced ground vibration is depending upon many factors as listed above, a large number of researchers have studied characteristics of blast-induced ground vibrations, their impacts on the surrounding environments, and methods for preventions or prediction of blast-induced ground vibration. In the field of blast-induced ground vibration, most of researches adopt the Peak Particle Velocity for evaluation the level of blast vibration. Each particle in the rock mass vibrates in a complicated motion, which is approximately elliptical motion in several cycles with varying amplitudes. The highest velocity during this motion is called as Peak Particle Velocity (PPV) [21]. A considerable number of prediction equations have been proposed on a basis of PPV. Until now, many researchers have evaluated the PPV and proposed the prediction equations. The most common empirical equations as shown in Table 1.2 [22].

Based on the prediction equations above, the level of ground vibration has been evaluated and the prevention methods of the vibrations have been proposed so far. For examples, N. Kunimatsu et al. and M. Toma et al. showed that ground vibrations can be controlled by selecting optimum delay time [23, 24]. In addition, as listed in Tables 1.3 [25], 1.4 [26] and 1.5 [27] criterions depending upon the building type or propagation medium (type of rock mass) have been suggested, and it can be said that the prediction method and guideline for controlling blast-induced ground vibration might be established.

Table 1.2 Common empirical equations for predicting PPV

Emprical formulas	Equations
USBM	$PPV = K[D/W^{1/2}]^n$
Ambraseys-Hendron	$PPV = K[D/W^{1/3}]^n$
Davies et al.	$PPV = K[D^b/W^{-a}]^n$
Indian Standard	$PPV = K[W/D^{2/3}]^{-n}$
Roy	$PPV = a+K[D/W^{1/2}]^{-n}$

Table 1.3 Limit values for vertical particle velocity for building damage [25]

Graund material beneath buildings			Result in normal residential area
Sand, gravel, clay	Morine, slate, soft limestone	Granite, gneiss, hard lime stone quartzite, sandstone, diabase	
mm/s	mm/s	mm/s	
18	35	70	No noticeable cracking
30	55	110	Fine cracks, and fall in plaster
40	80	160	Cracking
60	115	230	Serious cracking

Table 1.4 Recommended PPV in Germany according to DIN 4150 [26]

Building class	Maximum resultant of the PPV	Estimated maximum vertical particle velocity
	mm/s	mm/s
Residential buildings, offices and others similarly built in the conventional way and in normal condition	8	4.8-8
Stable buildings in normal condition	30	18-30
Other buildings and historical monuments	4	2.4-44

Table 1.5 Safe level blasting criteria (USBM RI 8570): thresholds of PPV value at different frequencies [27]

Structure	PPV, mm/s	
	＜40Hz	≧40Hz
Modern homes, dry wall interiors	18.75	50.0
Older homes	12.50	50.0

1.3.2. Flyrock

Flyrock is the most dangerous phenomena caused by rock blasting in open-pit mining excavation and it can directly influence on the surrounding structures. It is defined as the rock propelled beyond the blast area by the force of an explosion [28] and flyrock in rock blasting has been a serious problem. According to the statistic, approximately 70% of accidents caused by explosives is the flyrock disasters [29, 30]. Once the disaster occurs, mining companies must stop the operation in the worst case. Thus, they have to carefully control and prevent the flyrock accidents for safe and continuous mining operation. For this reason, a number of researches has been proposed on prediction and/or prevention methods of flyrock so far. The theory proposed by Langborg et al. made clear the relationship between hole diameter and velocity of fragmentation rock by semi-empirical approach [31]. The equations are as follow:

$$V_0=(10d \times 2600)/\left(T_b \times \rho_r\right) \quad (1)$$

$$L_m=260d^{(2/3)} \quad (2)$$

$$T_b=0.1d^{(2/3)} \quad (3)$$

where V_0 is initial velocity of rock, d is charge diameter (inch), L_m is the flight distance of blast-induced fragmented rock (m), T_b is the size of rock fragment (m), ρ_r is density of rock (g/cm^3). After his work, many researches have been performed on a basis of the equations [32-36]. For example, E. Ghasemi et al. simulated and discussed the effect of blasting designs on flying distance of fragmentation rocks [37]. M. Monjezi et al. and also simulated and proposed the prediction equations of the flight distance [38].

On the other hand, the prediction equations on a basis of flyrock mechanism as illustrated in Fig. 1.1 have been also proposed as listed in Table 1.6, where B is burden [m], SH is stemming length [m], m is the amount of charge explosive per burden [kg/m], g is acceleration of gravity and k is the constant reflected rock mass conditions [39]. Face burst type of flyrock can happen because of poor rock mass conditions such as

cracks or falt of burden. Cratering type of flyrock can occur if the stemming height to hole diameter ratio is too small or collar rock is weak [40]. Additionally, if the stemming length is adequate to prevent cratering, flyrock at a high trajectory can result from rifling the ejection of stemming material and loose rocks from the collar if there is insufficient stemming height or inappropriate stemming material is used. According to the mechanism described above, the outcome of blasting is primarily depending upon a number of factors such as rock mass conditions, explosive properties, blasting designs, and execution of blast according to the standard design procedures [41]. Especially, the different rock parameters and geological conditions empirically has an obvious impact on the flying characteristics of fragmentation rocks [42].

For this reason, recently, the prediction equations which consider such a condition can be evaluated and simulated with the development of computing technology. R. Trivedi et al. have considered the UCS and RQD as the rock mass conditions and simulated prediction equations [43]. RMR have employed in numerical simulations by F. Faramarzi et al [44]. Both of the results show that the rock mass conditions strongly influence on the flight distance of the fragmentation rock. However, to completely comprehend and evaluate the rock and geological conditions are still significantly difficult and research on generation mechanism and/or prediction methods of flyrock have not been discussed enough; therefore, further studies on the flyrock considering the blasting conditions have to be continued to conduct safety mining operation.

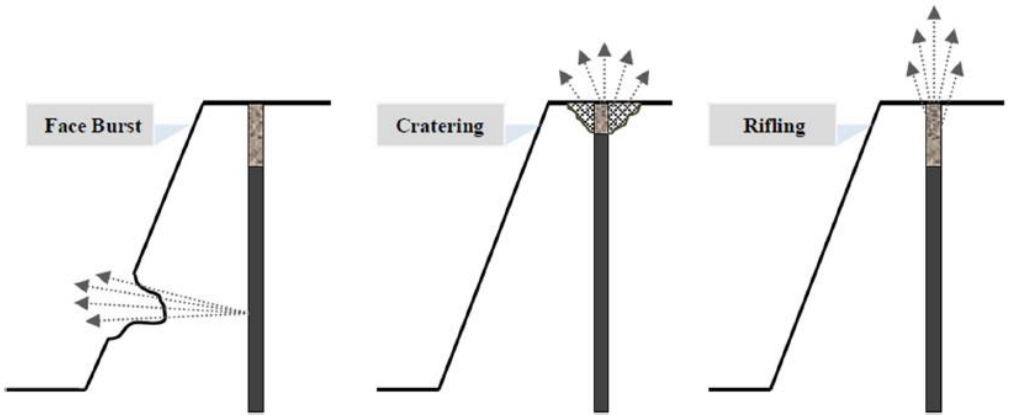

Fig. 1.1 Classification of flyrock mechanism [39]

Table 1.6 Prediction equations for each type of flyrock mechanism [39]

Type of flyrock	Equation
Face Burst	$L_{max}=\frac{k^2}{g}\left(\frac{\sqrt{m}}{B}\right)^{2.6}$
Cratering	$L_{max}=\frac{k^2}{g}\left(\frac{\sqrt{m}}{SH}\right)^{2.6}$
Rifling	$L_{max}=\frac{k^2}{g}\left(\frac{\sqrt{m}}{SH}\right)^{2.6} sin2\theta_0$

1.4. Flyrock accidents in Japan

Flyrock is one of the serious issues in the mining operation in Japan too. The size of the mine or quarry in Japan is relatively small and they are located in near buildings or town since the land of Japan is small. For this reason, the number of flyrock accidents have been reported so far. In recent 10 years (from 2005 to 2015), there were 31 accidents as shown in Fig .1.2 [45]. In Japan, the company must stop the operation in the worst case if the flyrock accidents occurs. Hence, mining companies have to carefully control and prevent flyrock accidents. However, the case of flyrock is complicated and rock mass conditions which is difficult to quantitatively evaluated before blasting strongly influence the occurrence of the accidents as describe above, In fact, as shown in Fig. 1.3 [45]. about 60% of the case of the flyrock accident in Japan is caused by insufficient understanding of rock mass conditions of blast face. Although 40% of the accident is occurred due to insufficient understanding of burden, it might caused by rock mass conditions. Moreover, Fig. 1.4 describes the flight distance of blast-induced fragmented rock of flyrock [45]. As shown in this figure, relatively short distance (0 m to 150 m) of the flight distance became flyrock. However, the distance can be acceptable depending on the mine site. In other words, the limitation of the flight distance change depending upon the mine site or blasting face, which is totally different from the blast-induced ground vibration. That is, for safe and efficient blasting operation, the flight distance of blast-induced fragmented rock have to be carefully controlled considering the miming situation, the location of blasting and so on.

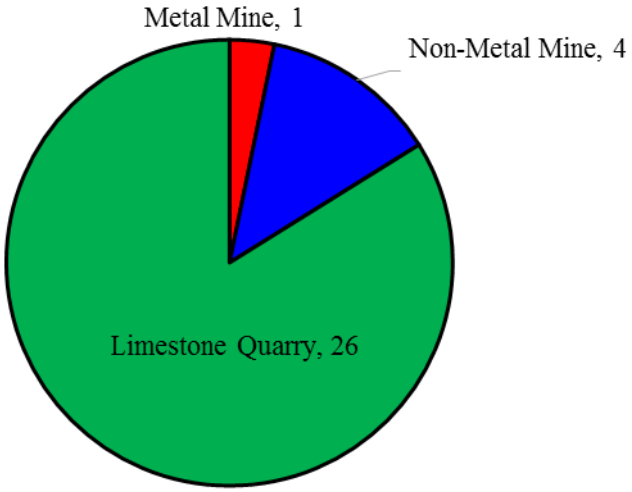

Fig. 1.2 The number of flyrock accidents in Japan from 2005 to 2015 [45]

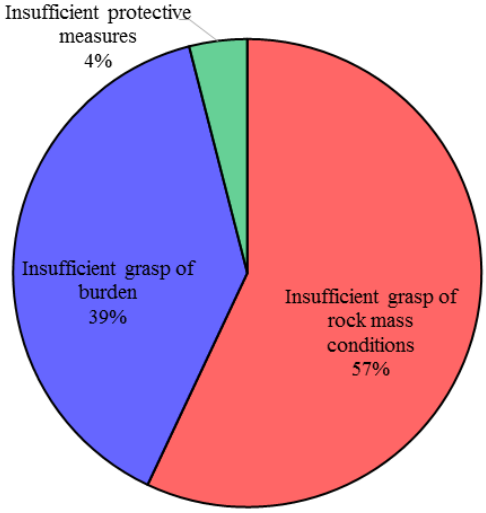

Fig. 1.3 The main cause of flyrock accidents in Japan from 2005 to 2015 [45]

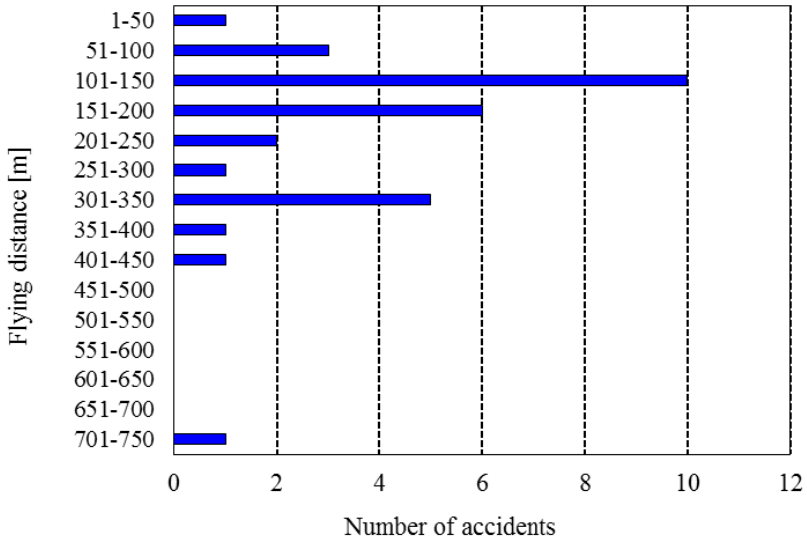

Fig. 1.4 The flight distance of the flyrock accidents from 2005 to 2015 [45]

1.5. Problem statement of rock blasting in Japan

As described above, in order to control flyrock and conduct safe and efficient mining operation, blasting designs have to be selected and changed considering rock mass conditions. On the other hand, various parameters influence on each other and change of one effects on whole of the system illustrated in Fig. 1.5 [46]. For this reason, several guidelines for blasting designs have established so far. However, once mining operation starts, the blasting designs are selected on a basis of the experience of the engineers, leading to occurrence of the accidents. Moreover, major counter measure for preventing flyrock is reduction of charge explosives, which may influence on the productivity of the mine since the size of blast-induced fragmented rock is depending upon it. In other words, safe and efficiency (productivity) is the trade-off relationship, which complicate the blasting operation.

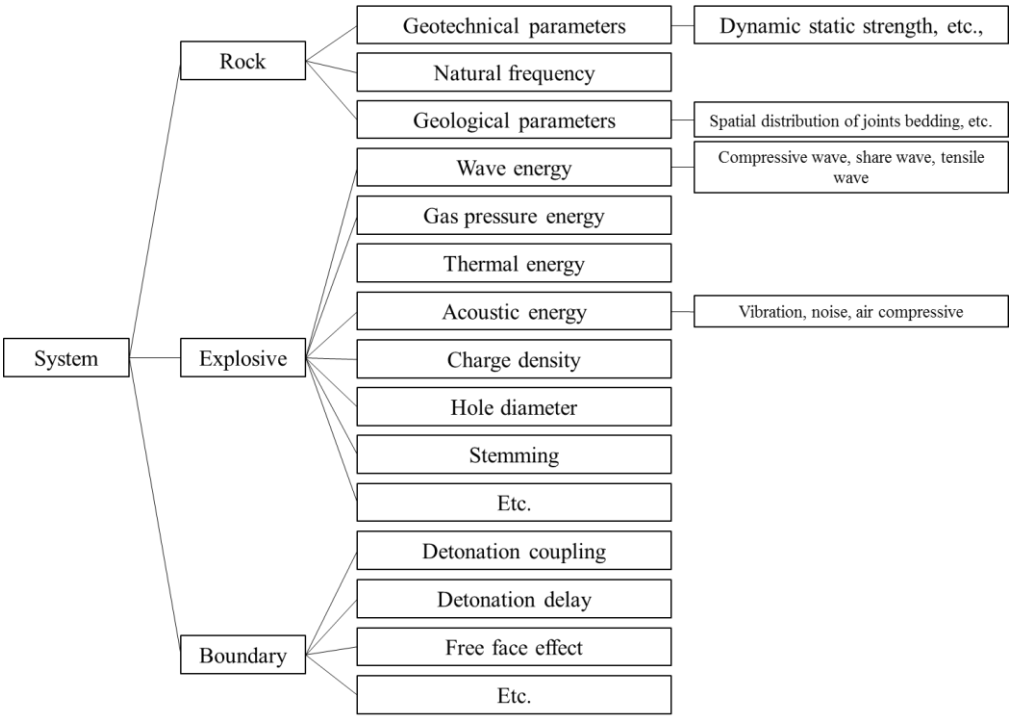

Fig. 1.5 Engineering for rock blasting system [47]

1.6. Composition of this study

This dissertation is composed of six chapters as follows:

Chapter 1 describes the background of this study, including mining industry in Japan, the accidents as a result of blasting, conventional blast-induced fracture theories, and the problems of blasting operation in Japan, in addition to the purpose of this study.

Chapter 2 discusses fracture mechanism induced by conducting in small-scale blasting experiment. The new evaluation method of the two dimensional dynamic strain of brittle material is developed by means of digital image correlation and the fracture mechanism is quantitatively discussed. In addition to the discussion of the fracture mechanism, fundamental information for making the numerical simulation model is obtained.

Chapter 3 elucidates the propagation behavior of stress wave and crack inside rock mass by means of numerical simulation built on a basis of the results of Chapter 2. The influence of rock mass strength and blasting designs on stress wave propagation behavior and crack propagation behavior are discussed.

Chapter 4 demonstrates flight characteristic of blast-induced fragmented rock in operating mine. By conducting field experiment, the effects of blasting designs such as powder factor, burden or delay time are discussed. The influence of rock mass conditions, such as strength and cracks, are also evaluated quantitatively. In addition to quantitative assessment of the flight characteristic, this chapter elucidates the maximum flight distance of blast-induced fragmented rock in each blasting and rock mass conditions in order to develop the guideline for preventing the flyrock accident.

Chapter 5 describes the controlling and prediction method of the size of blast-induced fragmented rocks. In addition to blasting designs, the more accurate prediction method is proposed by quantitatively evaluating the crack conditions before blasting. Moreover, firing pattern, which is generally set for reducing blast-induced ground vibration, is used for control of the size of fragmented rock in order to perform safe and efficient blasting operation.

Chapter 6 summarizes the results in each chapter, providing the fracture mechanism induced by rock blasting and proposing the guideline of safe and efficient blasting.

References

[1] M. Monjezi, A. Bahrami, and A. Yazdian Varjani : Simultaneous Prediction of Fragmentation and Flyrock in Blasting Operation Using Artificial Neural Networks. Int. J. of Rock Mech. and Min. Sci., 47, pp.476-480, 2010.

[2] J.M. Akande, A.E. Aladejare and A.I. Lawal : Evaluation of the Environmental Impacts of Blasting in Okorusu Fluorspar Mine, Namibia. Int. J. of Eng. and Tech., 4, 2, pp.101-108, 2014.

[3] Kyushu Industrial Safety and Inspection Department http://www.safety-kyushu.meti.go.jp/kouzan/gyoumu/minetoha.htm.

[4] Ministry of Economy, Trade and Industry http://www.meti.go.jp/statistics/tyo/seidou/result/ichiran/08_seidou.html.

[5] K. Matsui and H. Shimada : Study on Estimation of Rock Mass and Effect of Fracture on Blasting by Borehore Camera. J. of Limestone, 330, pp.57-61, 2004.

[6] A.K. Raina, V.M.S.R. Murthy, Abhay K. Soni : Estimating Flyrock Distance in Bench Through Blast Induced Pressure Measurements in Rock. Int. J. of Rock Mech. and Min. Sci., 76, pp.209-216, 2015.

[7] P. Y. Dhekne : Environmental Impacts of Rock Blasting and Their Mitigation. Int. J. of Chemical, Environmental & Biological Sci., 3, 1, pp.2320-4087, 2015.

[8] M. Khandelwal and M. Monjezi : Prediction of Flyrock in Open Pit Operation Using Machine Learning Method. Int. J. of Rock Mech. and Min. Sci., 23, pp.476-480, 2013.

[9] A. W. Daw and Z. W. Daw : Blasting of Rock, 2nd edition, E & F. N. Spon, 1909.

[10] T. Mrata and K. Tanaka : Science and Technology of Energetic Materials, 16, 1, pp.32-41, 1955.

[11] I .Ito, K. Sasa and C. Tanimoto : Mechanism of Rock Breakage under Pressure of Gas Explosion. J. of the Society of Materials Science, 20, 209, pp.203-208, 1971.

[12] K. Hino : Science and Technology of Energetic Materials, 15, 4, p235, 1954.

[13] S. Kubota, Y. Ogata, Y. Wada, G. Simangunsong, H. Shimada and K. Matsui : Estimation of Dynamic Tensile Strength of Sandstone. Int. J. of Rock Mech. and Min. Sci., 45, pp.397-406, 2008.

[14] S. H. Cho, Y. Ogata and K. Kaneko : Strain-rate Dependency of the Dynamic Tensile Strength of Rock. Int. J. of Rock Mech. and Min. Sci., 40, pp.763-777, 2003

[15] I. Ito and K. Sasa : Science and Technology of Energetic Materials, 84, p296, 1968.

[16] Shadanhoujin Kayaku Gakkai Happa Senmon Bukai : Genbagijyutsusha no Tameno Happakougaku Handobukku. 1st Eddition, Kyouritsu Shuppan Kabushiki Gaisha, 2001.

[17] M. Khandelwal and T.N Singh : Evaluation of Blast-Induced Ground Vibration Predictors. Soil Dynamics and Earthquake Engineering, 27, pp.116-125, 2007.

[18] M. Hasanipanah, M. Monjezi, A. Shahnazar, D. J. Armaghani and A. Farazmand : Feasibility of Indirect Determination of Blast Induced Ground Vibration Based on Support Vector Machine. Measurement, 75, pp.289-297, 2015.

[19] M. Khandelwal and T. N. Singh : Prediction of Blast-Induced Ground Vibration Using Artificial Neural Network. Int. J. of Rock Mech. and Min. Sci., 46, 7, pp.1214-1222, 2009.

[20] T.N. Singh and V. Singh : An Intelligent Approach to Prediction and Control

Ground Vibration in Mines. Geotechnical and Geological Engineering, 23, pp.249-262, 2005.

[21] M. Hasanipanah, R. Naderi, J. Kashir and A. Z. A. Qaleh : Prediction of Blast-Produced Ground Vibration Using Particle Swarm Optimization. Engineering With Computers, 2016.

[22] M. Monjezi, M. Hasanipanah and M. Khandelwal : Evaluation and Prediction of Blast-Induced Ground Vibration at Shur River Dam, Iran, by Artificial Neural Network. Neural Computing and Applications, 22, 7, pp.1637-1643, 2013.

[23] M. Toma, S. Murata, M. Sankoda, H. Ishida, T. Shodai, T. Yuasa, Y. Nara and T, Ishida : Optimal Delay Time of Blasting Caps to Reduce Vibration Due to the Infrasound Caused by Blasting. J. of MMIJ, 129, pp.626-634, 2013.

[24] S. Kunimatsu, T. Isei, M. A. E.Farsangi, S. Durucan and G. Johnston : Numerical Estimation Ground Vibration Control Method Based on Precise Delay Time Control, Sigen-to Sozai, 113, pp.100-106, 1997.

[25] U. Langefors and B. kihlstrom : The Modern Technique of Rock Blasting, 3rd Edition, Jphn Wiley & Sons, Inc., New York, p405, 1978.

[26] DIN4150 : Deutsche Normen, Vornorm, Erschutterungen in Bauwesen, 1975.

[27] S. Wahyudi, H. Shimada, G.M. Simangunsong, T. Sasaka, K. Matsui, S. Kramadibrata and B. Sulistianto : A Review Studyof Predictive Model Blast Vibration Attenuation Equation by Using Neural Network as an Evaluator. Int. J. of Mining Reclamationn and Environment, Publisher: Taylor & Francis; x, pp.1-17 ISSN 1748-0930, 2010.

[28] IME : Glossary of Commercial Explosives Industry Terms. 1st Edition, Institute of Makers of Explosives, 2007.

[29] L. Kricak, V. Kecojevic, M. Negovanovic, I. jankovic and D. Zekovic : Environmental and Safety Accidents Resulted to Blasting Operation, American J. of Environmental Science, 8, 4, pp.360-365, 2012.

[30] V. Kecojevic and M. Radomsky : Flyrock Phenomena and Area Security in Blasting-Related Accidents. Safety Science, 43, pp.739-750, 2005.

[31] N. Lungborg, N. Persson, A. Ladegaard and R. Holmberg : Keeping the Lid. on Flyrock in Open Pit Blasting, Engineering Mining J., 176, pp.95-100, 1975.

[32] S. Stojadinović, N. Lilić, R. Pantović, M. Žikić, M. Denić, V. Čokorilo, I. Svrkota, and Dejan Petrović : A New Model for Determining Flyrock Drag Coefficient. Int. J. of Rock Mech. and Min. Sci., 62, pp.68-73, 2013.

[33] E. T. Mohamad, D. J. Armaghani, M. Hajihassani, K. Faizi and A. Marto : A Simulation Approach to Predict Blasting-Induced Flyrock and Size of Throwbn Rocks. J. of Geotechnical Engineering, 18, pp.365-374, 2013.

[34] A. Marto, M. Hajihassani, D. J. Armaghani, E. T. Mohamad, and A. M. Makhtar : A

Novel Approach for Blast-Induced Flyrock Prediction Based on Imperialist Competitive Algorithm and Artificial Neural Network, The Scientific World J., pp.1-11, 2014.

[35] D. J. Armaghani, M. Hajihassani, E. T. Mohamad, A. Marto and S. A. Noorani : Blasting-Induced Flyrock and Ground Vibration Prediction through an Expert Artificial Neural Network Based on Particle Swarm Optimization. Arabian J. of Geosciences, 7, 12, pp.5383-5396, 2014.

[36] A.K. Raina, V.M.S.R. Murthy and Abhay K. Soni : Estimating Flyrock Distance in Bench through Blast Induced Pressure Measurements in Rock. Int. J. of Rock Mech. and Min. Sci., 76, pp.209-216, 2015.

[37] E. Ghasemi, M. Sari, and M. Ataei : Development of an Empirical Model for Predicting the Effects of Controllable Blasting Parameters on Flyrock Distance in Surface Mine. Int. J. of Rock Mech. and Min. Sci., 52, pp.163-170, 2012.

[38] M. Monjezi, A. A. Baharami, A. Yazdian Varjani : Simultaneous prediction of Fragmentation and Flyrock in Blasting Operation Using Artificial Neural Networks. Int. J. of Rock Mech. and Min. Sci., 47, pp.476-480, 2010.

[39] T. N. Little: EXPLO conference, Wollonggong, NSW., pp.35-43, 2007.

[40] A. J. Moore and A. B. Richards : Kalgoorlie Consolidated Gold Mines Golden Pike Cut-Back Flyrock Control and Calibration of a Predictive Model. Terrock Consulting Engineers, pdf https://superpit.com.au/wp-content/uploads/2015/05/Terrock-Golden-Pike-Flyrock-Modelling-Report.pdf, 2005.

[41] A. K Raina, V. M. S. R. Murthy and A. K. Soni : Flyrock in Bench Blasting: A Comprehensive Review. Bulletin of Engineering Geology and the Environment, 73, 4, pp.1199-1209, 2014.

[42] Y. Takahashi, T. Sasaoka, S. Wahyudi, H. Shimada, K. Takaeuchi and H. Tanaka : Fundamental Study on Behavior of Flyrock in Open-pit Metal Mine. Proc. Int. Symposium on Earth Science and Technology 2015, Fukuoka, 4-5, December 2015, pp.242-247, 2015.

[43] R. Trivedi, T. N. Singh and A. K. Raina : Prediction of Blast-induced Flyrock in Indian Limestone Mines Using Neural Networks. J. of Rock Mech. and Geotechnical Engineering, 6, pp.447-454, 2014.

[44] F. Faramarzi, H. Mansouri and M. A. E. Farsangi : Development of Rock Engineering Systems-Based Models for Flyrock Risk Analysis and Prediction of Flyrock Distance in Surface Blasting, Rock Mech. and Rock Eng., 47, 4, pp.1291-1306, 2014.

[45] kyushu Industrial Safety and Inspection : DepartmentHappa Tobiishi Taisakuni Tsuite , pdf

http://www.safety-kyushu.meti.go.jp/kouzan/shiryou/H28toukatsusya/H28shiryou03.pdf, 2016.

[46] S. Wahyudi : Study of Influential Site-Specific Characteristics on an Assessment Peak Particle Velocity for Prediction and Control of Ground Blast Vibration, Doctoral Thesis, 2011.

2. EXPERIMENTAL STUDY ON STRAIN RESPONSE AND CRACK PROPAGATION BEHAVIOR INDUCED BY BLASTING

2.1. Introduction

2.1.1. Rock fracture mechanism induced by blasting

Rock blasting is one of the most essential process in open-pit mining excavation in terms of economic and efficiency [(1)]. The application of this blasting technique, however, has been strictly regulated by law because it may cause serious accidents or environmental impacts such as ground vibration, flyrock or noise [(2)]. Rock fracture mechanism induced by blasting should be theoretically understood in order to control such negative impacts. Although a number of field experiment results have been reported, it is difficult to discuss the mechanism since rock mass conditions are different from each mine and blast faces.

For this reason, small-scale blasting experiment with mortar block have been conducted. In order to discuss rock fracture mechanism, strain of free face have evaluated by strain gauge. Nevertheless, accurate measurement could not been performed because of electrical noise on strain signal induced by detonation of detonator [(3)]. In addition, although wave interference generally influence on crack generation, a gauge can only evaluate point information even if a number of gauges are applied to the measurement.

Therefore, in order to solve above problems, the application of digital image correlation (DIC) method is discussed in this study. Two-dimensional strain distribution on surface of free face during blasting was visualized and evaluated quantitatively by means of DIC method. Then, crack generation and growth are discussed based on the DIC result.

2.2. Crack occurrence and its propagation behavior

2.2.1. Outline of small-scale blasting experiment

Small-scale blasting test was performed with mortar blocks as shown in Fig. 2.1 The block was 100 cm wide, 50 cm deep and 60 cm high. Two blasting holes with 13 mm in diameter and 200 mm in length were arranged in one row. Both burden and hole spacing were 100 mm. As explosives, one exploding-bridgewire (EBW) detonator with 1.3 g composition C4 was inserted into the bottom of each blasting hole. In this test, EBW detonator was adopted since time accuracy of detonation of detonator may be over shooting time by high-speed cameras. Each of two ignition control units charged a firing module up to firing voltage of 4,000 V for arming and each of the firing modules

fired by EBW detonator by an external trigger from digital delay generator. Moreover, for the purpose of comparison, biaxial strain gauge was attached on the surface at the center of bottom of two blasting hole as shown in Fig. 2.1. The point history of the dynamic strain was observed using biaxial strain gauges with a 10 mm gauge length (KYOWA KFG-10-120-D16-11L3M3S). The gauge signals were passed through a dynamic strain amplifier (KYOWA CDV-700A) and recorded by an oscilloscope (HIOKI HiCorder 8861) at a sampling rate of 1 MSa/s. The explosives were initiated simultaneously using the high–precision electric detonators (ED; Kayaku Japan Co., Ltd.). The high-precision ED was initiated by a high-voltage/high-current signal from a high–precision detonation control unit (Teledyne RISI, Inc.FS-43). A pulse/delay generator (Quantum composers 9528) adjusted and sent the trigger signals to flash lamps, the high-speed cameras, and the oscilloscope, and the detonation control unit. Mechanical properties of the mortar block is listed in Table 2.1 In this study, strain in x and y direction shown in Fig. 2.1 are defined as ε_{xx} and ε_{yy}, respectively.

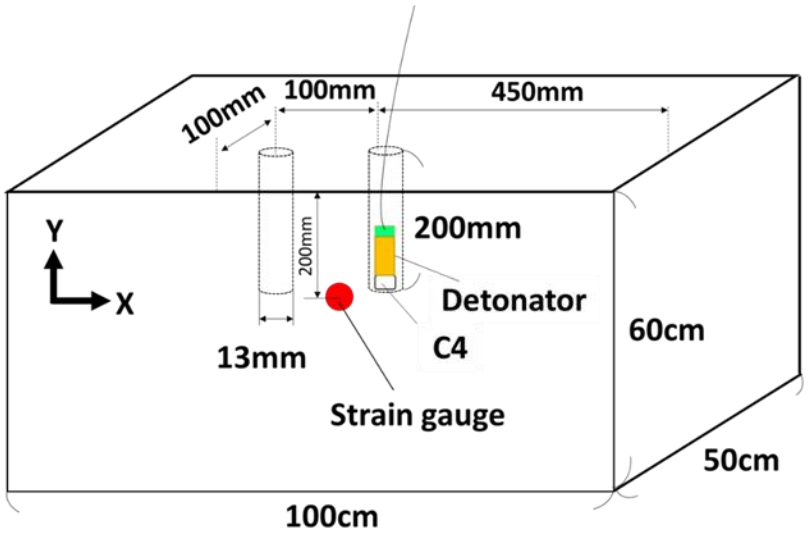

Fig. 2.1 Schematic view of mortar block and blasting designs

Dimension	100×60×40 cm		
Composition	mixing ratio	cement:water:sand	1770:919:5311
	sand material	surface-dry density	2.62 g/cm^3
		absolute-dry density	2.56 g/cm^3
		rate of water absorption	2.18 %
		the fineness modulus	2.83
Nominal strength	21 N/mm^2		
Mean strength	23 N/mm^2		
P wave velocity	3,557 m/s		
S wave velocity	2,102 m/s		

Table 2.1 Mechanical property of mortar block

2.2.2. Digital Image Correlation (DIC) Method

Recent development of the digital image technique puts the photographic method to practical and enables us to observe the dynamic displacement of object surface with the support of digital high-speed camera and computer system. DIC method is one of the image-based displacement measurement method and it can analyze displacement/strain of whole of shooting area on a basis of digital images taken by camera(s) [4]. In this analysis method, deformation and direction of the random pattern (speckle) drawn on evaluation area are visually traced by a correlation algorithm with a grey scale $G(x, y)$ of a pixel position (x, y) in images [5,6]. In other words, this method is non-contact and optical measurement system; therefore it is not affected by electrical noise and two or three dimensional analysis can be performed. Additionally, the method has wide dynamic range of strain (>100 %) and high sensitivity (1/100,000 of field of view). This method have recently started to apply to the field of rock mechanics for measurement of static strain or displacement [7].

For DIC analysis, random patterns (speckle) were drawn on the front surface of the mortar block. Series of photographs during blasting were taken by two high-speed cameras (SHIMADZU, HPV-1 and HPV-X) every 2 μs. It means the sampling rate of the analysis is 2 μs. Based on the photographs, DIC analysis was performed by using the software, VIC-3D (product by Correlated Solutions). Two cameras link together with a genlock and synchronize recording frames. Moreover, a strain gauge for comparison of strain with DIC analyzed data was also pasted on the surface at the center of mortar block as shown in Fig.4. The other shooting conditions of high-speed cameras are listed in Table 2.2 In addition, Fig. 2.2 is an illustration of the arrangement of equipment.

High-speed cameras and flash light were also triggered by digital delay signal. Before the experiment, the DIC system was calibrated with a planar calibration method [8].

Table 2.2 Shooting conditions of high-speed cameras

	Left : SHIMADZU HPV-X	Right : SHIMADZU HPV-1
Recording speed	500,000fps	
Exposure	1/1,000,000 sec	1/1,000,000 sec
Resolution	400×250	312×260
Lens	Tokina AT-X 840D	
	120 mm F3.5	220 mm F3.5

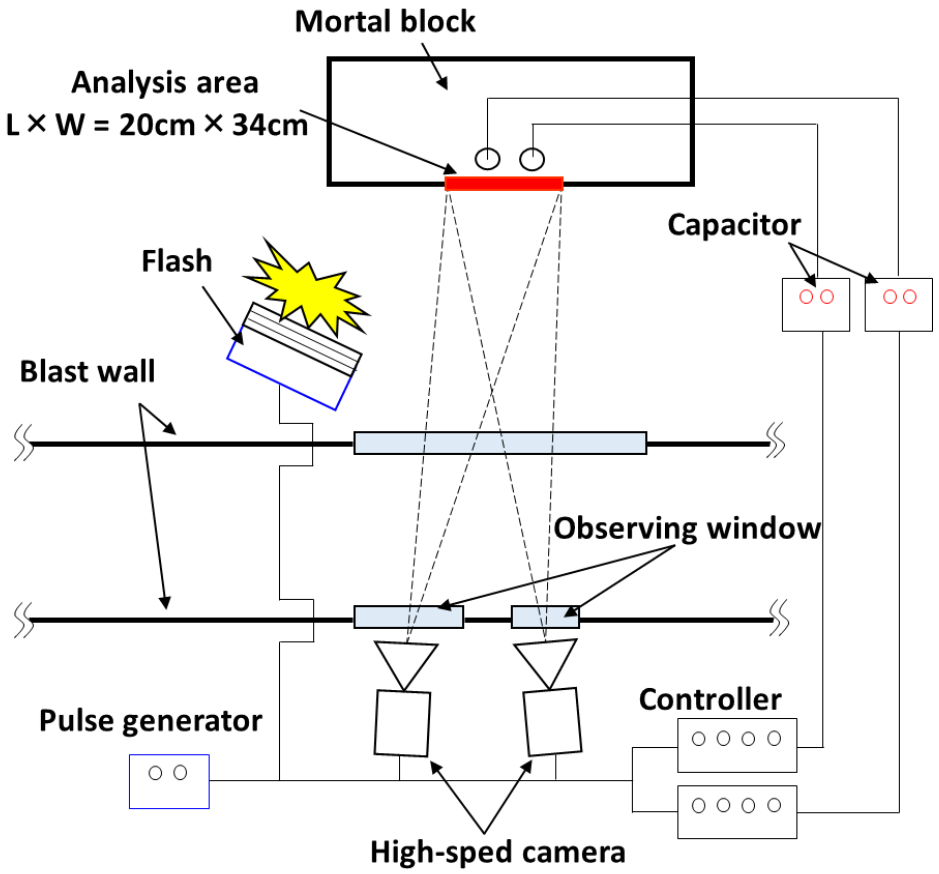

Fig. 2.2 Arrangement of equipment and mortar block

2.3. Results and discussions

2.3.1. Applicability of DIC method

The result of strain profile recorded by strain gauge and that of point a (analysis point on strain gauge) analyzed by DIC are shown in Figs. 2.3 (a) and (b), respectively. According to Fig. 2.3 (a), both ε_{xx} and ε_{yy} immediately change after the detonation of

detonator. In addition, recorded both strain values are too large for brittle material. This is because electrical noise is induced by the firing pulse for EBW detonator. On the other hand, as shown in Fig. 2.3 (b), both lateral and longitudinal strain gradually increase from approximately 50 μs elapsed after the detonation. This time is good accordance with arrival time of elastic wave (S wave) from the blasting holes to analysis point and the value of calculated strain is reasonable according to past researches [9, 10]. On the other hand, the strain induced by P wave was could not be detected due to the accuracy of this analysis in this study. Furthermore, as shown in Fig. 2.4, the occurrence of cracks can be recognized where tensile strain is larger than 7×10^{-9} by DIC. On a basis of these results, it can be said that a high speed strain of brittle material induced by blasting is assessed by applying DIC method.

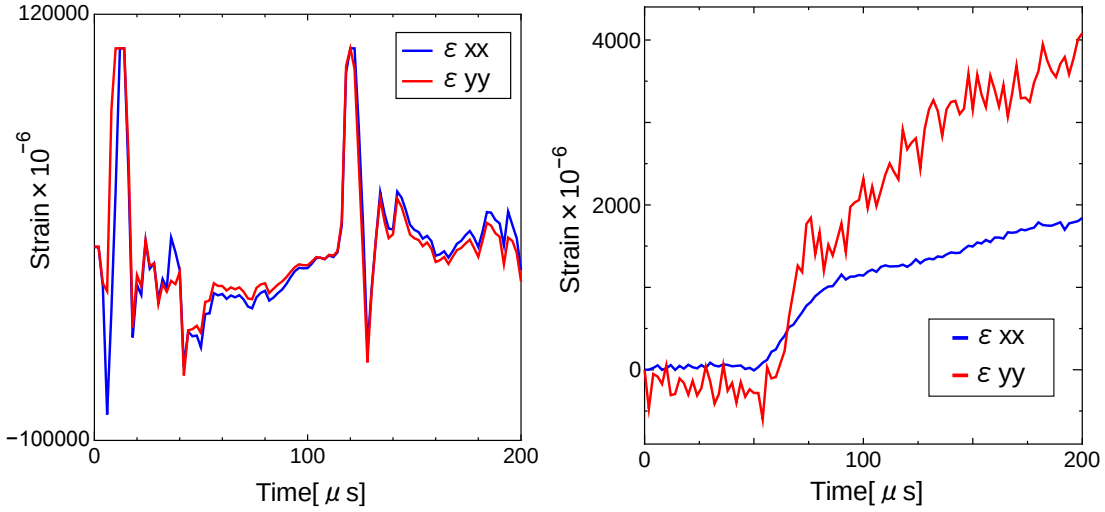

(a) (b)

Fig. 2.3 Strain histories on the point of interest: (a) measured by strain gauge, (b) obtained by DIC

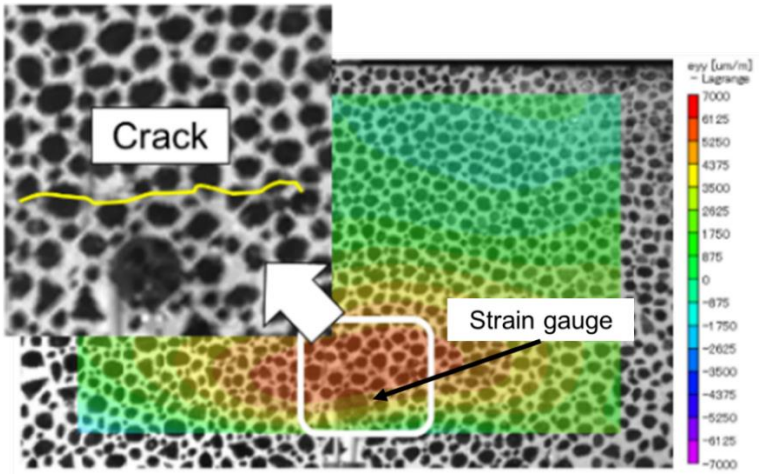

Fig. 2.4 Recognition of the crack occurrence in high tensile strain area at 200μs elapsed after blasting

2.3.2. Crack occurrence and its propagation behavior

Based on the strain distribution analyzed by DIC, fracture mechanism on free face induced by blasting is discussed in this section. Two analysis lines are set as shown in Fig. 2.5: line AB which is through the crack and line CD which is not through the crack. In addition, two analysis points are also set on line AB and line CD, respectively; point b is the starting point of crack and point c is the point above point b. By considering the direction of the propagated crack during analysis time, the ε_{yy} histories of both lines every 20 μs are shown in Figs. 2.6 (a) and (b), respectively. As shown in Fig. 2.6 (a), large strain was recorded around the area above two blasting holes. On the other hand, the ε_{yy} above the center between two blasting hole was larger than other area on line CD as shown in Fig. 2.6 (b). This is because stress wave interference lead the change of stress and strain distribution.

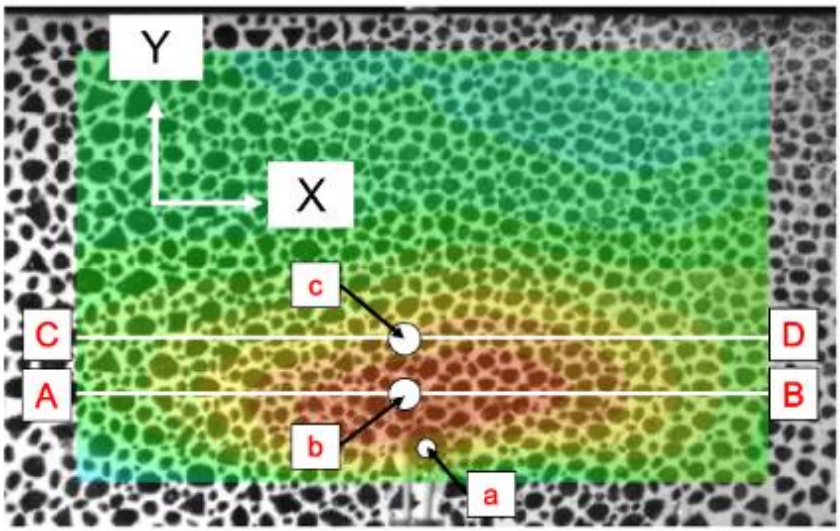

Fig. 2.5 Analysis lines and points

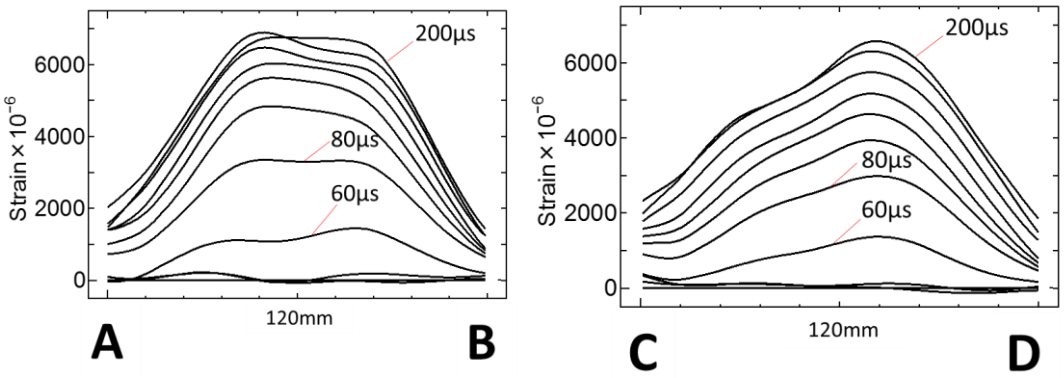

(a) (b)

Fig. 2.6 ε_{yy} profile (a) along with line AB and (b) along with line CD

Although strain distribution is different, there are not huge difference of the value of recorded strain between two lines. In other words, by only considering the value of strain, crack could occur on line CD, especially around the center between two blasting hole like point c. Moreover, in this experiment, crack appeared from point b on line AB at approximately 70 μs after the detonation. This result indicated that there is other factor which influence on crack generation except for strain. By comparing ε_{yy} histories of both lines, there is obvious difference of the amount of change of strain between 60 μs and 80 μs. In other words, the strain rate can effect on the crack generation. For this, strain history and strain rate history (15 moving average) of point b on line AB and point c on line CD are compared as shown in Figs. 2.7 (a) and (b), respectively. As shown in these figures, there are clear difference of strain rate of ε_{yy} ($\dot{\varepsilon}_{yy}$) although large strain difference cannot be seen between points b and c. It can be said that not only strain but also strain rate influence on crack occurrence.

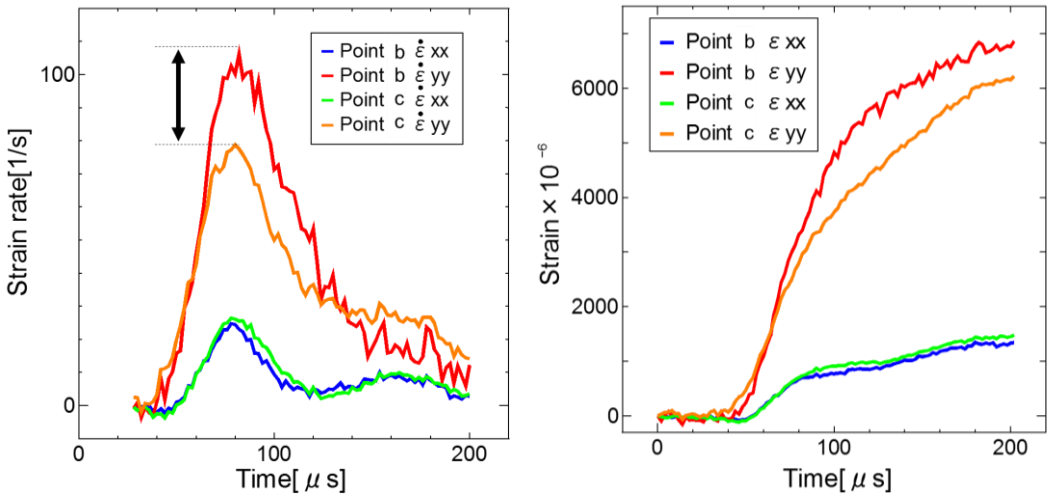

(a) (b)

Fig. 2.7 (a) Strain history at points b and c. (b) Strain rate history at points b and c (15 moving average)

Hence, as a next step, 10 points are extracted from line AB and $\dot{\varepsilon}_{yy}$ of these points are analyzed and compared as shown in Fig. 8 in order to discuss crack growth. As can be seen in Fig. 2.8, all strain rates at all points reach their peak at the same time and $\dot{\varepsilon}_{yy}$ of points on crack record over a certain value. In other words, crack occurred and propagated to the area where strain rate is over a certain value at a certain timing. In this experiment, crack can be recognized at the points where $\dot{\varepsilon}_{yy}$ is over approximately 100 s^{-1}.

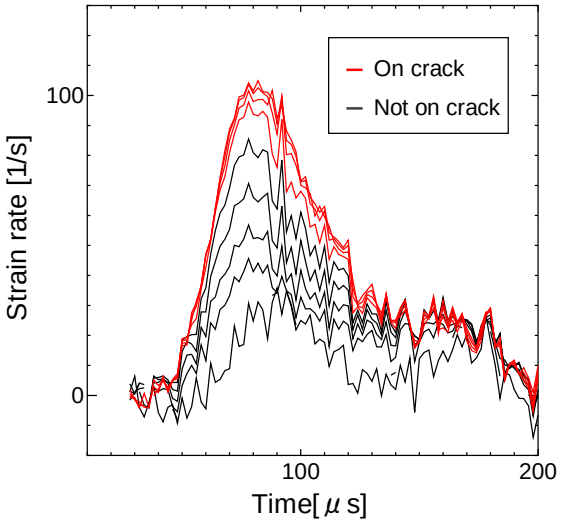

Fig. 2.8 Strain rate history of ε_{yy} at 10 points on line AB (15 moving average)

2.4. Effect of rock mass strength and blasting designs on rock fracture mechanism

2.4.1. Redesigns of small-scale blasting experiment

In former section, the method to evaluate the two dimensional dynamic strain and make clear the fracture mechanism of free face after blasting successfully could be developed and discussed. As a next step of this study, small-scale blasting experiment was redesigned. The next series of small scale blasting tests was performed by using concrete blocks. The dimension of new blocks was 40 cm wide, 30 cm deep and 30 cm in height. Two vertical blasting holes with 3.8 mm in diameter and 120 mm in length were drilled and arranged in one row and hole spacing was 88 mm. As explosives, 1.2 g of C-4 was filled into fluorine resin tube which is 120 mm in length and 3.72 mm and 3.0 mm outside and inside diameter (see Fig. 2.9). They were insert into each blasting hole and detonated by precision detonator. In this experiment, an acrylic set to fix EBW detonator was combined with the tube at the top as a detonation system in order to detonate it from outside of the block (see Fig. 2.10). In order to control the influence of reflected stress wave from side, back and bottom free face, each free face was fixed by other concrete blocks. The dimension of the side concrete block was 20 cm wide, 30 cm deep and 30 cm high and that of the back concrete block was 80 cm wide, 20 cm deep and 30 cm high. A test block was surrounded by the blocks and the blocks were fixed by fixture made by metal (see Fig. 2.11). In this study, two types of concrete blocks were prepared; one was made from normal mortar, the other one was made from lightweight mortar. As blasting designs, burden and hole spacing were focused on in this experiment. The blasting designs are listed in Table 2.3 and mechanical properties of concrete block are shown in Table 2.4. In this test cases, series of photographs during blasting were taken every 8 μs for recording longer strain profiles than previous section. Other

shooting conditions were listed in Table. 2.5.

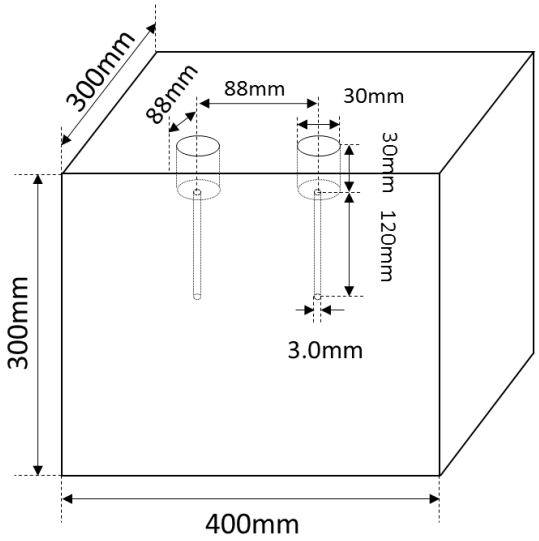

Fig. 2.9 Outline of mortar block and blasting designs

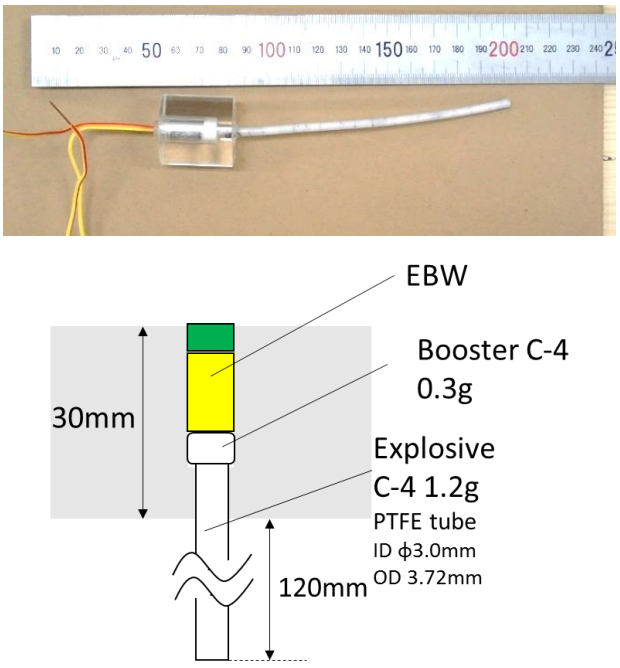

Fig. 2.10 EBW and detonation system in this experiment

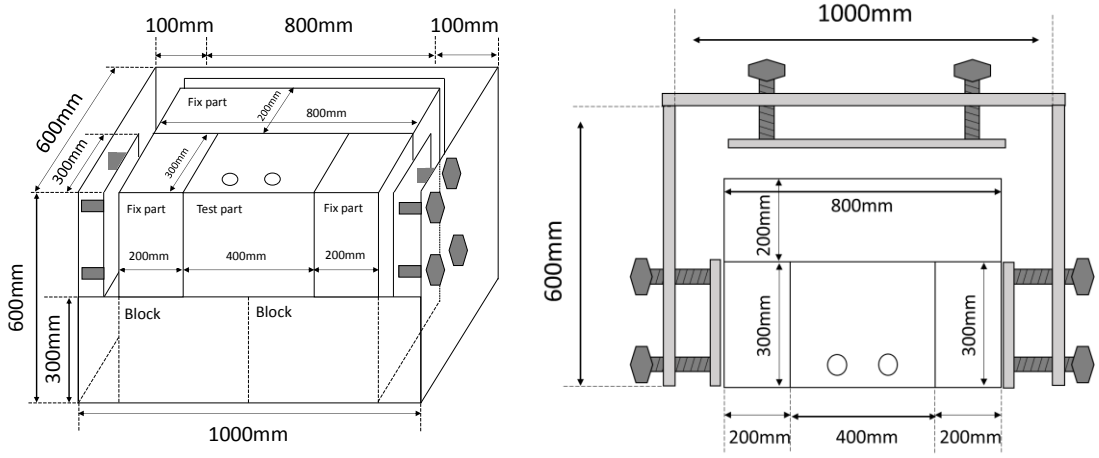

Fig. 2.11 Outline of control system for reflection wave from free faces

Table 2.3 The blasting designs

Charge explosive	1.2 g/hole
Hole diameter	3.8 mm
Hole length	120 mm
Hole spacing	88 mm
Burden	88 mm
Hole number	2

Table 2.4 Shooting conditions of high-speed cameras

	Left : SHIMADZU HPV-1	Right : SHIMADZU HPV-X
Shatter speed	125,000fps (every 8μs)	
Exposure	4μs	4μs
Resolution	312×260	400×250
Lens	Tokina AT-X 840D	
	380mm F11	110mm F16

Table 2.5 Mechanical properties of two types of concrete blocks

	Normal mortar	Light-weight mortar
Density t/m^3	2.32	1.72
Porosity %	4.5	5.0
P-wave velocity m/s	3.70×10^3	3.17×10^3
S-wave velocity m/s	2.47×10^3	2.11×10^3
Uniaxial compressive strength (UCS) MPa	26.3	19.3
Young's modulus GPa	30.6	22.3
Poisson's ratio	0.17	0.20
Brazilian tensile strength (BTS) MPa	12.6	7.2

2.4.2. Effect of rock mass strength on rock fracture mechanism induced by blasting

Final crack formation (crack conditions at 808 μs after detonation) was compared at first. The crack conditions of normal mortar (larger strength) and lightweight mortar (smaller strength) are shown in Figs. 2.12 (a) and (b), respectively. As shown in these figures, several short cracks can be seen in the case of normal mortar. On the other hand, one long crack is generated in the case of light-weight mortar. Cho et al. reported that relatively short length and multiple cracks are generated by blasting in the case of high dynamic strength and relatively long length and a few cracks are generated in the case of low dynamic strength [(11)].

As a next step, the results of DIC analysis are discussed for further discussion. As show in Fig. 2.12, the appeared cracks are propagated in the longitudinal direction, so the time history of stain distribution of ε_{yy} are listed in Figs. 2.13 (a) and (b), respectively. In the case of normal mortar, larger strength, high tensile strength area is spread on the two blasting holes. On the other hand, high tensile strain area can be seen on the center of two blasting holes. In addition, in order to discuss the crack generation depending upon the strength of rock, the strain profile on the points A and B illustrated in Figs. 2.13 (a) and (b) are shown in Figs. 2.14 (a) and (b). The measured strain on the crack of normal mortar is larger than that of light weight mortar. Furthermore, the remarkable strain risings start after 40 μs (between 40 μs and 48 μs) in both history. Here, the arrival time of P-wave from blast source to free face in the case of normal and light-weight mortar is around 24 μs and 28 μs, respectively. On the other hand, that of S-wave in the case of normal and light-weight mortar is 36 μs and 42 μs, respectively. On a basis of these arrival times, the remarkable strain change might be caused by S-wave. As the same way above, strain rate (4 moving average) of point A and B are also shown in Figs. 2.15 (a) and (b). In this study, first crack could be seen by visual

observation at 72 μs and 80 μs after initiation in the case of normal and light-weight mortar, respectively. On the other hand, the first peak of strain rate can be seen in both profiles at around 50 μs after the detonation. This result suggests that the peak is caused by reflection wave of S-wave and invisible cracks or core of the cracks are generated at the peak. Moreover, the value of normal mortar is larger than that of light-weight mortar. The value of strain rate of normal mortar is approximately 30 1/s and that of light-weight mortar is approximately 20 1/s. Second peak is located around 200 μs in both profiles. The distance from blasting source to side free faces 132 mm and the distance to the bottom free face is 150 mm. By considering the time when reflection S-wave reach at evaluation area, the second peak might be caused by the reflection waves from the free faces and crack opening can be recognized around this time by visual observation. This result indicated that the core of the cracks are generated by first stress waves and then the cores are spread by secondly waves. From the results of this section, strain rate at the time of fracture is depending upon the rock mass strength, resulting in the difference of crack formation.

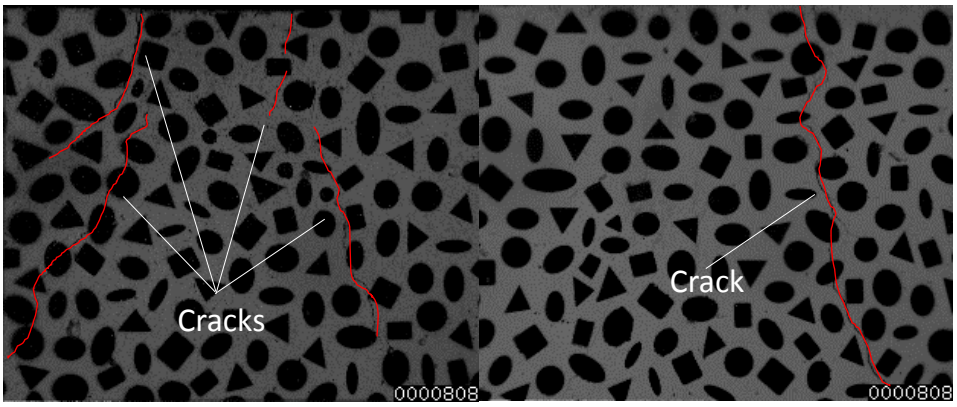

(a) (b)

Fig. 2.12 Final crack propagation behavior at 808 μs (a) Normal mortar and (b) Light-weight mortar

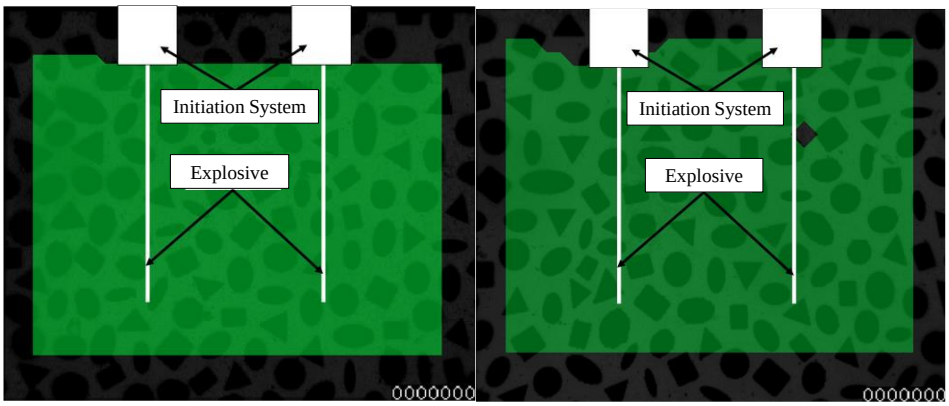
Initiation System
Explosive
0000000
Initiation System
Explosive
0000000

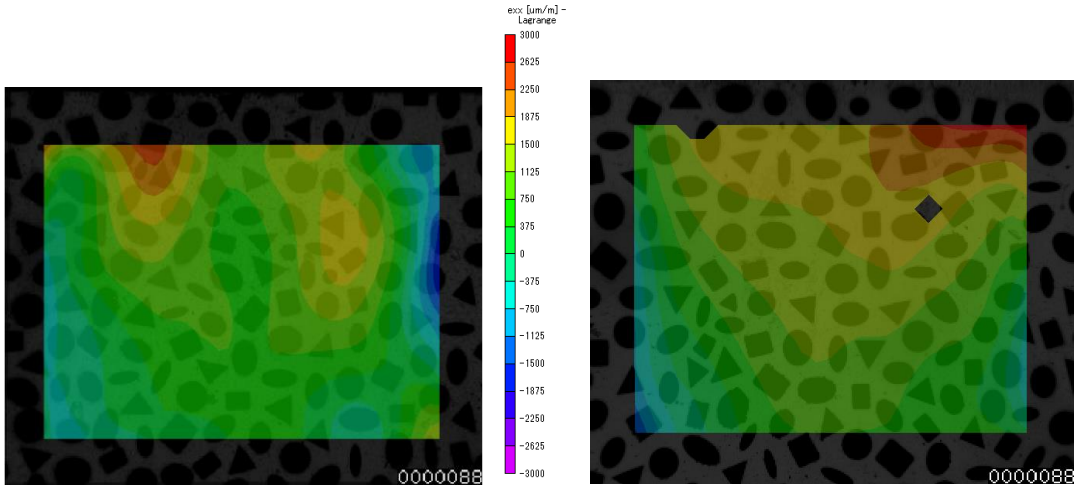
exx [um/m] - Lagrange
3000
2625
2250
1875
1500
1125
750
375
0
-375
-750
-1125
-1500
-1875
-2250
-2625
-3000
0000088
0000088

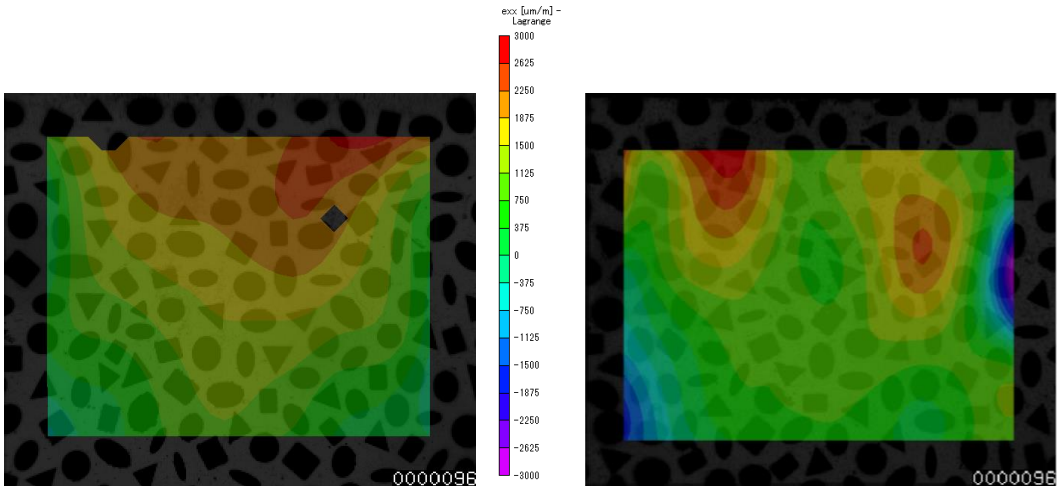
exx [um/m] - Lagrange
3000
2625
2250
1875
1500
1125
750
375
0
-375
-750
-1125
-1500
-1875
-2250
-2625
-3000
0000096
0000096

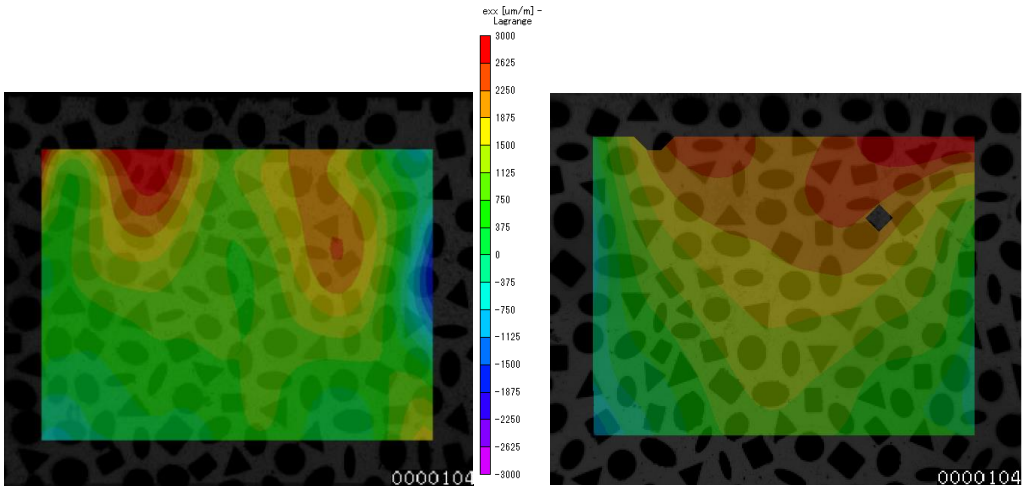

(a) (b)

Fig. 2.13 The time history of stain distribution of ε_{xx} at 0 μs, 88 μs, 96 μs and 104 μs (a) Normal mortar and (b) Light-weight mortar

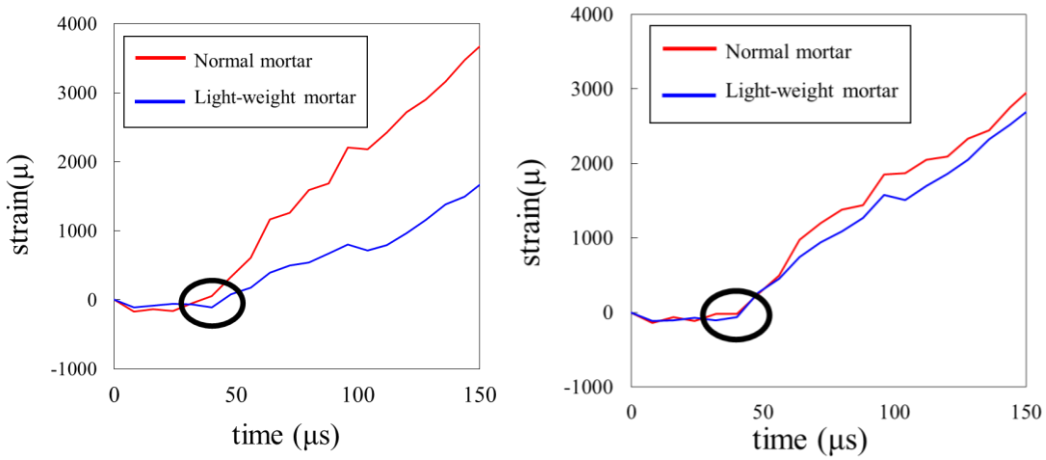

(a) (b)

Fig. 2.14 The strain profiles of ε_{xx} on the cracks at (a) Point A and (b) Point B

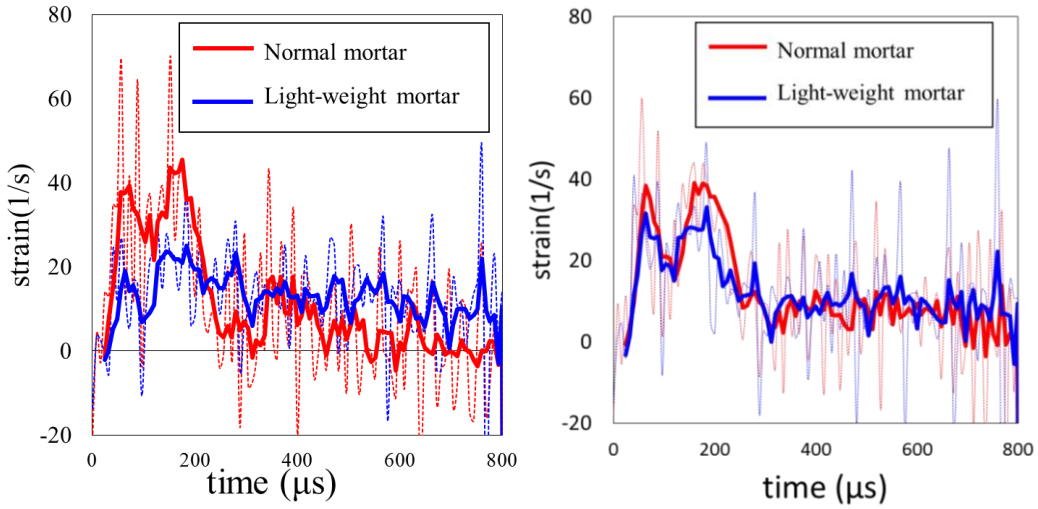

Fig. 2.15 The strain rate profiles of ε_{xx} on the cracks at (a) Point A and (b) Point B

2.4.3. Effect of blasting designs on rock fracture mechanism induced by blasting

2.4.3.1 Effect of burden on rock fracture mechanism induced by blasting

Effect of burden is discussed in this section. In this study, the burden is reduced and the light-weight mortar test sample of 75 mm of burden is prepared and performed the blasting experiment. Crack propagation behavior of analysis areas are compared based on the images captured by high-speed camera. Figs. 2.16 (a) and (b) are high-speed photographs of crack conditions of 88 mm and 75 mm of burden, respectively. As shown in these figures, the number of cracks in the case of 75 mm of burden is larger than that of 88 mm of burden. This is because charge volume per unit volume of concrete block (powder factor) is large when burden is small. In addition, since the distance from blasting holes and free face (analysis area) becomes small in the case of 75 mm burden, the energy of explosive is more likely to contribute fracture of the block. This result suggested that crack can be effectively generated by reducing burden length even though same charge volume is consumed.

Figs. 2.17 (a) and (b) shows strain distribution of 88 mm and 75 mm of burden in horizontal direction (ε_{xx}), respectively. Both of them show high tensile strain area in the direction perpendicular to the crack direction. For further discussion, Fig. 2.18 shows strain history on analysis points (on crack) in Figs. 2.17 (a) and (b). As shown in these profiles, both results remarkable strain rising start from 40 μs and 32 μs, respectively. In this experiment, reaching time of P-wave of 88 mm and 75 mm of burden from blasting source to analysis point is approximately 28 μs and 24 μs and that of S-wave is from blasting source to analysis point is 42 μs and 36 μs, respectively. Same as above section, this is because the strain is generated by reflected wave of P-wave and then

remarkable strain change is induced by S-wave. Moreover, as a next step, strain rate history (4 moving average) is calculated based on the strain profiles as shown in Fig. 2.19. As shown in this graph, first spike peak of the strain rate can be seen approximately 50 μs after detonation, after S wave reflected at free face, in both profiles. On the other hand, in this experiment, first crack can be appeared by visual observation at 88 μs and 72 μs in the case of 88 mm and 75 mm of burden, respectively. This result might suggested that micro crack which cannot be captured by is generated at the first peak, and then visible cracks are generated. Moreover, the value of the spike peak of small burden is larger than that of large one. The value of strain rate of 75 mm of burden is approximately 50 1/s. It should be noted that the second spike peak can be seen in the graph can be induced by reflected wave from the side or bottom free faces.

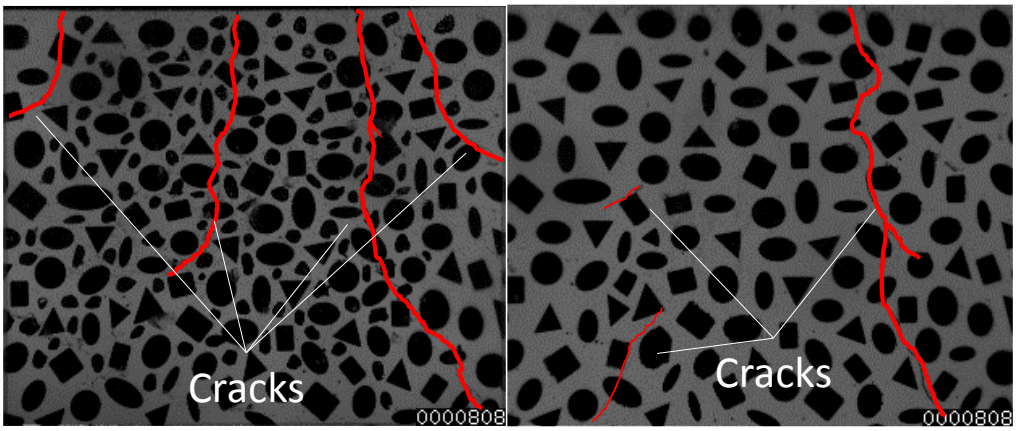

(a) (b)

Fig. 2.16 Final crack propagation behavior at 808 μs (a) Burden: 75 mm and (b) Burden: 88 mm

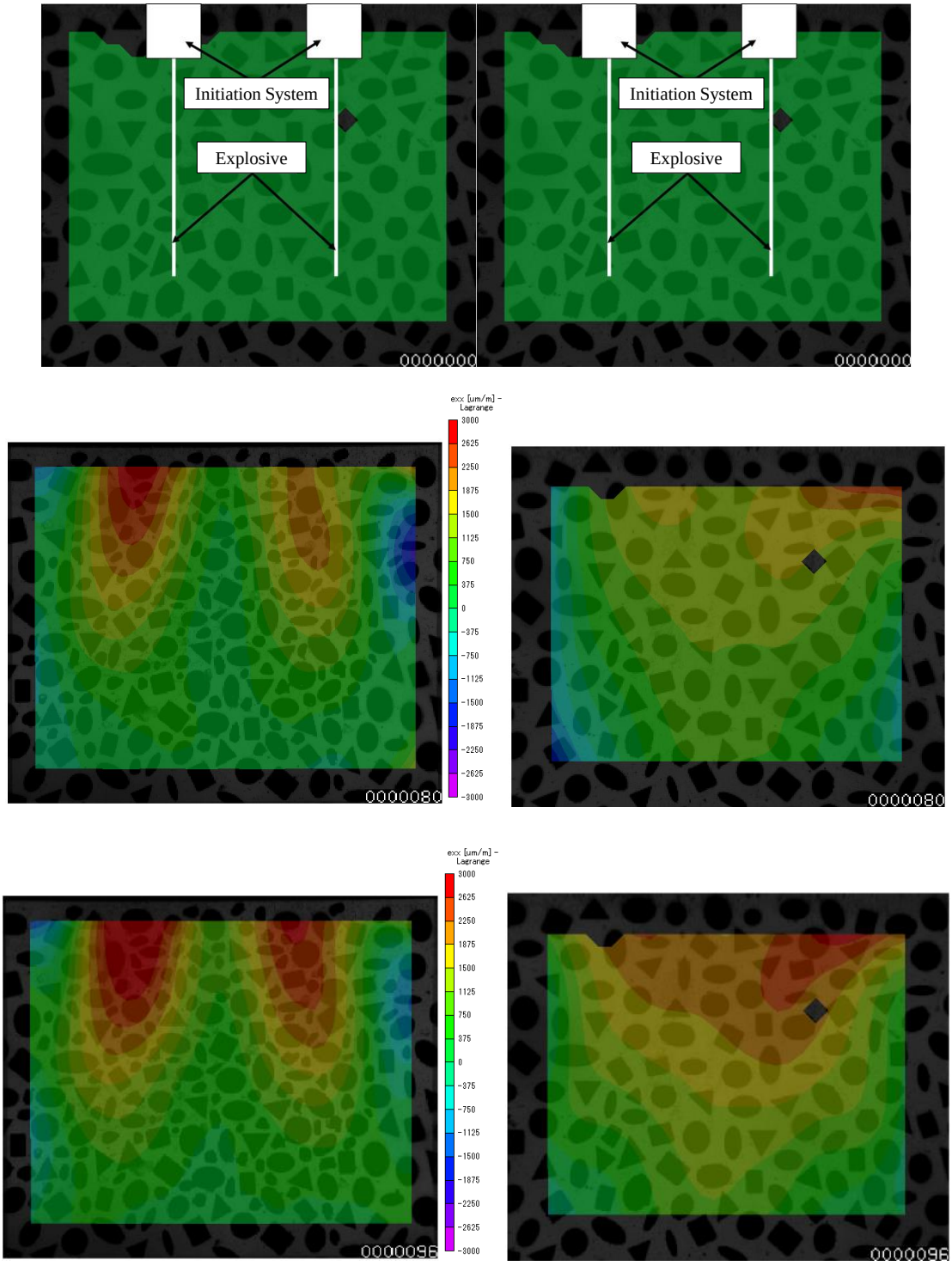

(a) (b)

Fig. 2.17 The time history of stain distribution of ε_{xx} at 0 μs , 80 μs, and 96 μs (a) Burden: 75 mm and (b) Burden: 88 mm

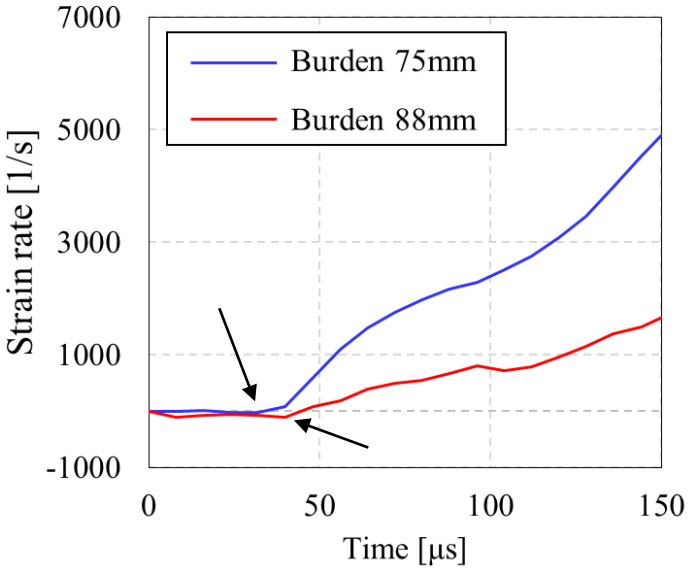

Fig. 2.18 The strain profiles of ε_{xx} on the cracks at Point A2

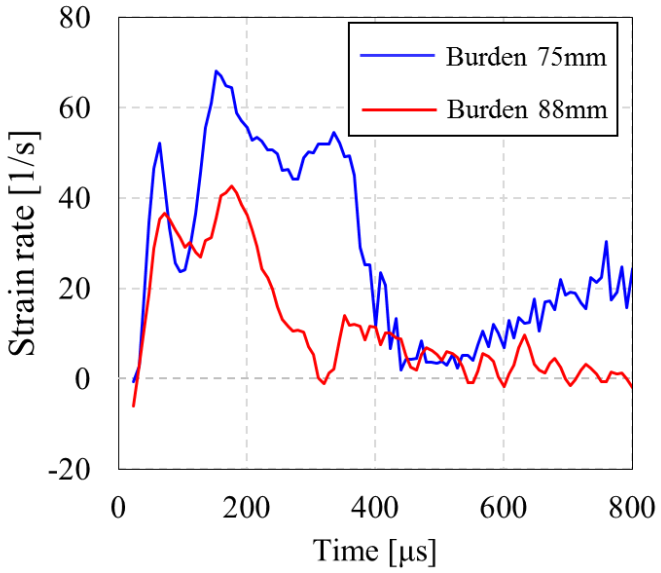

Fig. 2.19 The strain rate profiles of ε_{xx} on the cracks at Point A2

2.4.3.2 Effect of hole spacing on rock fracture mechanism induced by blasting

Finally, effect of hole spacing is discussed in this section. Two types of hole spacing, 88 mm and 132 mm are prepared and performed the blasting experiment with the light-weight mortar. It should be noted that other blasting designs are same as section **2.4.2.** High-speed photographs of final crack conditions of 88 mm and 132 mm of hole spacing are arranged in Fig. 2.20 (a) and (b), respectively. In this case, there is not big difference of crack propagation behavior between 88 mm and 132 mm of hole spacing.

In other words, the number and the shape of cracks are almost similar. In addition, the cracks are located on two blasting holes the in both cases. Hence, in the case of 132 mm of hole spacing, cracks is more difficult to generate around the center of two blasting holes, which can result in larger size of blast-induced fragmented rocks. This is because powder factor become small by enlarging hole spacing.

Fig. 2.21 (a) and (b) shows comparison of strain distribution of 88 mm and 132 mm of hole spacing in horizontal direction (ε_{xx}), respectively. Both of them show high tensile strain area in the direction perpendicular to the crack direction same as above sections. Moreover, Fig. 2.22 (a) and (b) are strain profiles on analysis points (on crack) in Fig. 2.21 (a) and (b). As can be seen in these profiles, both results remarkable strain rising start from 40 μs. Same as above section, this is because the strain is generated by reflected wave of P-wave and then remarkable strain change is induced by S-wave. Moreover, as a next step, strain rate history (4 moving average) is calculated based on the strain profiles as shown in Fig. 2.23. In both profiles, first spike peak of the strain rate can be seen approximately 50 μs after detonation, after S-wave reflected at free face. In addition, the value of the peak of strain rate is almost same. This is the one of the reason for similar crack propagation behavior.

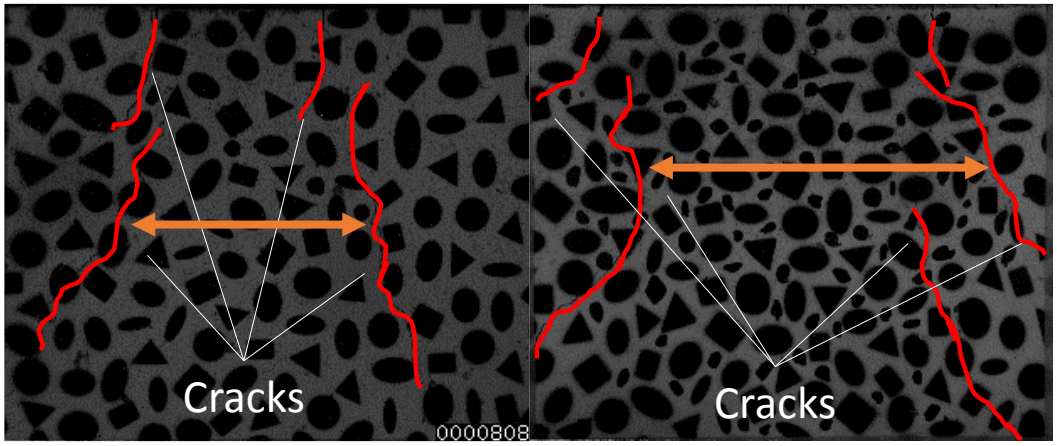

(a) (b)

Fig. 2.20 Final crack propagation behavior at 808 μs (a) Hole spacing: 88 mm and (b) Hole spacing: 132 mm

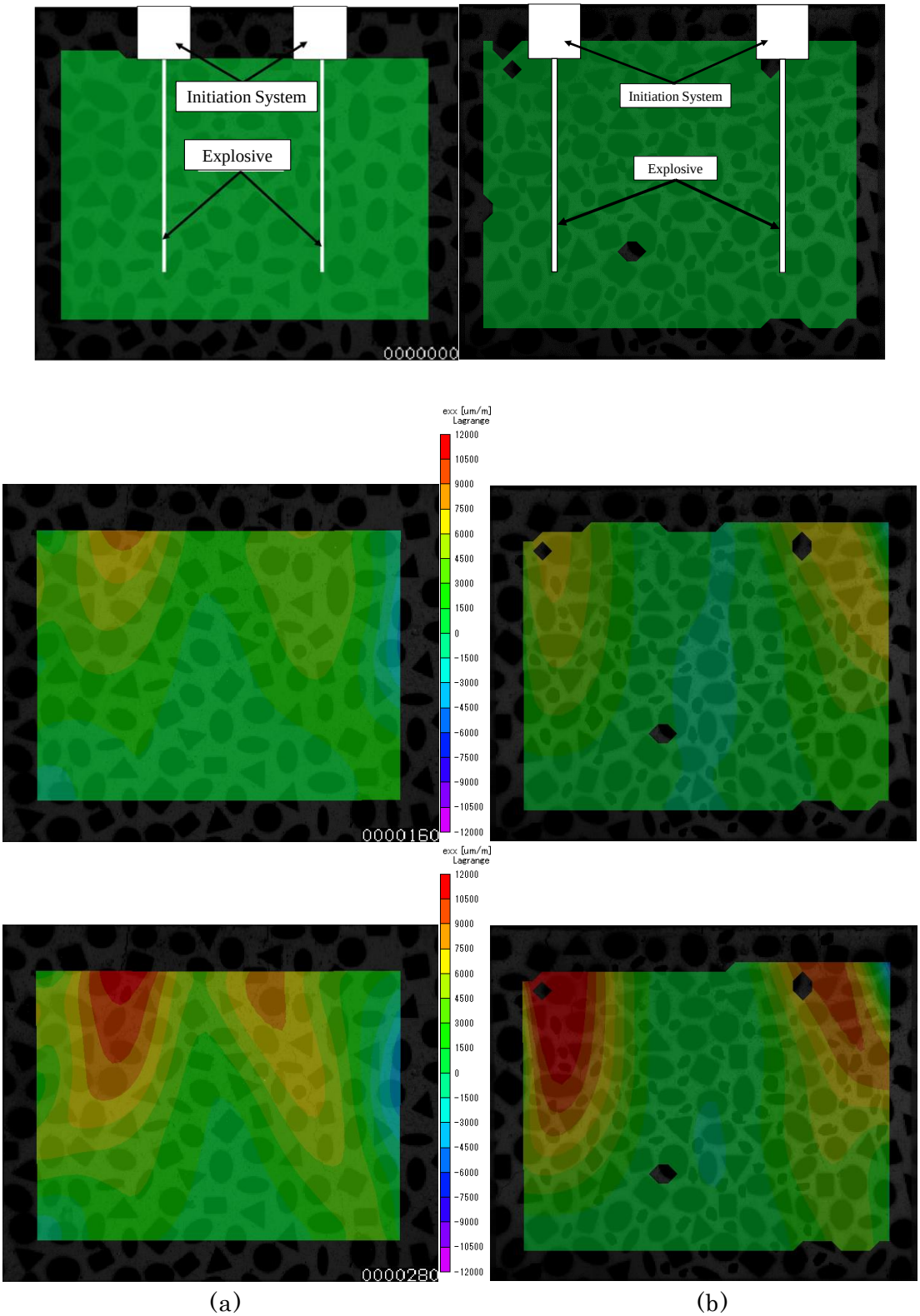

Fig. 2.21 The time history of stain distribution of ε_{xx} at 0 μs, 160 μs, and 240 μs (a) Hole spacing: 88 mm and (b) Hole spacing: 132 mm

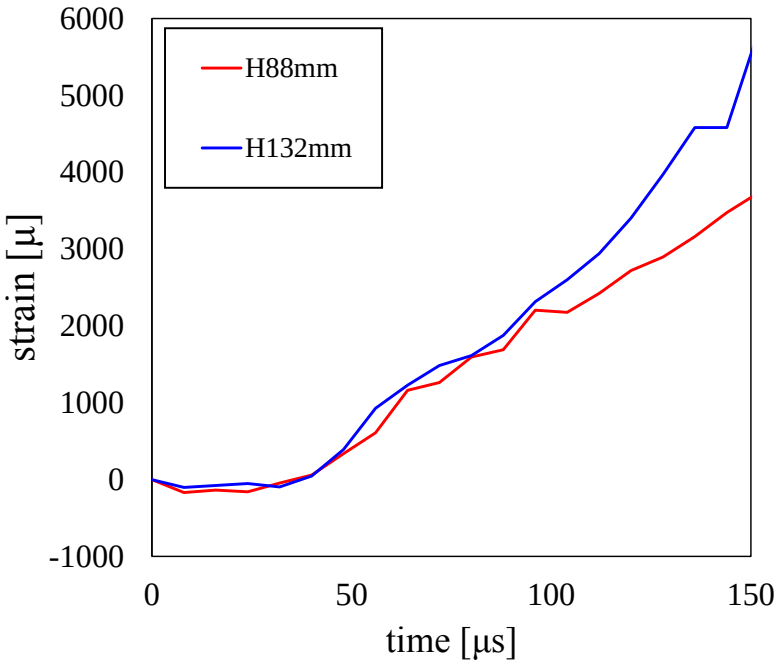

Fig. 2.22 The strain profiles of ε_{xx} on the cracks at Point A3

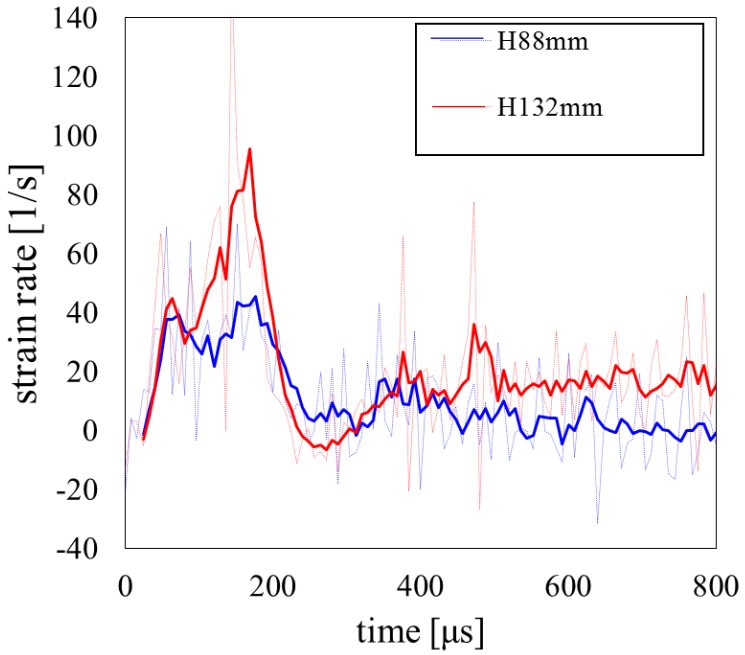

Fig. 2.23 The strain rate profiles of ε_{xx} on the cracks at Point A3

2.5. Conclusions

In this chapter, brand-new two dimensional dynamic strain/displacement measurement method were developed by applying DIC with high-speed photographs. In

addition, crack occurrence, its propagation behavior, the effect of rock mass strength and blasting designs were successfully understood by applying DIC method. The main findings are following:

1. By applying digital image correlation method, two dimensional dynamic strain of brittle material were successfully developed. Due to the electrical noise induced by detonating EBW, strain gauge was difficult to evaluate the strain of the surface of the mortar block. On the other hand, DIC could recorded two dimensional reasonable value without electrical noise.
2. Remarkable strain change on the surface of the block was induced after S wave arrived at the surface and then the strain gradually increased. However, clear influence of the strain on the crack occurrence could not be seen based on the result of the strain profiles.
3. On the other hand, relationship between crack occurrence and strain rate was made clear. After the peak of the strain rate crack started to appear. In addition, cracks propagated to the place where the peak was over the certain value.
4. Rock mass strength strongly influence of the crack propagation behavior. Several short cracks can be seen in the case of normal mortar. On the other hand, one long crack is generated in the case of light-weight mortar. In addition, approximately 30 % of the difference of the rock mass strength (UCS) made the 34 % of difference of the value of strain rate when crack are generated.
5. By reducing the burden, the number of the crack generated by blasting increased since powder factor increased and the energy of explosive more likely to contribute to the fracture energy. Moreover, the strain rate when crack are generated increased around 60 %.

References

[1] M. Monjezi, A. Bahrami, and A. Y. Varjani : Simultaneous Prediction of Fragmentation and Flyrock in Blasting Operation Using Artificial Neural Networks. Int. J. Rock Mech. Min. Sci., 47, 476-480, 2010.

[2] K. Matsui and H. Shimada : Study on Estimation of Rock Mass and Effect of Fracture on Blasting by Borehore Camera. J. Limestone, 330, 57-61, 2004. (in Japanese).

[3] Y. Takahashi, T. Saburi, T. Sasaoka, S. Wahyudi, S. Kubota, H. Shimada and Y. Ogata, Proc. MMIJ Spring Meeting (2016). (in Japanese)

[4] T. P. Chu, W. F. Ranson and M. Sutton : Application of Digital-Image-Correlation Techniques to Experimental Mechanics. Experimental Mech., 25, pp.232-244, 1985.

[5] M. A. Sutton, J. J. Orteu and H. W. Schreier, “Image Correlation for Shape, Motion and Deformation Measurement”, Springer Science and Business Media (2009).

[6] T. Saburi, Y. Takahashi, S. Kubota and Y. Ogata : Dynamic Response Analysis of Mortar Block under Blast Loading Using Digital Image Correlation. M.S.F., 910, pp.161-166, 2018.

[7] H. Munoz, A. Taheri and E. K. Chanda : Pre-Peak and Post-Peak Rock Strain Characteristics During Uniaxial Compression by 3D Digital Image Correlation. Rock Mech. Rock Eng., 49, pp.2541-2544, 2016.

[8] C. H. Hwang, W. C. Wang and Y. H. Chen, Proc. 37th NCTAM 2013 & The 1st ICM, 2013.

[9] M. Beppu, K. Miwa and J. Takahashi : Failure Mechanism of the Scabbing of Concrete Plates Subjected to High Velocity Impact and Effects of Fiber Sheet Reiforcement. J. Japan Society of Civil Eng. Ser. A1, 68, pp.398-412, 2012.

[10] M. Beppu, K. Miwa, T. Ono and M. Siomi : An Experimental Study on the Local Damage of Concrete Plate Due to High Velocity Impact of Steel Projectile. J. Japan Society of Civil Eng. Ser A1, 63, pp.178-191, 2007.

[11] S. H. Cho, S. Nohara and K. Kaneko : Numerical Approach for Strain Rate Dependency on the Dynamic Tensile Strength of Rock. Science and Technology of Energetic Materials, 64, 2, pp.87-96, 2003.

3. NUMERICAL STUDY ON STRESS WAVE AND FAILURE PROPAGATION BEHAVIOR INSIDE ROCK MASS

3.1. Introduction

In Chapter 2, the fracture mechanism on the surface of rock mass could discussed successfully. However, the fracture mechanism induced by blasting side rock mass could not be evaluated quantitatively. In addition, although stress wave interference may influence on the mechanism, small-scale blasting experiment could not describe it. Therefore in this section, the stress wave propagation behavior and influence on interference of the stress wave on rock fracture is discussed by means of numerical simulation. In addition, the effect of distribution and interference of stress wave are also discussed. Moreover, quantitative data which is necessary for building numerical simulation model could be obtained from the experiment; therefore, numerical simulation model is built on a basis of the result of quantitative information. Then, the influence of the blasting designs on stress wave and crack propagation behavior is discussed by using established simulation model.

3.2. Numerical simulation model

3.2.1. Numerical simulation model

On a basis of the small-scale blasting experiment, three dimensional numerical simulation model is built by means of three dimensional finite element method impact analysis software, AUTDYN-3D [(1)]. This software is non-linear and time history response analysis software with explicit method solver and it can be applied the phenomena which occur large displacement.

In this discussion, the explosive part is Euler solver and equation of state (EOS) was Jones-Wilkins-Lee (JWL) [(2)]. On the other hand, the dimension of the model is same as the concrete block which was used in Section **2.4.** in Chapter 2. The concrete part is Lagrange solver and EOS is linear. In addition, non-linear Drucker-Prager model which is often adopted to the numerical simulation of concrete or soil is adopted as constitutive law [(3)]. Failure criterion is set as Hydro (tensile failure criterion). Moreover, based on the recorded first spike peak of strain rate in the experiment, static strength is correlated to dynamic strength. In this numerical analysis, 40 1/s and 30 1/s are set as representative value of normal and light-weight mortar, respectively. In this experiment, for correlating the static strength to dynamic strength, equation (3.1) for compressive strength proposed by Fujikake et al.[(4)] and equation (3.2) for tensile strength proposed by Ross et al. [(5)] were used in this study.

$$\frac{f_{cd}{}'}{f_{cs}{}'} = \left(\frac{\dot{\varepsilon}}{\dot{\varepsilon}_s}\right)^{0.006\left[Log\left(\frac{\dot{\varepsilon}}{\dot{\varepsilon}_s}\right)\right]^{1.05}} \quad (3.1)$$

Where, $f_{cs}{}'$ is static compressive strength, $f_{cd}{}'$ is dynamic compressive strength, $\dot{\varepsilon}$ is strain rate and $\dot{\varepsilon}_s$ is strain rate for static compressive, 1.2×10^{-5} 1/s.

$$\eta(\dot{\varepsilon}) = \frac{f'_{td}}{f'_{ts}} = exp\left[0.00126\left(Log\frac{\dot{\varepsilon}}{\dot{\varepsilon}_s}\right)^{3.3373}\right] \quad (3.2)$$

Where, f'_{ts} is static tensile strength, f'_{td} is dynamic tensile strength, $\dot{\varepsilon}$ is strain rate and $\dot{\varepsilon}_s$ is strain rate for static tensile strength, 1.0×10^{-7} 1/s. Additionally, in order to reduce the influence from reflected wave from side, bottom and back free face, these free faces are set as transmission boundary. The kind of input parameters are listed in Table. 3.1.

Table 3.1 The input parameters for numerical simulations

	Concrete	C-4
Mesh type	Lagrange	Euler
Equation of state	Linear	JWL
Constitutive law	Drucker-Prager	-
Failure criterion	Hydro (tensile failure)	-
Reference density g/cm^3	2.4	1.4
UCS (Dynamic, Normal mortar) MPa	48.9	-
UCS (Dynamic, Light-weight mortar) MPa	36.8	-
BTS (Dynamic, Normal mortar) MPa	14.4	-
BTS (Dynamic, Light-weight mortar) MPa	11.6	

3.2.2. Applicability of the numerical simulation

By comparing the result obtained from laboratory tests in Chapter 2 and numerical simulation, the applicability of the numerical simulations is discussed in this section. At first, the result of final cracks formation is compared. The crack formation of top face of experiment (Normal mortar, Burden 88 mm, Hole spacing 88 mm and numerical simulation is shown in Figs. 3.1 (a) and (b), respectively. It should be noted that the red color in the numerical simulation result is failure mesh, light-blue color is plastic area and green one is the concrete block. As shown in these figures, including the bowl-shaped crack formation, the crack propagation behavior of numerical simulation is

remarkably similar to the result of small-scale blasting experiment.

In addition, the horizontal strain distribution obtained by DIC and numerical simulation is compared in Figs. 3.2 (a) and (b). As can be seen in these figures, although it cannot be said that the result of the numerical simulation quantitatively match with the result of the strain distribution calculated by DIC, numerical simulation might reproduce the result of small-scale blasting experiment at least qualitatively in terms of the position of remarkable tensile and compressive strain zone. In other words, stress wave and crack propagation behavior inside rock mass can be accessed by using the numerical simulation model built in this section

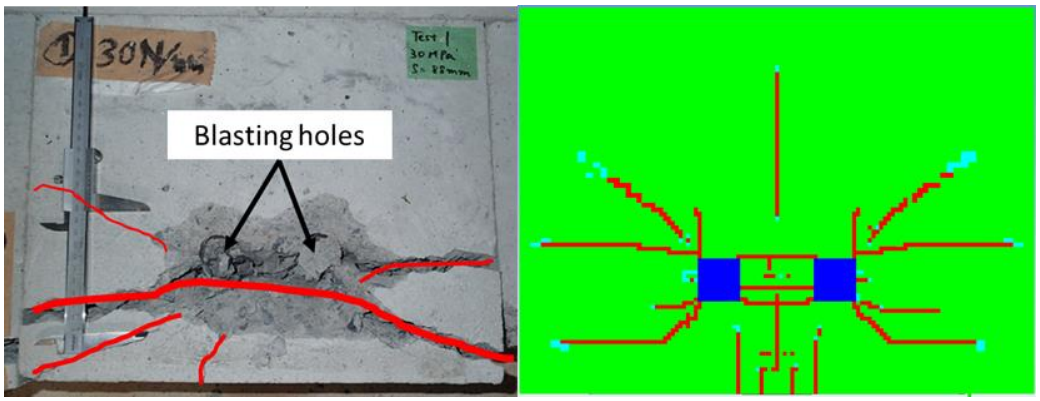

(a) (b)

Fig. 3.1 Comparison of crack propagation behavior (a) Small-scale blasting experiment (b) Numerical simulation

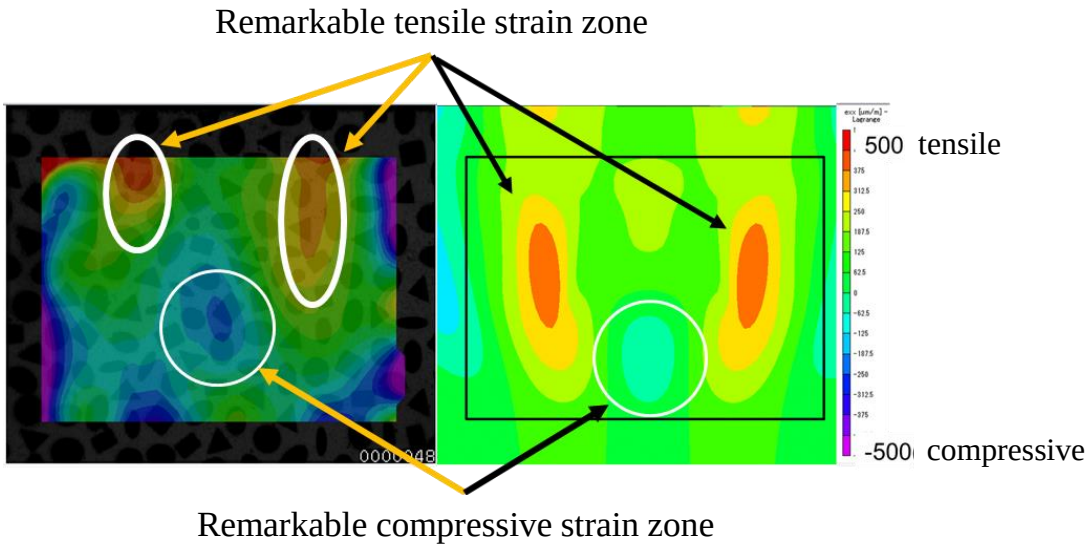

Fig. 3.2 Comparison of horizontal strain distribution at 50 [μs] (a) Small-scale blasting experiment (b) Numerical simulation (same contour scale)

3.3. Results and discussions

3.3.1. Crack occurrence on free face

At first, the crack occurrence on free face (front face) is discussed. The results of Chapter 2 indicated that the crack occurred when the strain rate become peak value (the first peak). On the other hand, by visual observation of the images captured by high-speed camera, cracks could not be seen at the first peak of strain rate (around 50μs), but around 80 μs. Here, the pressure contour and crack propagation behaviors around 50 μs obtained by numerical simulation are illustrated in Figs. 3.2 (a) and (b). In these right figures, red color is the failure cells which are over the failure criterion. As shown in these figures, the first cracks in numerical simulation appear in 46 μs, which is good accordance with the time of fist strain rate peak in the experiment. In addition, the pressure contour suggested that the crack is caused by negative pressure, tensile pressure, induced by reflected wave of compressive stress wave.

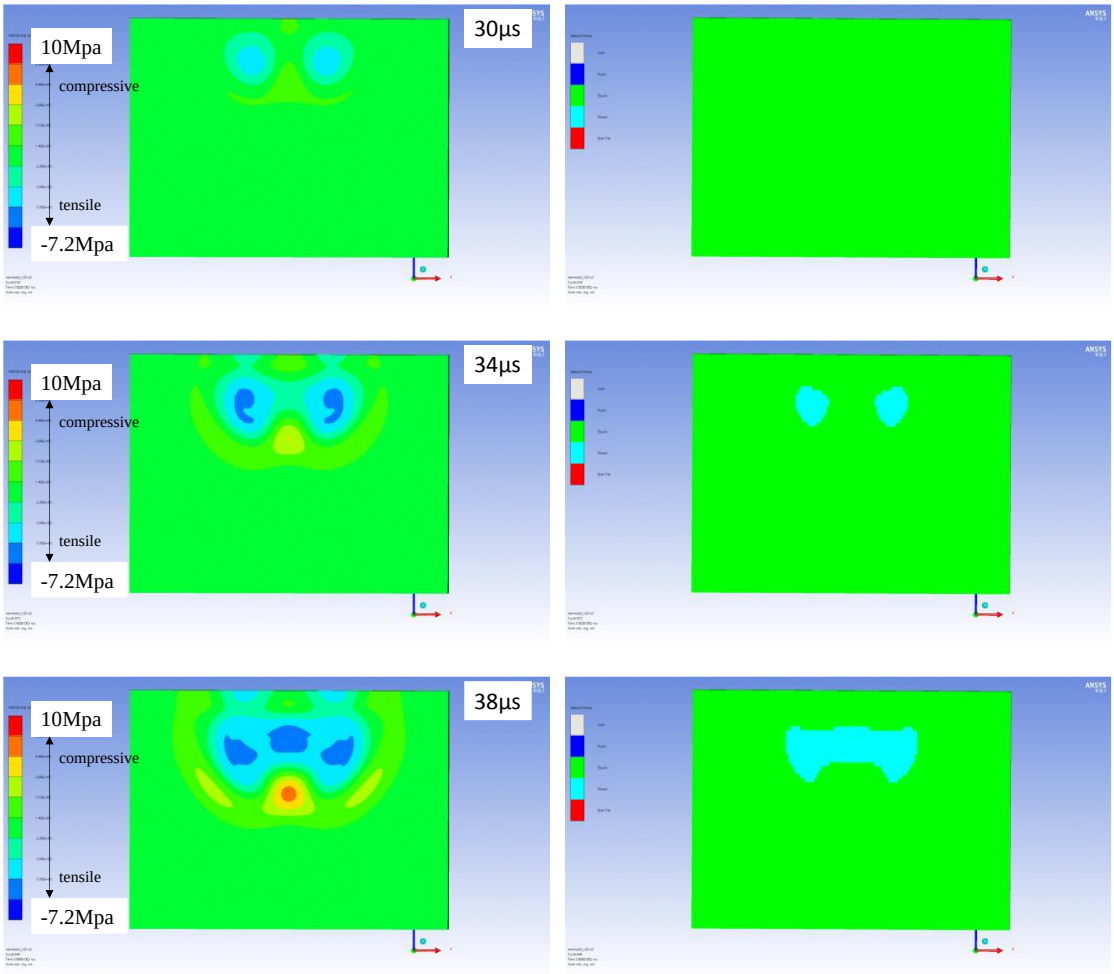

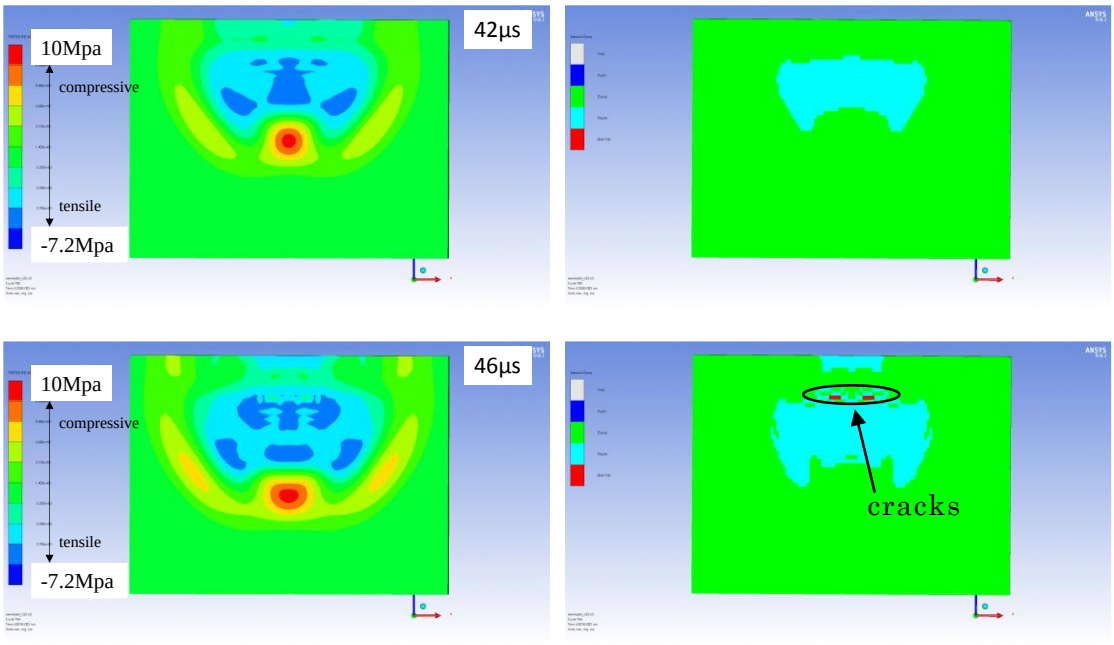

(a) (b)

Fig. 3.2 The result of numerical simulation of front face (a) pressure contour and (b) crack conditions

3.3.2. Stress wave propagation behavior and fracture behavior inside rock mass

Next, stress wave and crack propagation behavior inside rock mass is discussed. A series of contours of pressure and material states in the case of normal mortar, 88 mm of burden and 88 mm of hole spacing at the cross section of middle of the blasting holes of top face are arranged in Figs. 3.3(a) and (b). As shown in these figures, high compressive pressure waves propagate in concentric circles. These compressive waves reflect at the free face and change into tensile stress wave. Compared with the pressure and material state, tensile failure is generated not immediately after stress waves reflect at the free face, but after reflected tensile stress waves from two blasting holes superpose and failure propagate with spreading tensile stress wave. This result suggested that tensile wave interference has strong influence on the fracture induced by blasting and it can be key to control the size of blast-induced fragmented rocks.

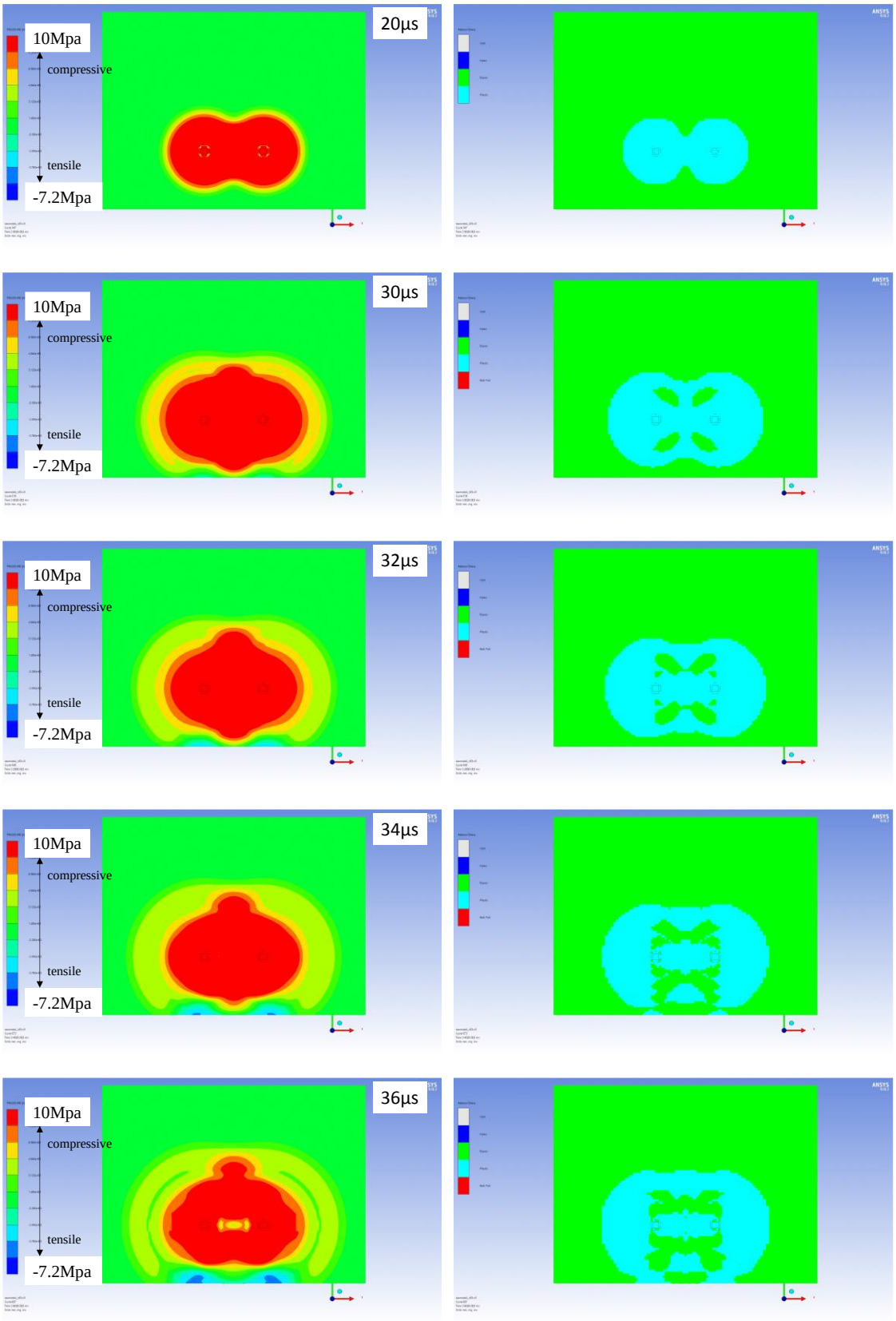
20μs
10Mpa
compressive
tensile
-7.2Mpa
30μs
10Mpa
compressive
tensile
-7.2Mpa
32μs
10Mpa
compressive
tensile
-7.2Mpa
34μs
10Mpa
compressive
tensile
-7.2Mpa
36μs
10Mpa
compressive
tensile
-7.2Mpa

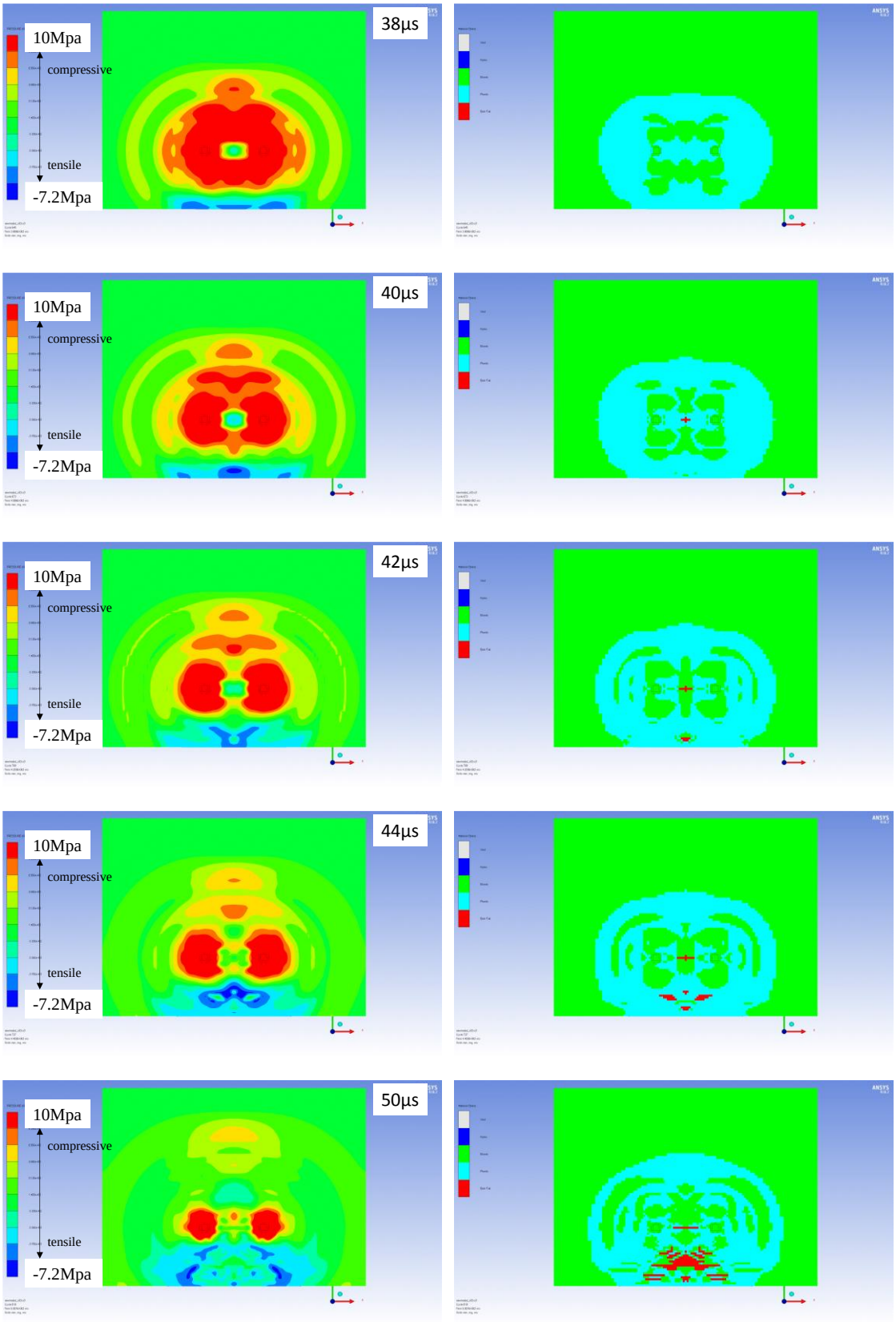
38μs
40μs
42μs
44μs
50μs
10Mpa
compressive
tensile
-7.2Mpa

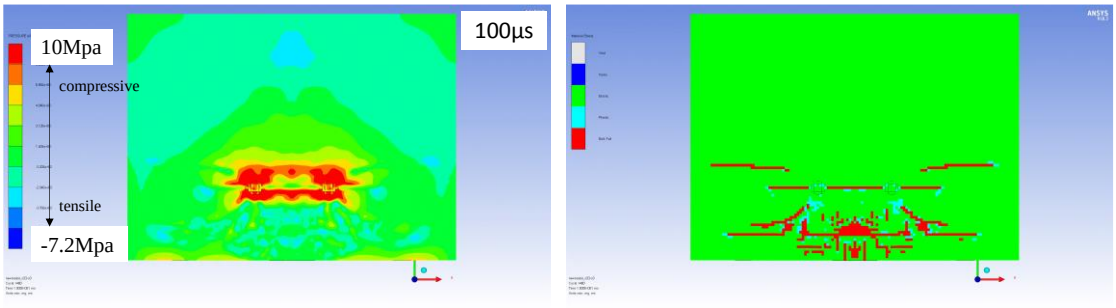

(a) (b)

Fig. 3.3 Stress wave and crack propagation behavior inside rock mass (a) pressure contour and (b) crack conditions

3.4. Effect of rock mass conditions and blasting designs on stress wave and fracture propagation behavior inside rock mass

3.4.1. Effect of rock mass strength on stress wave and fracture propagation behavior inside rock mass

Contours of pressure and material states in the case of light-weight mortar at the cross section of middle of the blasting holes of top face are shown in Figs. 3.4 (a) and (b). In this case, although the first crack can be seen at 48 μs between two blasting holes, the fracture mechanism is almost same as the result of normal mortal. Since the velocity of stress wave becomes slow due to the decreasing of the strength, crack start to appear around the free face later than case of normal mortar. Same as the case of normal mortar, crack occurs and failure zone spreads with spreading the superposed tensile stress wave. Small-scale experiment result showed smaller number of cracks on the surface of the block in the case of light-weight mortar in comparison to normal mortar. However, considering the failure conditions inside rock mass, the failure zone became large compared with the case of normal mortar due to the decreasing the rock mass strength. This is because superpose of the tensile waves occur not on the free face but a little far from the free face.

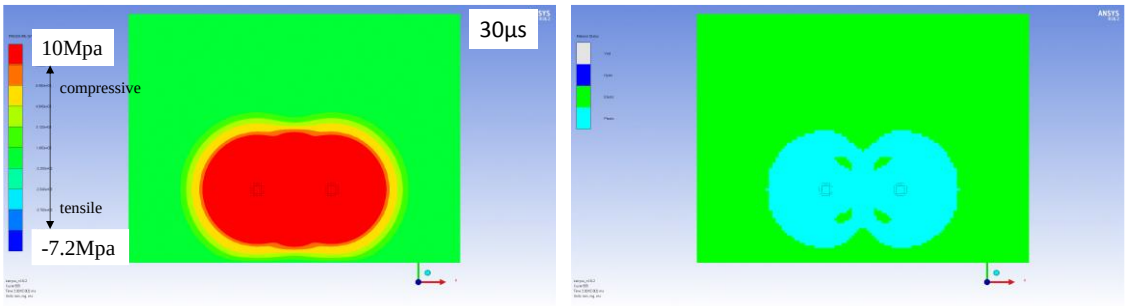

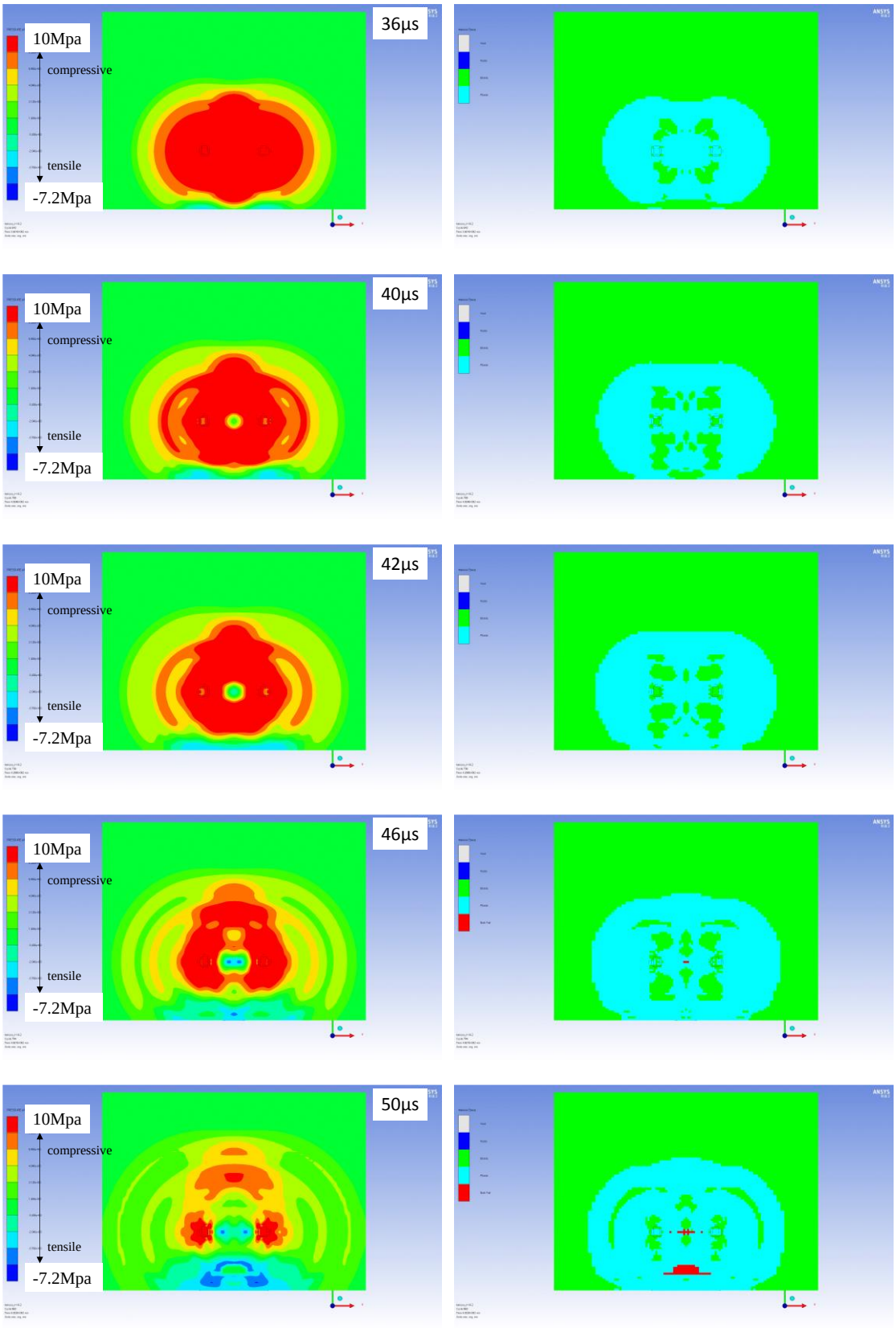
36μs
40μs
42μs
46μs
50μs
10Mpa
compressive
tensile
-7.2Mpa

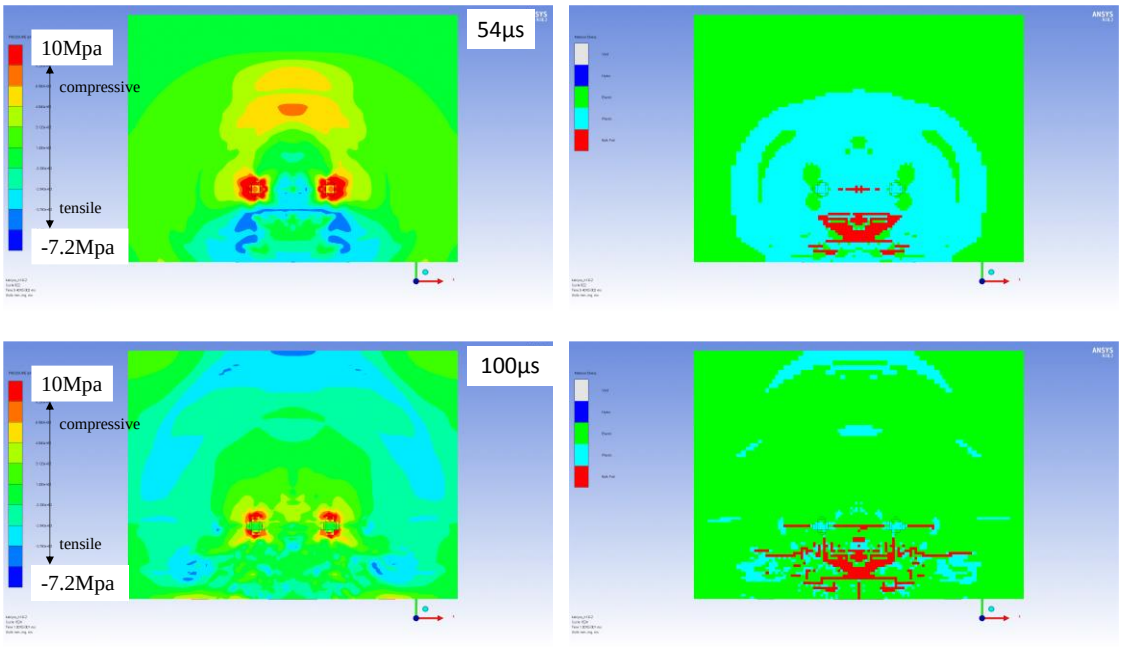

(a) (b)

Fig. 3.4 Stress wave and crack propagation behavior inside rock mass in the case of light-weight mortar (a) pressure contour and (b) crack conditions

3.4.2. Effect of burden on stress wave and fracture propagation behavior inside rock mass

A series of contours of pressure and material states in the case of 75 mm burden at the cross section of middle of the blasting holes of top face are shown in Fig. 3.5 (a) and (b). In this simulation, the dynamic strength is correlated by strain rate 40 1/s based on the result of small-scale blasting experiment. Same as Fig. 3.3(a) and (b), high compressive pressure waves propagate in concentric circles and reflected wave turn into tensile stress wave. However, compared with 88 mm of burden, the position where tensile failure is superposed move to forward and crack occur earlier than in the case of 88 mm of burden. As the result, remarkable failure zone can be seen around the free face in the case of 75 mm of burden. That is why the number of cracks in the case of 75 mm of burden is larger than that of 88 mm of burden in the small scale experiment. This result indicated that the size of blast-induced fragmented rock can decrease by reducing the burden.

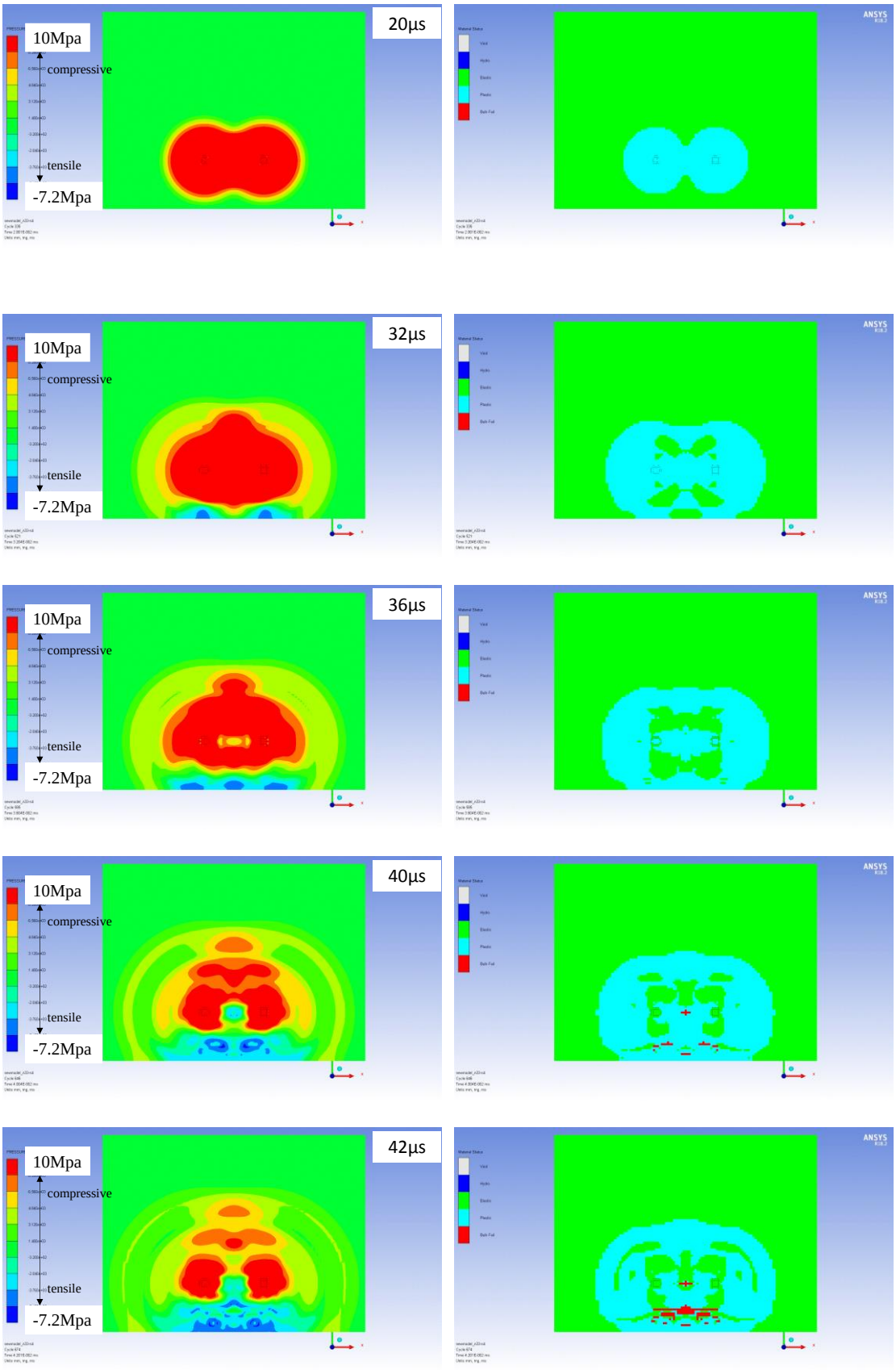
20μs
10Mpa
compressive
tensile
-7.2Mpa
32μs
10Mpa
compressive
tensile
-7.2Mpa
36μs
10Mpa
compressive
tensile
-7.2Mpa
40μs
10Mpa
compressive
tensile
-7.2Mpa
42μs
10Mpa
compressive
tensile
-7.2Mpa

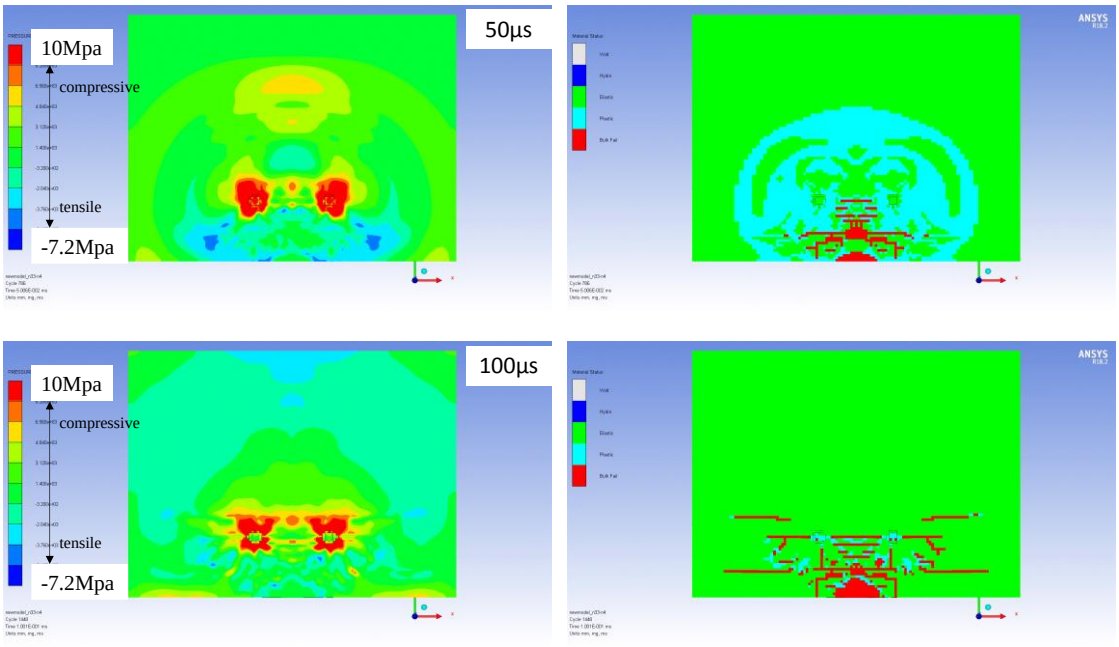

(a) (b)

Fig. 3.5 Stress wave and crack propagation behavior inside rock mass in the case of 75 mm of burden (a) pressure contour and (b) crack conditions

3.4.3. Effect of hole spacing on stress wave and fracture propagation behavior inside rock mass

A series of contours of pressure and material states in the case of 132 mm of hole spacing at the cross section of middle of the blasting holes of top face are show in Figs. 3.6 (a) and (b). In this case, cracks start to appear not around free face in front of two blasting holes which is a little different from Fig. 3.3(a) and (b). This is because the value of tensile stress wave reaches the criteria of tensile strength of this concrete before two tensile waves are superposed. On the other hand, same as 88 mm of hole spacing, failure zone is generated where two tensile waves are superposed. However, compared with 88 mm of hole spacing, the failure zone between two blasting hole is relatively small. By increasing the hole spacing, tensile stress wave which value is over the tensile criterion is difficult to spread, resulting in the decreasing the failure zone, especially the middle of blasting hole and free face (circle in Fig 3.6 (a) and (b)). That is why crack propagation behavior captured by high speed camera is similar. However, increasing hole spacing can make the size of blast-induced fragmented rocks large by considering the failure zone in side rock mass.

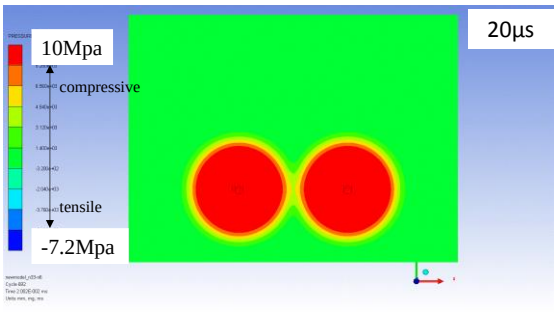
20μs
10Mpa
compressive
tensile
-7.2Mpa

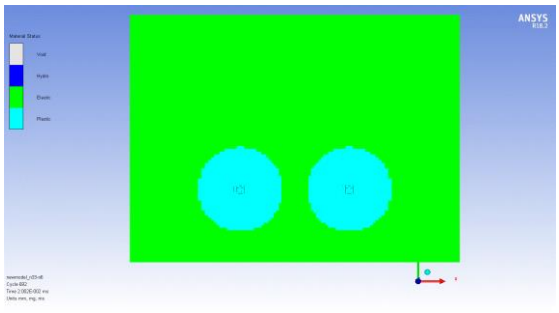
ANSYS

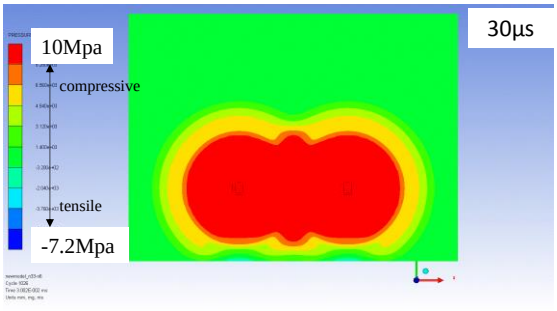
30μs
10Mpa
compressive
tensile
-7.2Mpa

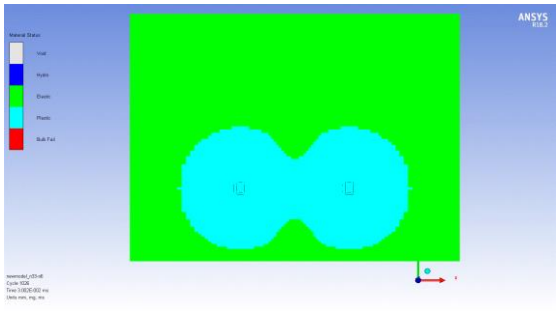
ANSYS

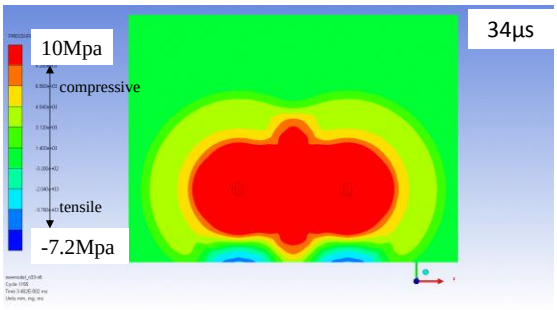
34μs
10Mpa
compressive
tensile
-7.2Mpa

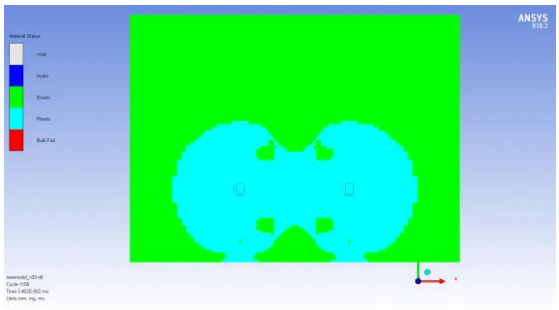
ANSYS

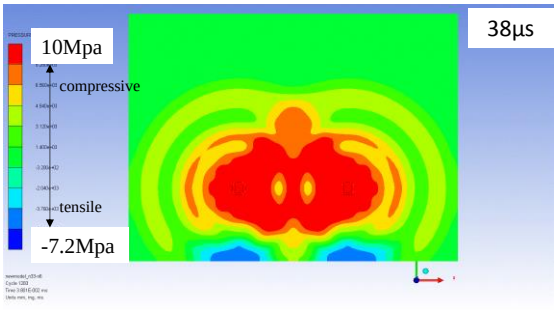
38μs
10Mpa
compressive
tensile
-7.2Mpa

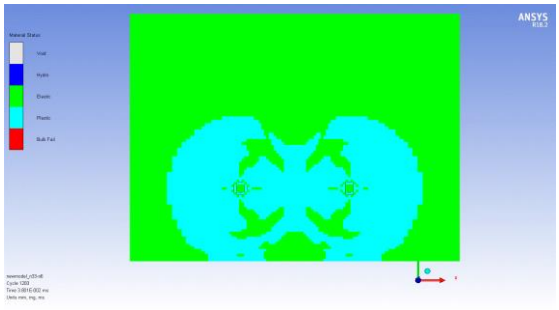
ANSYS

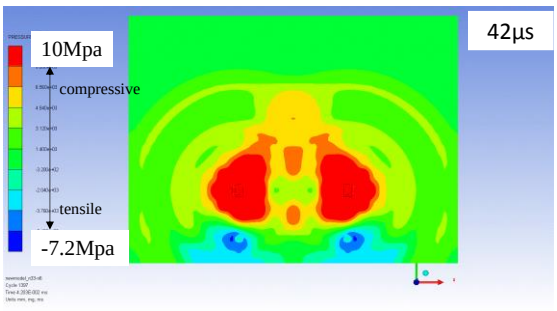
42μs
10Mpa
compressive
tensile
-7.2Mpa


ANSYS

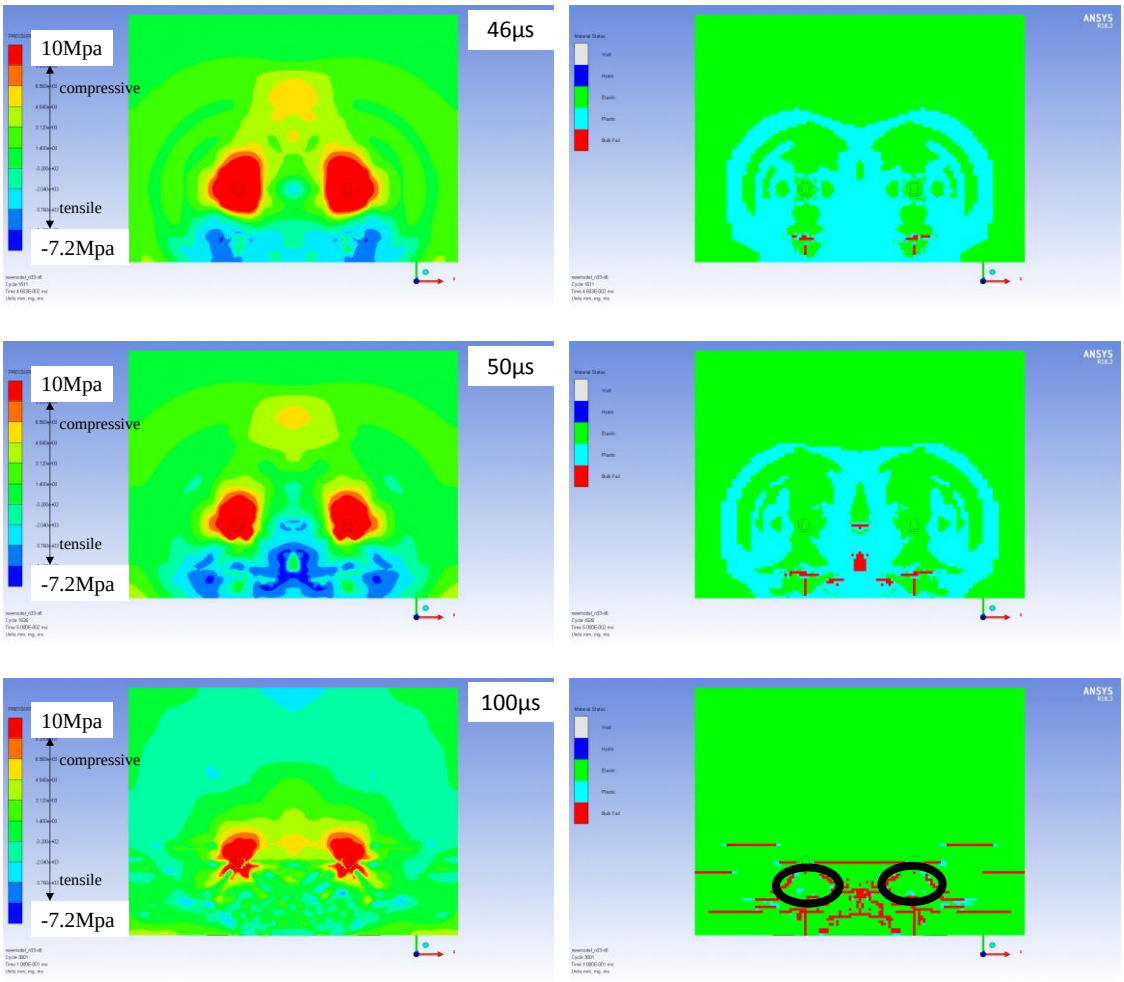

(a) (b)

Fig. 3.6 Stress wave and crack propagation behavior inside rock mass in the case of 132 mm of hole spacing (a) pressure contour and (b) crack conditions

3.4.4. Effect of delay time on stress wave and fracture propagation behavior inside rock mass

Usually, the delay blasting is performed in order to control blast-induced ground vibration. On the other hand, several research works suggested that size of blast-induced fragmented rocks can be controlled by setting optimum delay time. Hence, in this simulation, in order to obtain fundamental knowledge for establishing the guidelines of optimum delay time. In this study, three types of delay times are discussed by considering the reaching time of stress wave (P-wave) at the neighboring blasthole. 24 μs is arrival time of P-wave at neighboring blasthole, so 72 μs and 108 μs of delay blasting are numerically simulated in addition to 24 μs of delay blasting.

At first, the result of 24 μs of delay blasting is illustrated in Figs. 3.7 (a) and (b). First cracks can be seen around in front of first firing blasthole. This crack is caused by

reflection tensile wave from first firing blasthole. In other words, the first crack is not caused by superpose of the two tensile stress wave. Although similar cases happen in the discussion of effect of hole spacing, the failure zone tends to small when crack is not generated by superpose of two reflection tensile waves. Moreover, 62 μs after first blast hole is detonated, superpose of the tensile waves can be seen around the free face. In the case of 72 μs and 108 μs of delay time, however, the superpose of tensile stress waves cannot be seen (see Figs. 3.8 (a) and (b) and Figs. 3.9 (a) and (b)). In these cases, the effect of stress wave induced by first firing blasthole is lost around the time when the stress wave generated by second blasthole reach at the free face. Because of that, the failure zone in the case of 72 μs and 108 μs is relatively small compared with 24 μs of delay blasting. On the other hand, from different perspective, it can be said the second firing blasthole is detonated after free face is generated in the case of 72 μs and 108 μs, which might result in enlarging the failure zone. In this numerical simulations, the effect of new created free face cannot simulated, therefore the failure zone in real conditions can be lager. However, the result of simultaneous blasting suggested that the most important point to increase failure zone is occurrence of superposition of reflected tensile stress wave; therefore; it can be concluded that it is important to evaluate the velocity of stress wave and set the delay time to generate the superposition of the stress wave in order to reduce the size of blast-induced fragmented rocks.

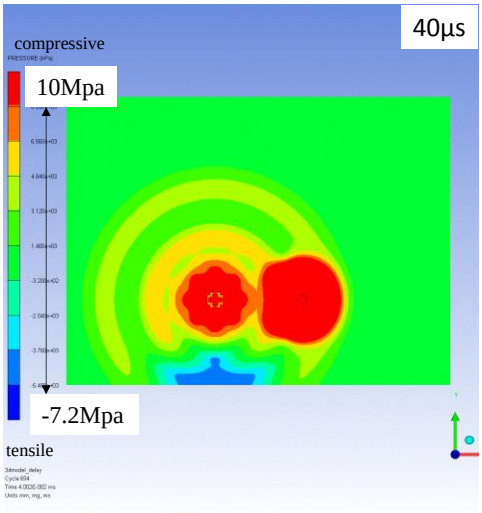

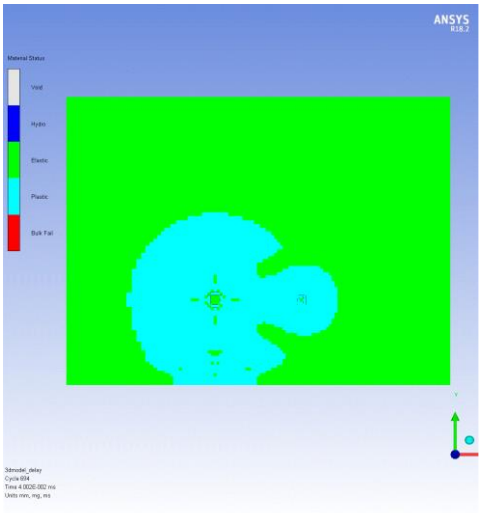

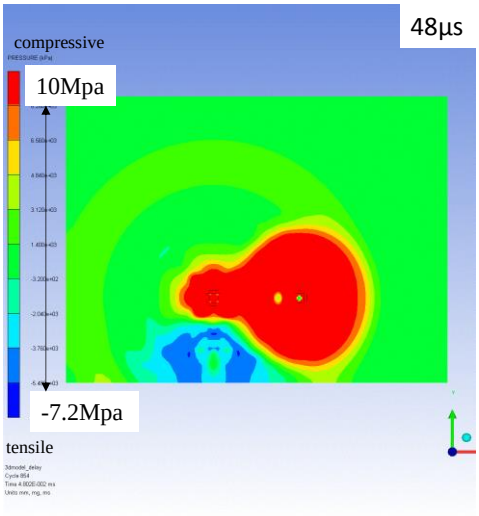
48μs
compressive
10Mpa
-7.2Mpa
tensile

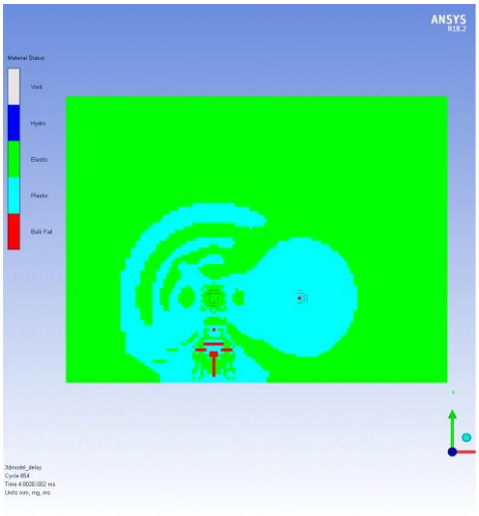
ANSYS

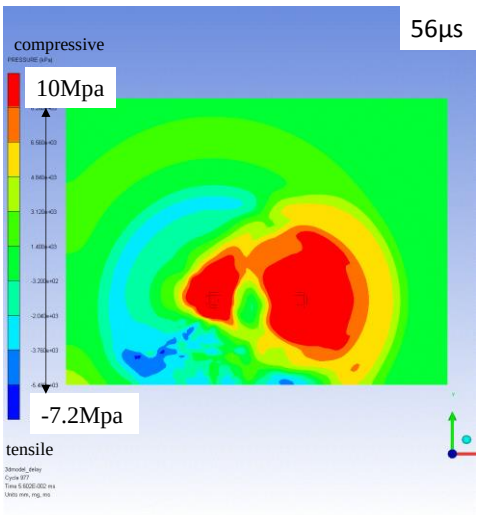
56μs
compressive
10Mpa
-7.2Mpa
tensile

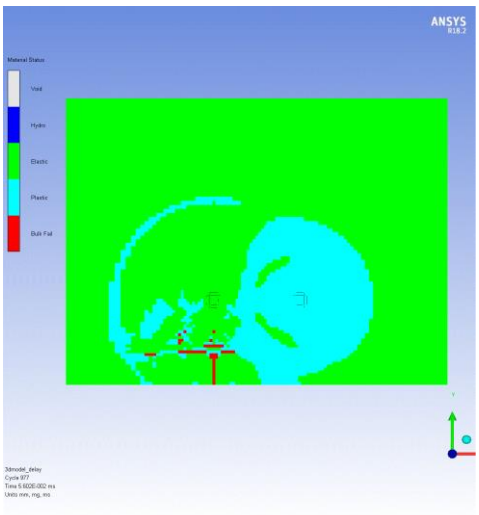
ANSYS

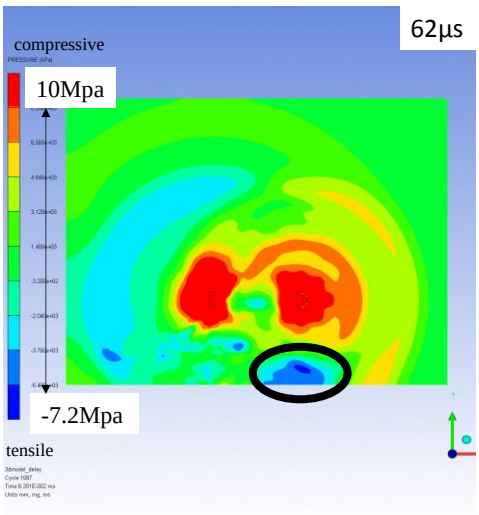
62μs
compressive
10Mpa
-7.2Mpa
tensile

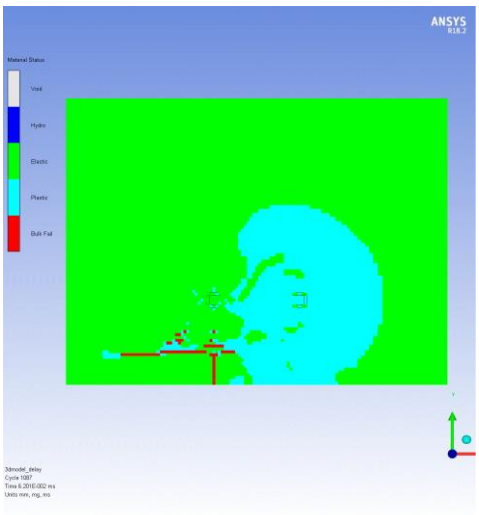
ANSYS

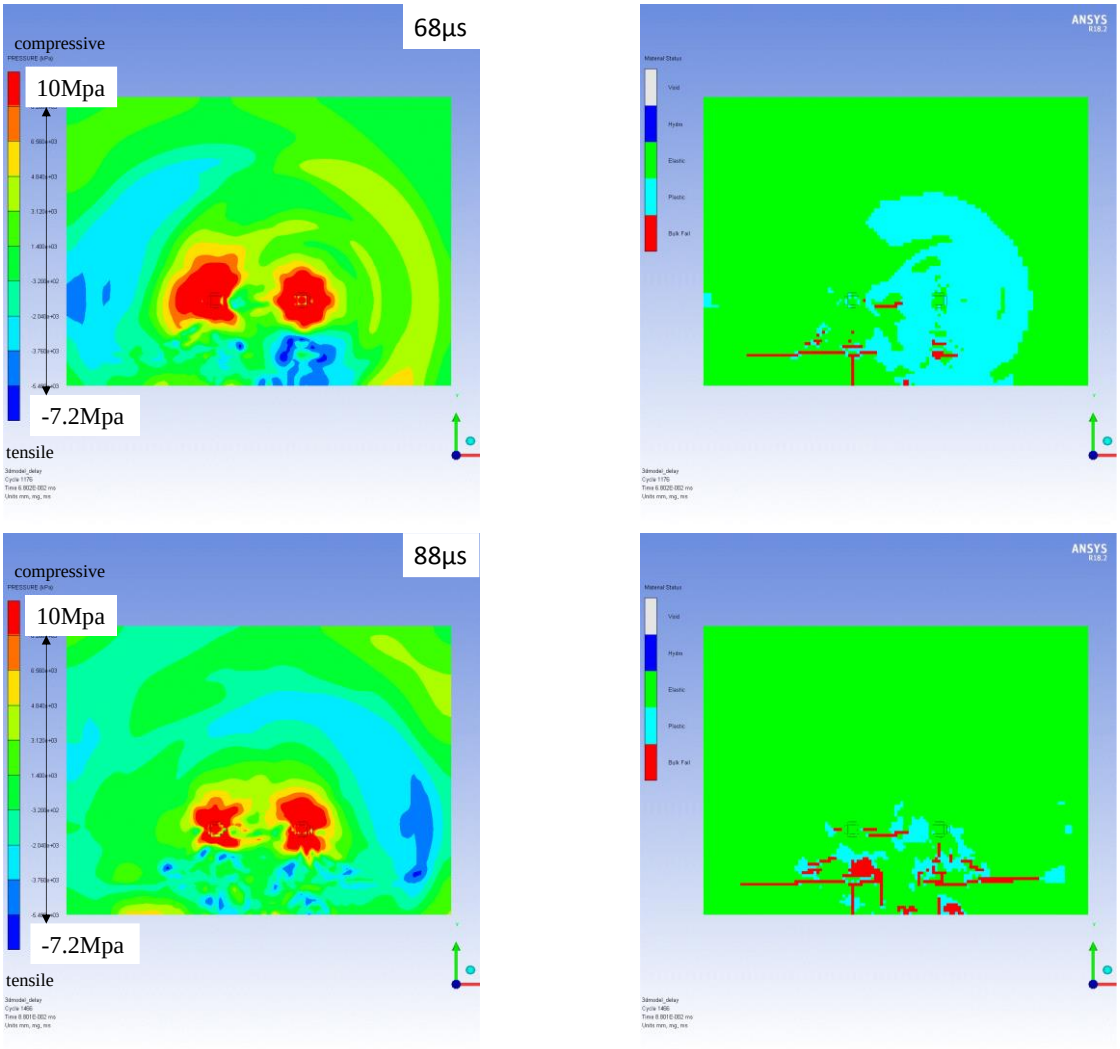

(a) (b)

Fig. 3.7 Stress wave and crack propagation behavior inside rock mass in the case of 24 μs of delay time (a) pressure contour and (b) crack conditions

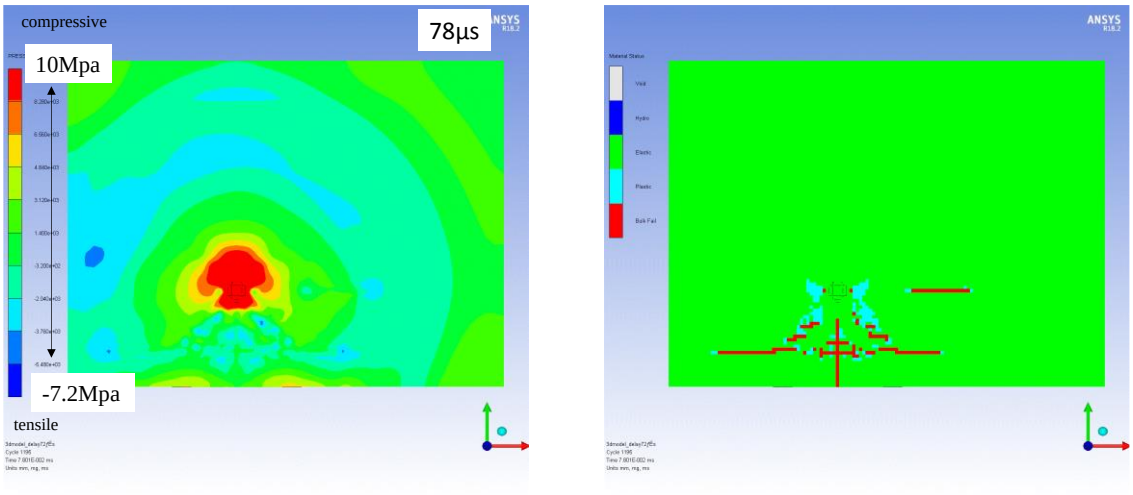

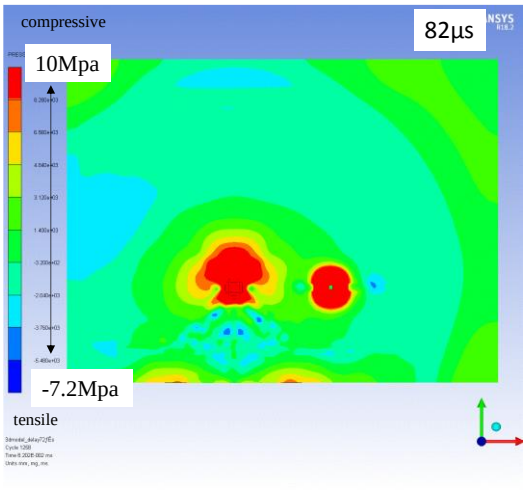
compressive
82μs
10Mpa
-7.2Mpa
tensile

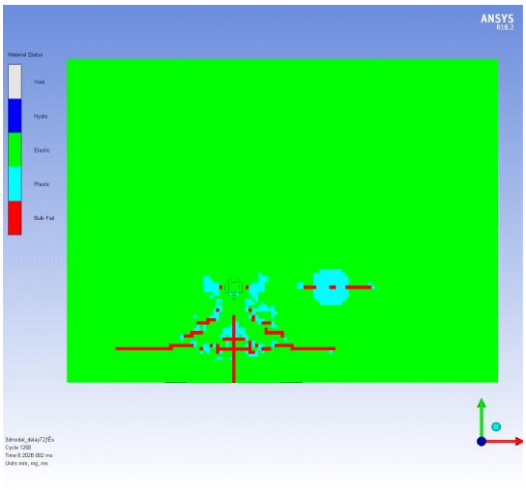
ANSYS

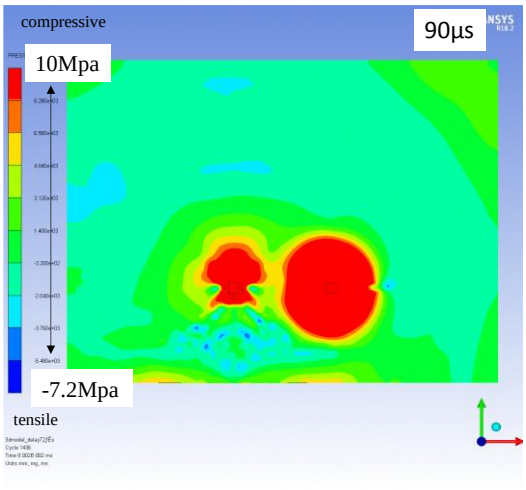
compressive
90μs
10Mpa
-7.2Mpa
tensile

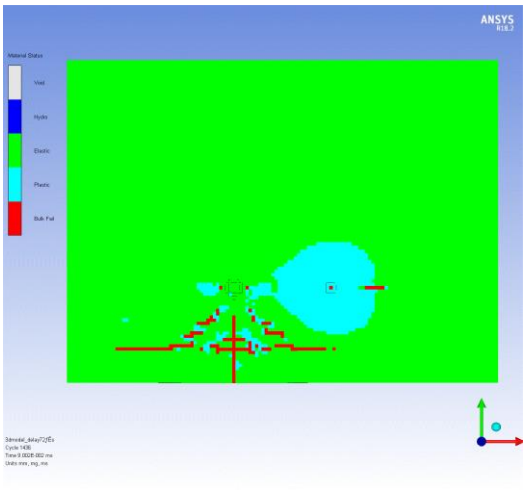
ANSYS

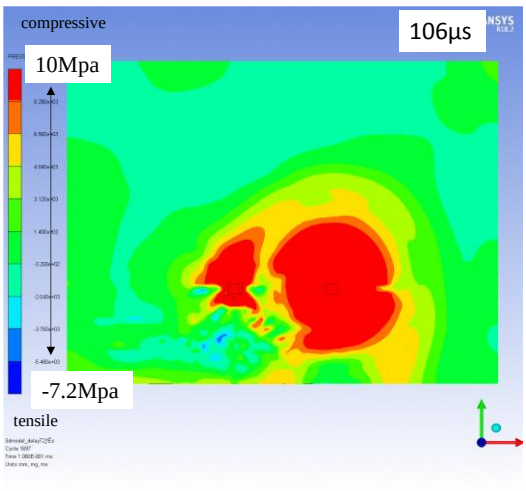
compressive
106μs
10Mpa
-7.2Mpa
tensile

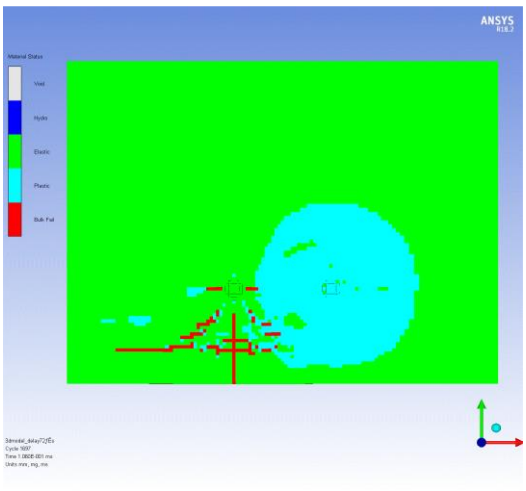
ANSYS

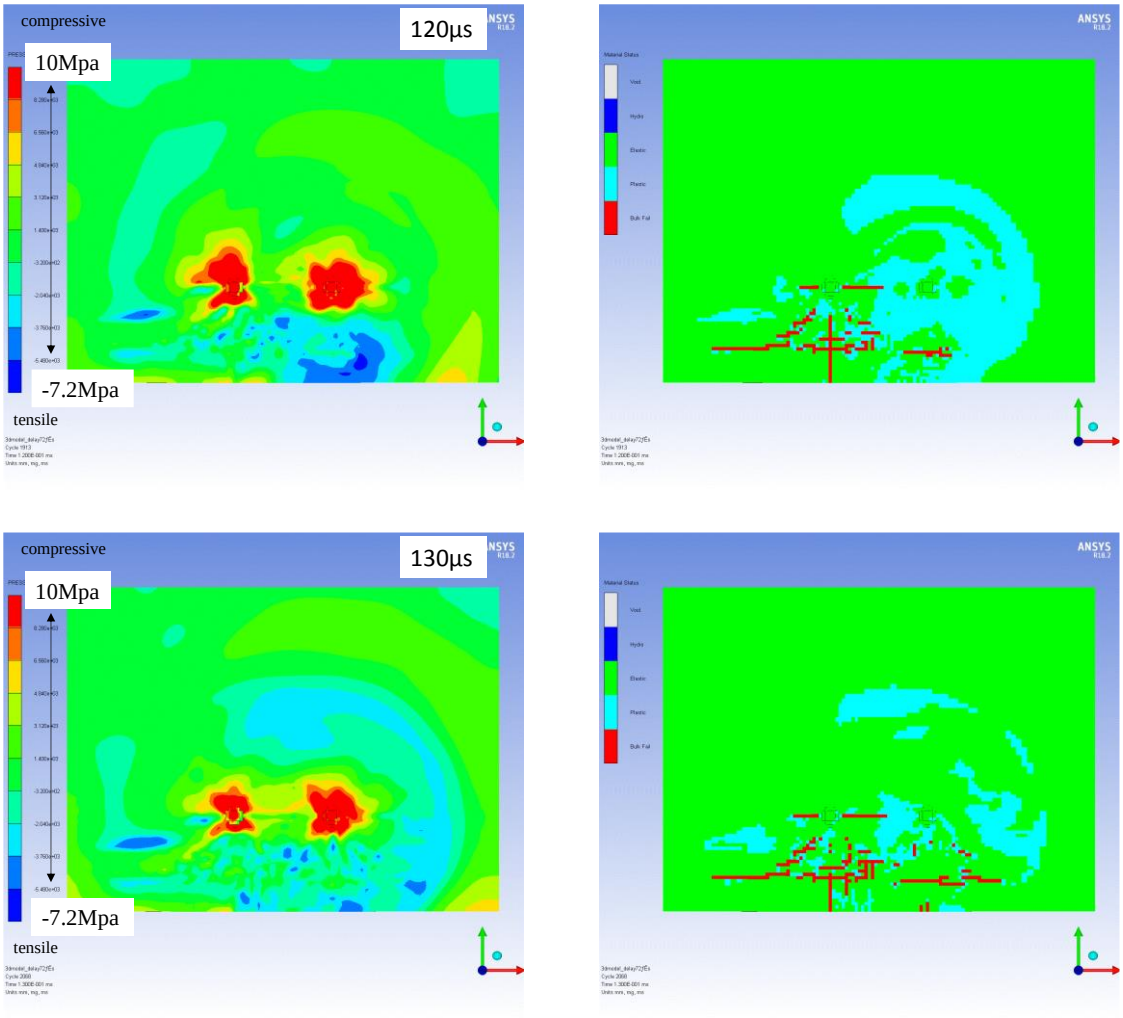

(a) (b)

Fig. 3.8 Stress wave and crack propagation behavior inside rock mass in the case of 72 μs of delay time (a) pressure contour and (b) crack conditions

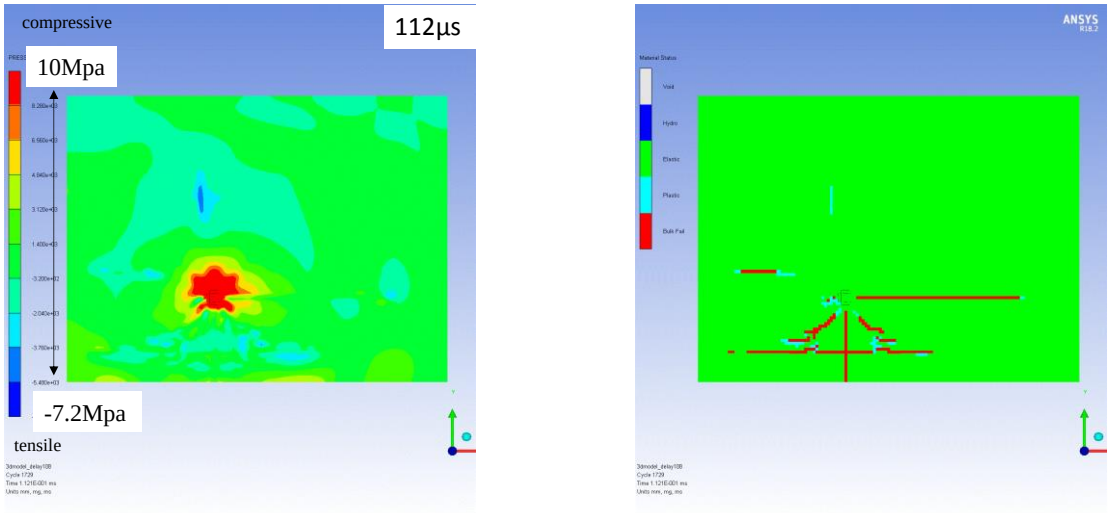

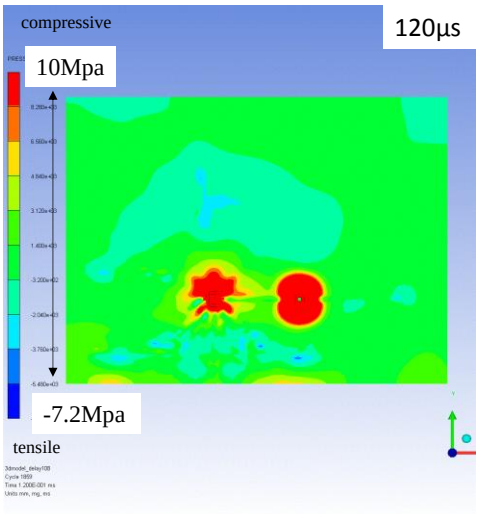
compressive
120μs
10Mpa
-7.2Mpa
tensile

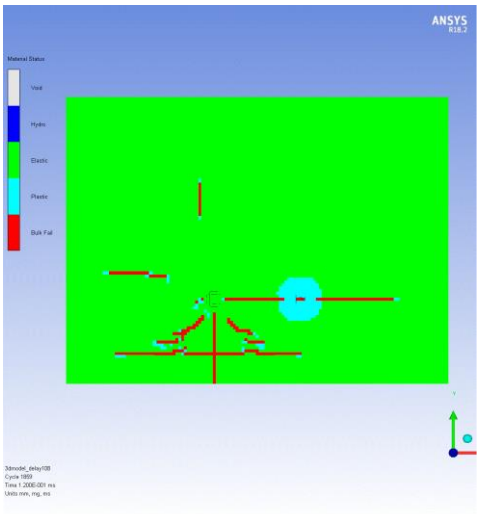
ANSYS

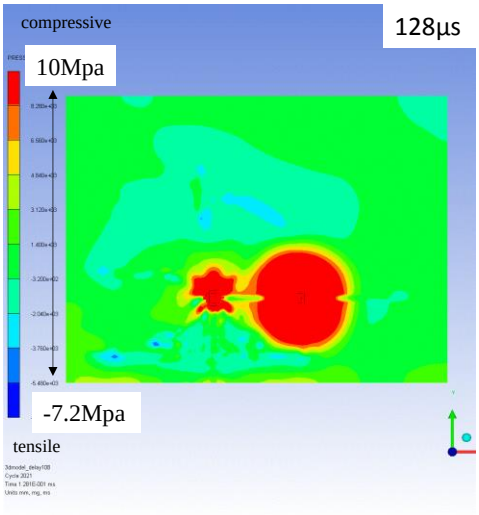
compressive
128μs
10Mpa
-7.2Mpa
tensile

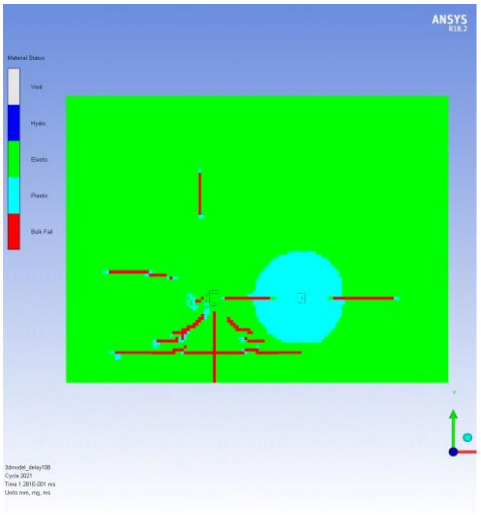
ANSYS

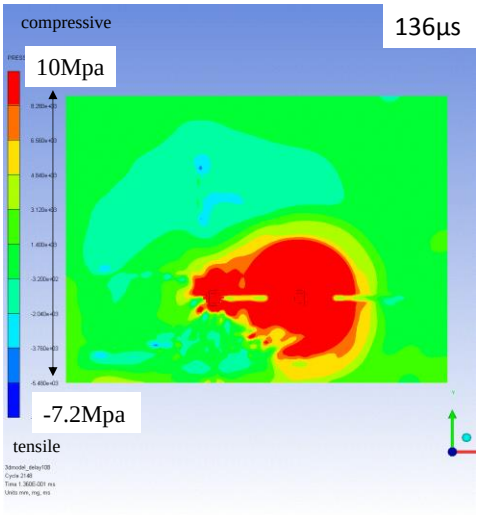
compressive
136μs
10Mpa
-7.2Mpa
tensile

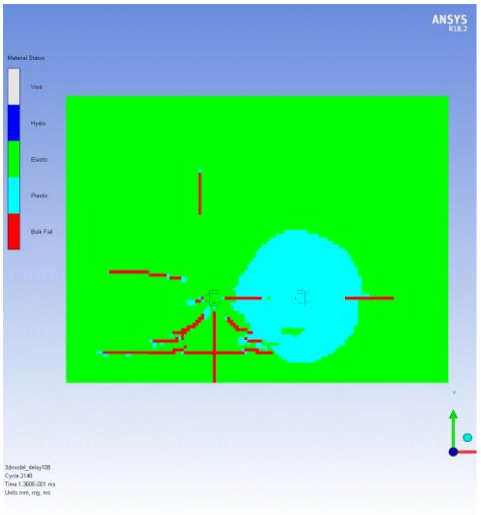
ANSYS

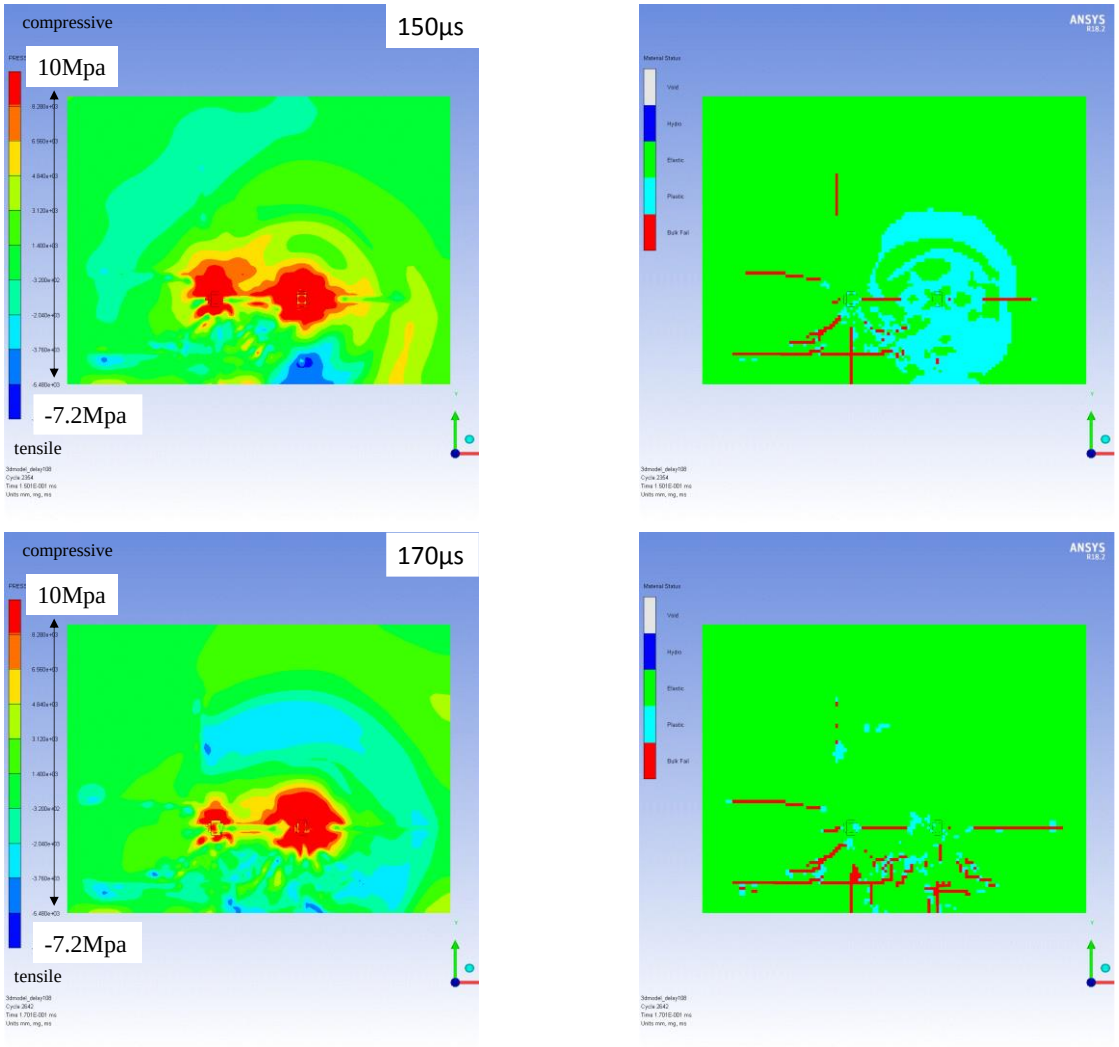

(a) (b)

Fig. 3.9 Stress wave and crack propagation behavior inside rock mass in the case of 108 μs of delay time (a) pressure contour and (b) crack conditions

3.5. Conclusions

In this chapter, numerical simulation model is built based on the result of small scale blasting experiment and the stress wave and failure propagation behavior inside rock mass were discussed. The main results are summarized as follows:

1. Numerical simulation model based on the result of small-scale blasting experiment successfully built by using AUTODYN software. Two dimentional strain information could obtain in Chapter 2, which result in more accurate verification of numerical simulation model.
2. It is numerically showed that cracks are generated at the first peak of strain rate evaluated by experiment in Chapter 2 even though it is difficult to see by visual

observation. In addition the crack is caused by tensile stress wave reflected at the free face.

3. Inside rock mass, high compressive pressure waves propagate in concentric circles after explosives are detonated and these compressive waves reflect at the free face and change into tensile stress wave. Then, the tensile failure is generated not immediately after stress waves reflect at the free face, but after reflected tensile stress waves from two blasting holes superpose and failure propagate with spreading tensile stress wave.
4. Even though the cracks on the surface of the block is fewer since superpose of the tensile waves occur not at the free face but at a little far from the free face, considering the failure conditions inside rock mass, the failure zone became larger under the smaller rock mass strength of normal mortar due to the decreasing the rock mass strength.
5. The position where tensile failure is superposed move to forward and crack occur earlier by reducing the length of burden. As the result, remarkable failure zone can be seen around the free face, which might result in reducing the size of blast-induced fragmented rock.
6. Cracks start to appear not around free face but in front of two blasting holes by increasing the hole spacing 1.5 times as large as burden. This is because the value of tensile stress wave reaches the criteria of tensile strength of this concrete before two tensile waves are superposed. On the other hand, the failure zone between two blasting hole is relatively small since the area superposed tensile stress waves which value is over the tensile criterion reduced, resulting in the decreasing the failure zone, especially the middle of blasting hole and free face.
7. By setting the delay time more than three times as long as arrival time of P-wave to neighboring blasthole, superposition of tensile stress wave is difficult occur and second blasthole was detonated after new free face was generated.

References

[1] AUTODYN Technical Manual
http://www.engineering-eye.com/AUTODYN/customer/download/index.html

[2] Bakuhatsu Genshouno Suutikaiseki Shuhou
http://www.engineering-eye.com/rpt/r094_jsdfe/pdf/20100903_2.pdf

[3] M. Beppu, K. Miwa, M. Itoh, M. Katayama and T. Ohno：A Numerical Study on Mechanism of the Local Damage of Concrete Plate Subjected to Impact by Rigid Projectile, JSCE J. Materials, Concrete Structures and Pavements. 63, 1, pp.178-191, 2007

[4] K. Fujikake, K. Uebayashi, T. Ono, A. Mizuno and A. Suzuki：Formation of Orthotropic Constitutive Model for Concrete Materials Under High Starain-Rate and Triaxial Stress State. J. of JSCE, 669, 50, pp.109-123, 2001. (in Japanese)

[5] C. A. Ross, P. Y. Thompson and J. W. Tedesco ： Split-hopkinson Pressure-Bar Tests on Concrete and Mortar in Tension and Compression, ACI Material J., 85, pp.475-481, 1989.

4. FLIGHT CHARACTERISTIC AND PREDICTION OF BLAST-INDUCED FRAGMENTED ROCKS IN BENC BLASTING

4.1. Introduction

In previous chapters, the fracture mechanism induced by blasting was discussed by a series of small-scale blasting experiment and numerical simulation. As a next step of this study, in this chapter, field scale experiment was performed in operating mine in order to understand flight characteristic of blast-induced fragmented rock as a real scale experiment. Flyrock is defined as the rock propelled beyond the blast area by the force of an explosion [(1)]. It is one of the serious problems induced by blasting in open-pit mining excavation. According to statistics, approximately 70 % of accidents caused by explosives is the flyrock disaster [(2)]. Compared with other blasting problems such as blast-induced blasting vibration or noise, it may directly damage surrounding structures or cause fatality in the worst case. In Japan, if flyrock accident happens repeatedly, in the worst case, the company must stop the mining operation. Thus, mining companies have to carefully control and prevent the occurrence of flyrock.

For this reason, a large number of researches on flyrock and its impacts on the surrounding environment have been conducted and several methods for prediction and prevention of the flyrock have proposed so far [(3-7)]. Since the rock mass conditions such as strength, crack or joint system generally influence on the occurrence of flyrock, the control and prediction method of flyrock considering the rock mass conditions have not been established yet. If the effect of rock mass conditions can be quantitatively evaluated, flyrock can be controlled effectively by altering blasting designs resulting in safe and efficient blasting operations.

Hence, in this chapter, a series of blasting tests under different rock mass conditions was conducted at metal mine in Japan in order to comprehend the flight behavior of fragmented rocks induced by blasting. At first, the relationship between initial velocity and blasting designs were discussed. As a next step, the effect of rock mass conditions on the initial velocity was evaluated and the prediction equation for the flyrock was finally established based on the experimental data. In other word, this chapter discussed the impacts of rock mass conditions such as uniaxial compressive strength (UCS), Rock Mass Rating (RMR), or crack density and blasting standards on initial velocity and flight direction of fragmented rocks.

4.2. Overview of Field Experiment

4.2.1. Outline of test field

A series of blasting experiments were conducted at Iwado mine. This mine is located in Makurazaki city in Kagoshima prefecture, Japan. This mine applies open-cut mining system and produces silicic acid ore contain gold. Table 4.1 shows the blasting standard in Iwado mine. In this study, the flight distance and direction of the fragmented rocks were measured, and then the effects of the blasting standard and the rock mass condition on the flying behavior of rock fragmentation were discussed. In order to measure the initial velocity of blast induced fragmented rocks, a high-speed camera was installed perpendicular to the face direction, and then the initial velocity and elevation angle of the fragmented rocks were measured. As for consideration of the flight direction, it focused on azimuth angles that was defined as the angle formed by the line connecting the furthest point of rock fragmentations and the center of the face and the face. In order to evaluate rock mass condition, a photo of the face was taken with a digital camera. Moreover, representative strikes of joints or rock mass were measured by using clinometer and crack density (explained in next section) of rock mass was evaluated from the photo image. Moreover, in each blasting test, the rock samples obtained in order to measure the mechanical properties. A series of the tests was summarized in Fig. 4.1.

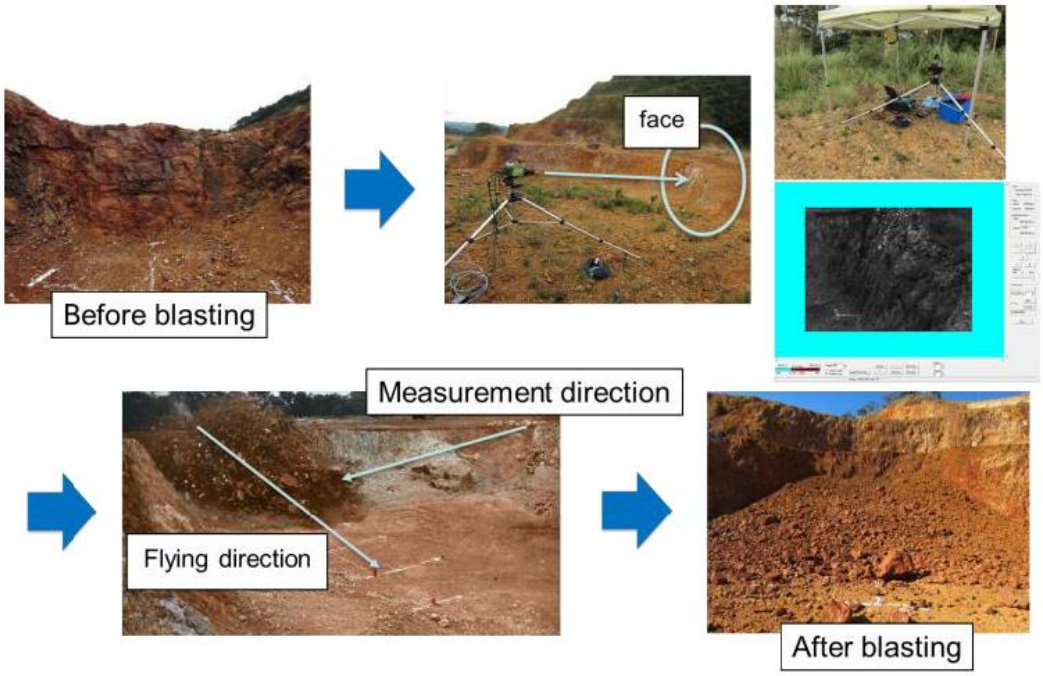

Fig. 4.1 Outline of field experiment

4.2.1.1 Crack density

Before the blasting test, the photograph of each face wall of blasting face was taken by digital camera and the crack condition of the rock mass was investigated based on it. As shown in Fig. 4.2, 10 courses of traverse were set at the face wall (every 2 m), and the number of cracks on the lines were counted. Based on the sum of the ten courses of the traverse and the number of the counted cracks, cracks per 1m length of the courses of traverse was calculated and the value is defined as “crack density” (cracks/m) in this study as a representative of crack condition of face of blasting tests [8].

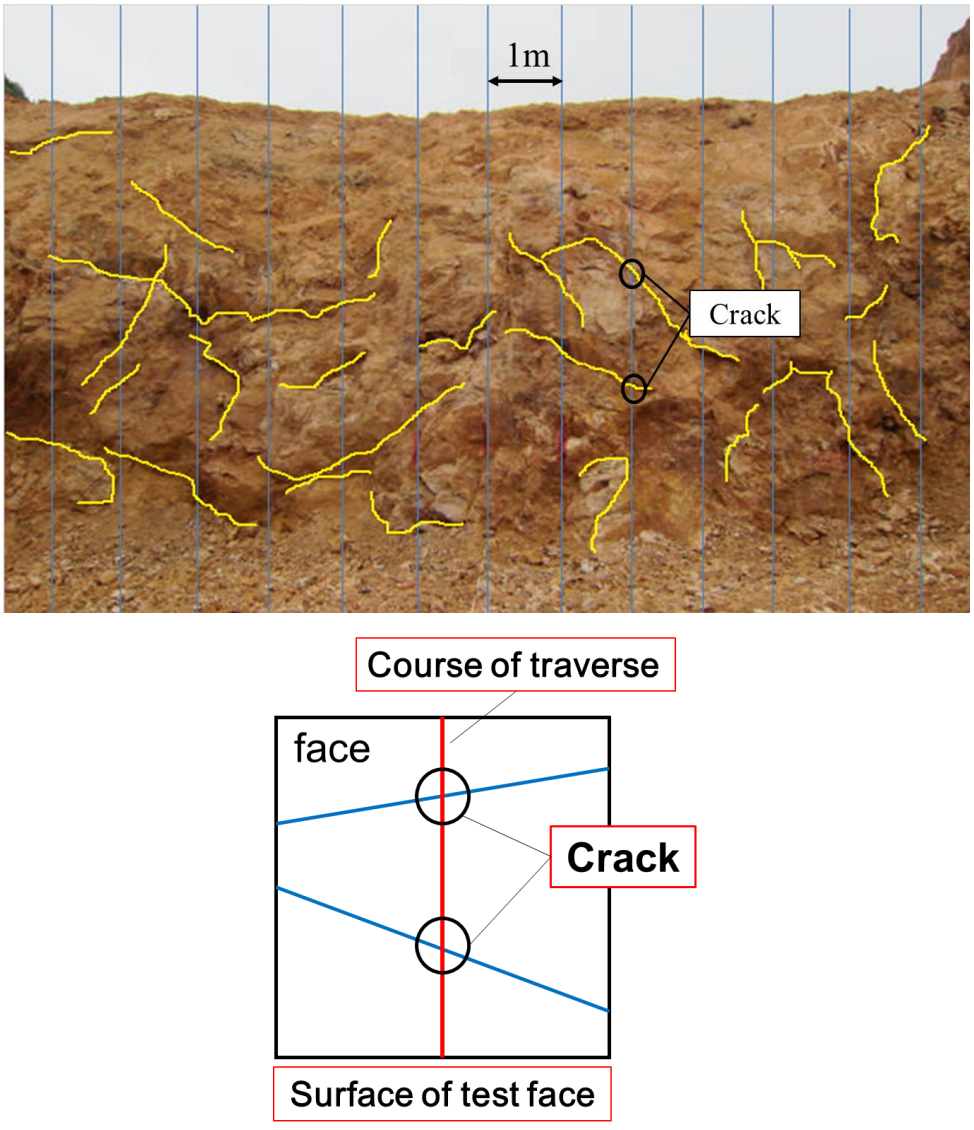

Fig. 4.2 Outline of evaluation method of crack condition of blast wall

4.2.2. Initial Velocity of Blast-Induced Fragmented Rock

According to the previous research works, an initial velocity of blast-induced fragmented rock is one of the important parameters to predict the flyrock accident. The

velocity would provide the flying distance; therefore, the risk of the accident can be assessed on a basis of the initial velocity. For this reason, the effect of rock mass conditions and burden, powder factor on the initial velocity of rock fragmentation were discussed in this study.

The initial velocity of rock fragmentation was calculated based on a series of digital image data observed by high-speed camera (Vision Research, Phantom Ver. 7.3). As the scale, a 2 m length of white line was drawn close and perpendicular to the bench face in this test (see Fig. 4.3). Compared to the traveled distance of fragmented rocks at every 1 ms (1,000 fps) and this scale, the initial velocity was estimated by image analysis. In this test, the traveled distance of 12 blast-induced fragmented rocks which can be distinguished in the image at every 50 ms was calculated from the time of initiation and when 400 ms had elapsed after ignition, and then the average velocity was calculated and determined as the initial velocity of blast-induced fragmented rock [9]. The one which has the largest initial velocity is defined as “maximum initial velocity” of blast-induced fragmented rock. In addition to the observation by high-speed camera, normal video camcorder was set perpendicular to the face of blasting test in order to understand the flight direction of blast-induced fragmented rock (see Fig. 4.4). On a basis of obtained fright direction, the initial velocity captured by high-speed camera was correlated.

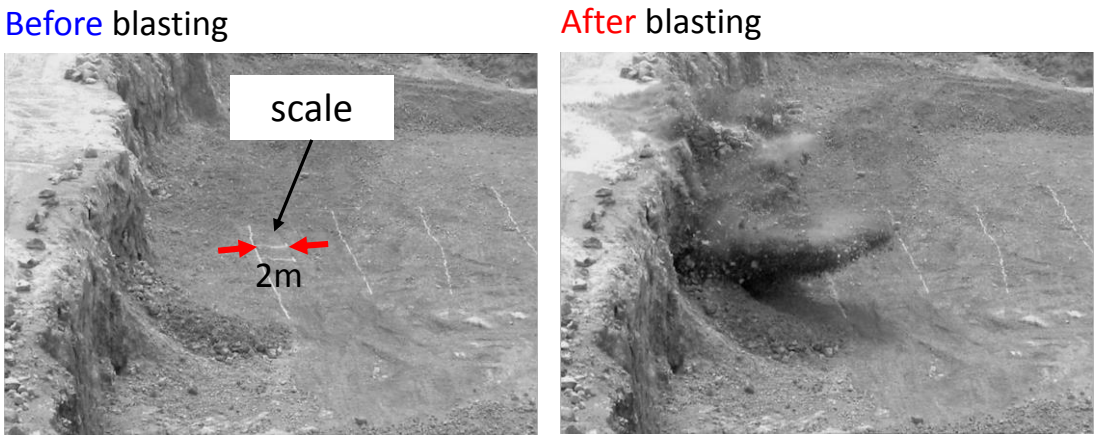

Fig. 4.3 The digital images of before and after blasting captured by high-speed camera and 2 m of scale for calculating initial velocity

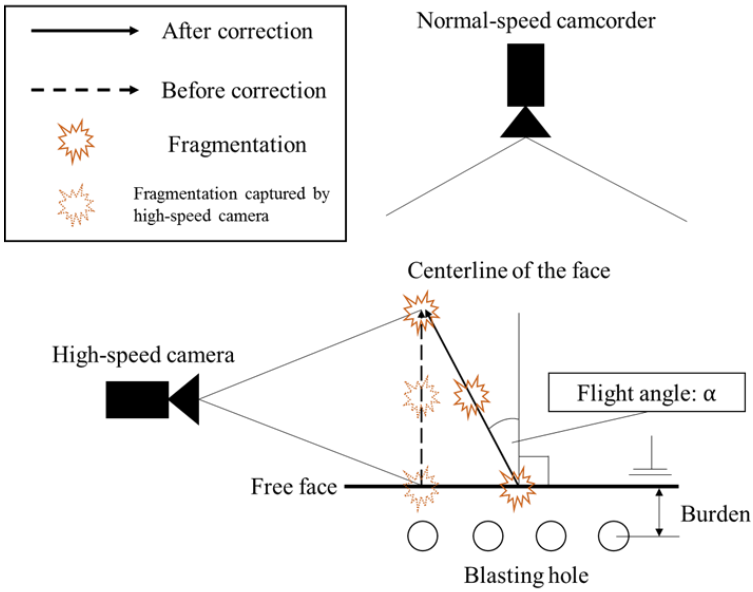

Fig. 4.4 Layout of high-speed camera and normal-speed camcorder and definition of flight angle

4.2.3. Flight Direction

When a flyrock problem is discussed, not only its distance, but also its direction is important factor in order to predict and prevent accidents. Hence, the effect of rock mass condition and blasting standard on flight direction of fragmented rocks was assessed as shown in Fig. 4.4. In this study, the angle α between face and the line connecting center of the face and fragmented rock which flew farthest was defined as "flight direction".

4.3. Flight Characteristic of Blast-Induced Fragmented Rock

4.3.1. Effects of blasting standards on the initial velocity

The effects of powder factor and burden on the initial velocity is discussed in this section. The relationship between powder factor and maximum initial velocity in each burden is shown in Fig. 4.5. As shown in this figure, although initial velocity of blast-induced fragmented rock increases with increasing powder factor because the energy of explosive increased and contribute to flying of rock fragmentation, there is a variation in measurement and it shows a weak association between powder factor and the initial velocity. On the other hand, the relationship between burden and the initial velocity is shown in Fig. 4.6. Moreover, the average maximum initial velocities in the case of 1.5 m, 2.0 m and 2.5 m of burden are 27.2 m/s, 24.2 m/s and 12.6 m/s, respectively. As suggested by these results, in the case burden is short, the initial velocity is more likely to be large since the explosion energy spend for movement of

rock increases with decreasing the distance between the free face and energy sources. These results suggested that blasting designs strongly influence on the flying distance of rock fragmentation.

However, even though the blasting designs were almost the same, there were huge gaps of initial velocity at several points. This result indicated that the initial velocity is depending upon not only blasting designs but also rock mass conditions; therefore, as a next section, the effects rock mass conditions: crack density and Brazilian Tensile Strength (BTS) are discussed.

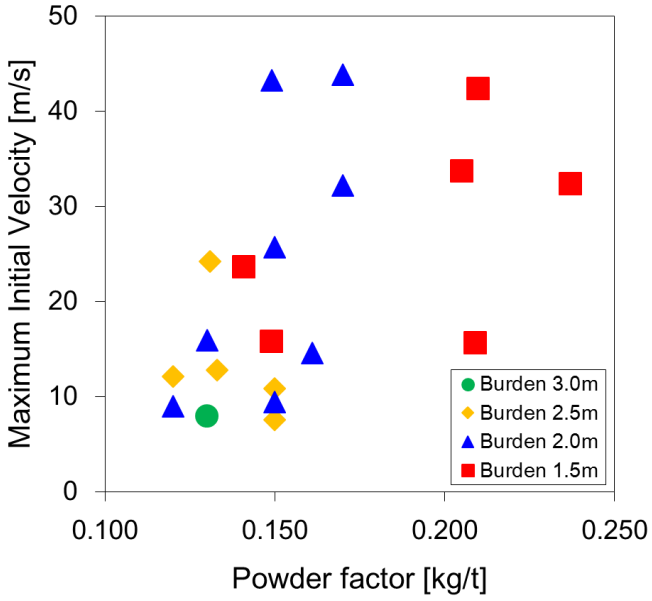

Fig. 4.5 The relationship between powder factor and maximum initial velocity of blast-induced fragmented rocks

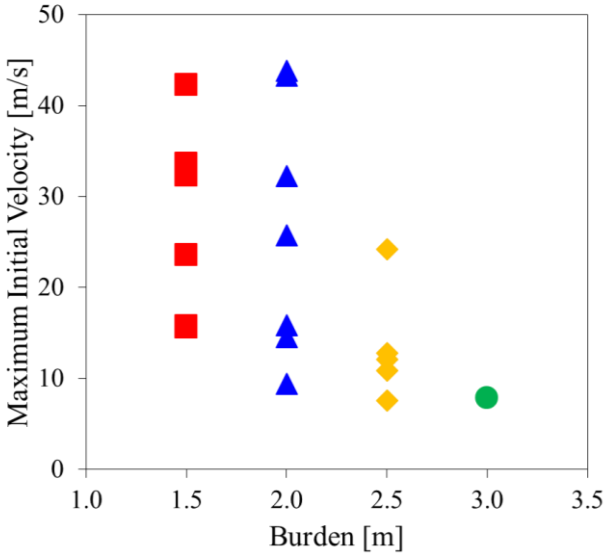

Fig. 4.6 The relationship between burden and maximum initial velocity of blast-induced fragmented rocks

4.3.2. Effects of crack conditions on the initial velocity

The effect of crack density is discussed at first as a rock mass conditions. Since the energy of explosive generally contribute to expansion or propagation of exiting cracks or pores and generation of new cracks, the energy which contributes rock fracture might decrease in the fractured rock mass [10], resulting in larger initial velocity of blast-induced fragmented rock. The relationship between crack density and the maximum initial velocity in each burden is listed in Fig. 4.7. As shown in this figure, the maximum initial velocity is likely large with increasing crack density, but it is difficult to say that there is clear association between crack density and maximum initial velocity.

As a next step, in order to eliminate the influence of blasting designs, Figs. 4.8 (a), (b) and (c) summarizes the relationship between crack density and maximum initial velocity under similar powder factor and burden conditions. In the case of 2.0 m and 1.5 m of burden, crack density is good accordance with maximum initial velocity. On the other hand, the clear association cannot be seen when burden is 2.5 m; therefore, larger burden can control the effect of crack on the surface of blasting wall. In other words, 2.5 m of burden is one of the indicator to reduce the influence of crack in this test site.

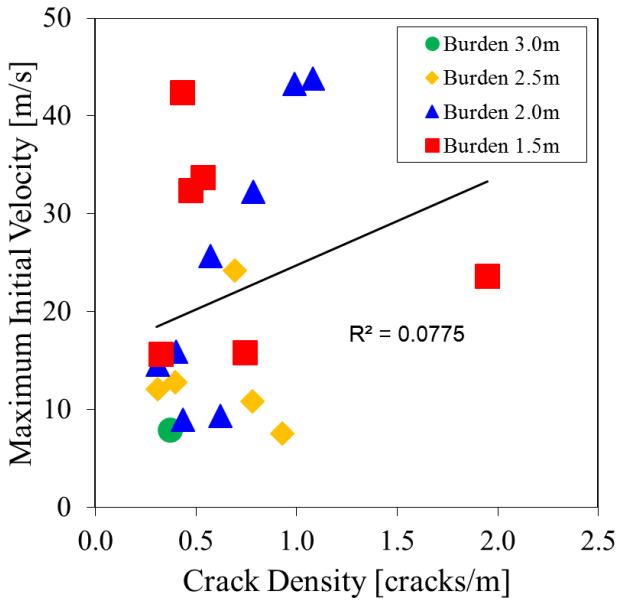

Fig. 4.7 The relationship between crack density and maximum initial velocity of blast-induced fragmented rocks

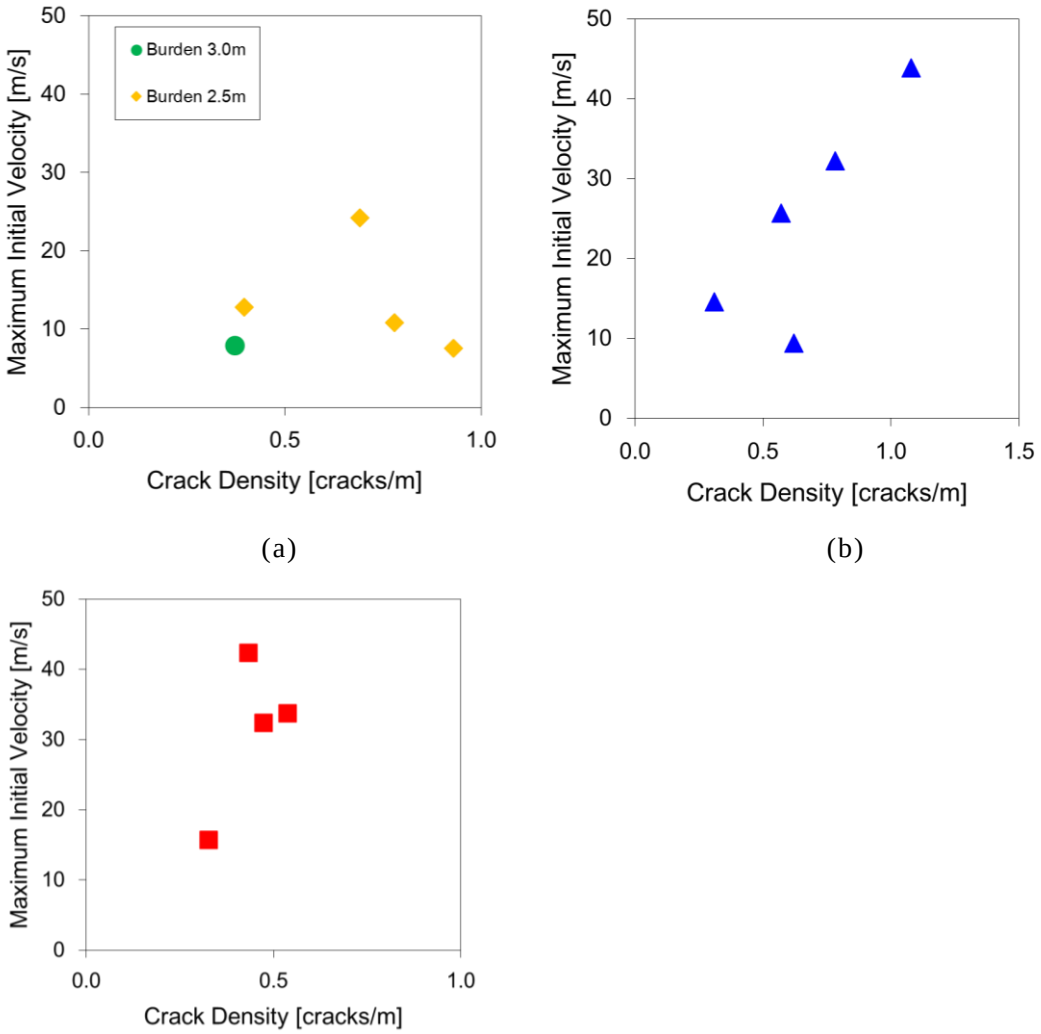

Fig. 4.8 The relationship between crack density and maximum initial velocity of blast-induced fragmented rocks in similar blasting designs; (a) Powder factor: 0.130-0.150 kg/t, Burden: 2.5-3.0 m, (b) Powder factor: 0.149-0.170 kg/t, Burden: 2.0 m, (c) Powder factor: 0.205-0.237 kg/t, Burden: 1.5 m

4.3.3. Effects of rock mass strength on the initial velocity

As a next step, the effect BTS on the initial velocity is discussed since rock is generally fractured by tensile strength. The relationship is not clear, but maximum initial velocity is likely to be large with decreasing the crack BTS (see Fig. 4.9). As well as the case of crack density, the influence of blasting designs is eliminated and the relationship between BTS and maximum initial velocity under similar powder factor and burden conditions are shown in Figs. 4.10 (a), (b) and (c). From these figures, though there is a weak associations, it can be see that BTS influence on the initial velocity on a basis of this experiment. This is because much more explosive energy

contributes to flight energy rather than rock fracture in small strength rock mass.

Based on above discussion, maximum initial velocity is depended upon burden and its value decreases with decreasing burden on average. On the other hand, there is a variation in initial velocity caused by rock mass conditions. In the rock mass conditions, crack condition and strength of rock mass have obvious impacts on the initial velocity and its influence could evaluated quantitatively. In other words, rock mass conditions should be investigated before blasting operation and burden length should be enlarged in the case of high crack density in order to control flyrock accidents. Moreover, in this test site, maximum initial velocity is less than 30 m/s when powder factor is less than 0.15 kg/t or the burden is more than 2.5 m and these value is one of the index to prevent flyrock accidents.

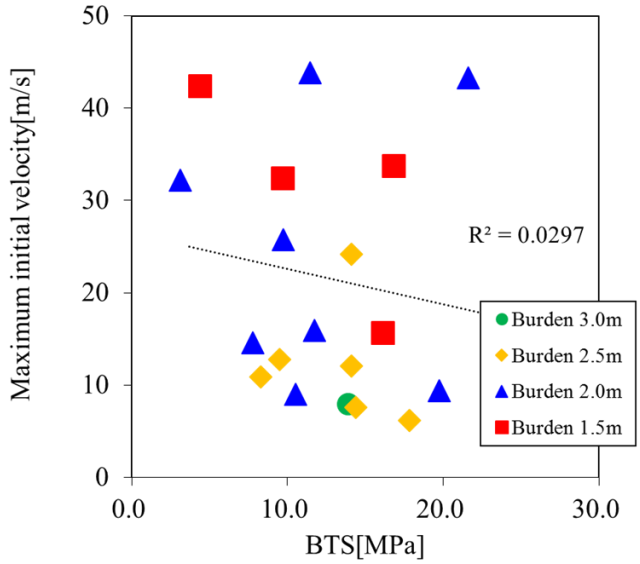

Fig. 4.9 The relationship between BTS and maximum initial velocity of blast-induced fragmented rocks

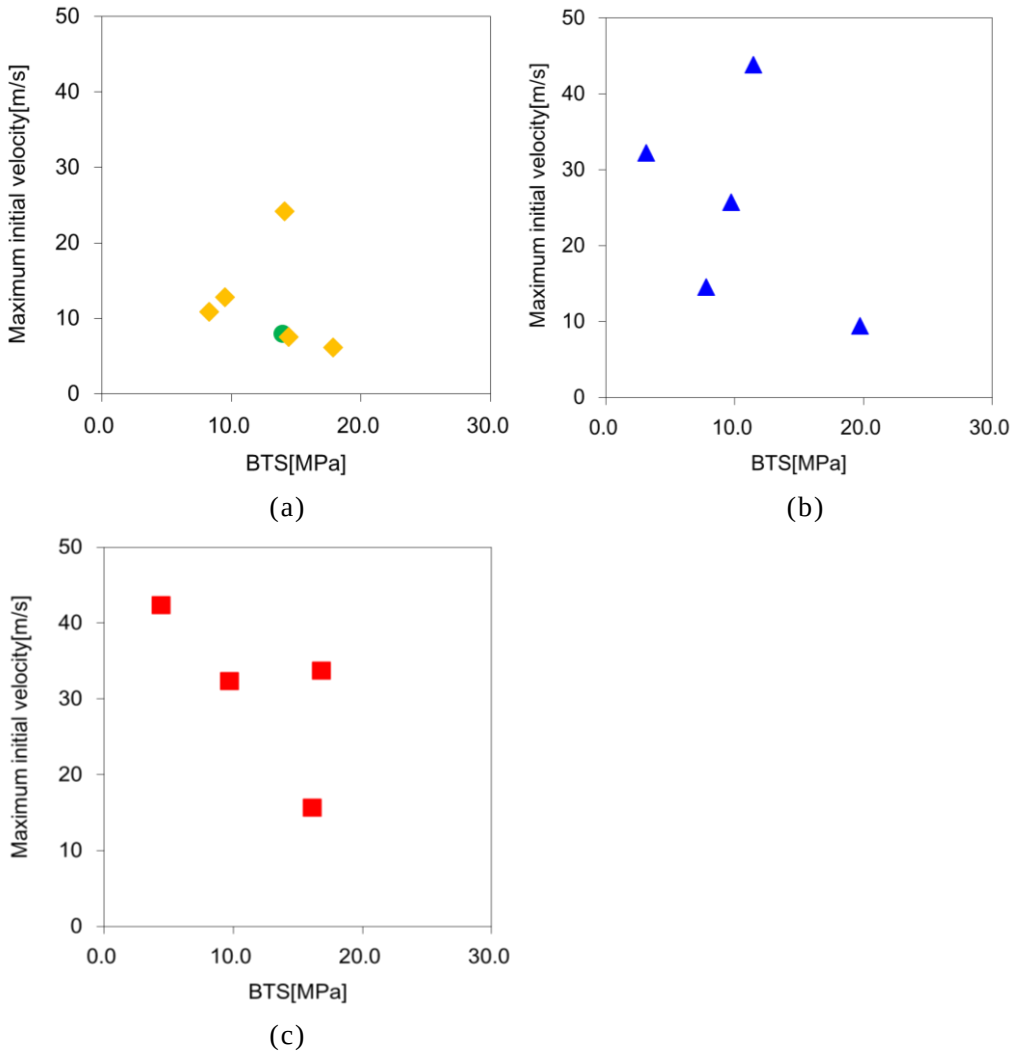

Fig. 4.10 The relationship between BTS and maximum initial velocity of blast-induced fragmented rocks in similar blasting designs; (a) Powder factor: 0.130-0.150 kg/t, Burden: 2.5-3.0 m, (b) Powder factor: 0.149-0.170 kg/t, Burden: 2.0 m, (c) Powder factor: 0.205-0.237 kg/t, Burden: 1.5 m

4.4. Prediction of Flight Distance of Blast-Induced Fragmented Rock

4.4.1. Introduction of RMR

The effect of blasting designs and rock mass conditions could be discussed quantitatively in previous section. Especially, as the rock mass conditions, several parameters, such as strength or crack density influence on the maximum initial velocity. However, there is weak association between maximum initial velocity and crack density or BTS. In addition, in order to evaluate rock mass conditions comprehensively, RMR is introduced as a representative value of rock mass conditions. This RMR was proposed by Bieniawski in 1976 and it is rock mass evaluating method which is rated in 100 point

scale by UCS, rock quality designation (RQD), spacing of discontinuities, groundwater conditions and orientation of discontinuities. The evaluate sheet of RMR is listed in Table 4.2 [11].

Fig. 4.11 shows the relationship between RMR and the initial velocity of fragmented rock under similar blasting designs. As shown in this figure, the maximum initial velocity has good accordance with the number of RMR and tends to be large at the test face which has large number of RMR since the energy of explosive is more likely to contribute to fracture of rock mass rather than flight under good rock mass conditions. From these results, in next chapter, the prediction equation of maximum initial velocity of blast-induced fragmented rock is discussed.

Table 4.2 Evaluation sheet of RMR [12]

A. CLASSIFICATION PARAMETERS AND THEIR RATINGS									
Parameter			Range of values						
1	Strength of intact rock material	Point-load strength index	> 10MPa	4-10MPa	2-4MPa	1-2MPa	For this low range-uniaxial compressive test is preferred		
		Uniaxial comp. strength	> 250MPa	100-250MPa	50-100MPa	25-50MPa	5-25Mpa	1-5MPa	< 1MPa
	Rating		15	12	7	4	2	1	0
2	Drill core Quality RQD		90%-100%	75%-90%	50%-75%	25%-50%	< 25%		
	Rating		20	17	13	8	3		
3	Spacing of		> 2m	0.6-2m	200-600mm	60-200mm	< 60mm		
	Rating		20	15	10	8	5		
4	Condition of discontinuces(See E)		Very rough surfaces	Slightly rough surfaces	Slightly rough surfaces	Sickensided surfaces	Soft gouge>5mm thick		
			Not continucs	Separation<1mm	Separation<1mm	or Gouge<5mm thick	or Separation>5mm Continuous		
			No separation	Sligthly weathered walls	Highly weathered walls	or Separation 1-5mm Continuous			
			Unweathered walls						
	Rating		30	25	20	10	0		
5	Groundwater	inlow per 10m tunnel length	None	< 10	10-25	25-125	> 125		
		(joint water press)	0	< 0.1	0.1-0.2	0.2-0.5	> 0.5		
		General conditions	Completed dry	Damp	Wet	Dripping	Flowing		
	Rating		15	10	7	4	0		
B. RATING ADJUSTMENT FOR DISCONTINUITY ORIENTATIONS(See F)									
Strike and dip orientations			Very favourable	Fovourable	Fare	Unfovourable	Unfovourable		
Ratings	Tunnels&mines		0	-2	-5	-10	-12		
	Foundations		0	-2	-7	-15	-25		
	Slopes		0	-2	-25	-50			
C. ROCK MASS CLASSES DETERMINED FROM TOTAL RATINGS									
Ratings			100-81	80-61	60-41	40-21	< 21		
Class number			Ⅰ	Ⅱ	Ⅲ	Ⅳ	Ⅴ		
Description			Very good rock	Good rock	Fair rock	Poor rock	Very poor rock		
D. MEANING OF ROCK CLASSES									
Class number			Ⅰ	Ⅱ	Ⅲ	Ⅳ	Ⅴ		
Average stand-up time			20 yrs for 15 m span	1 year for 10 m span	1 week for 5 m span	10 hrs for 2.5 m span	30 min for 1 m span		
Conhesion of rock mass			> 400	300-400	200-300	100-200	< 100		
Friction angle of rock mass			> 45	35-45	25-35	15-25	< 15		
E. GUIDELINES FOR CLASSFICATION OF DISCONINUITY conditions									
Discontinuity length(persistence) rating			< 1m 6	1-3m 4	3-10m 2	10-20m 1	> 20m 0		
Separation(apature) rating			None 6	<0.1m 5	0.1-1.0mm 4	1-5mm 1	> 5mm 0		
Roughness rating			Very rough 6	Rough 5	Slightly rough 3	Smooth 1	Slickensided 0		
Infilling(gouge) rating			None 6	Hard sling < 5mm 4	Hard sling > 5mm 2	Soft filling < 5mm 2	soft filling > 5mm 0		
Weatherig rating			Unweathered 6	Slightly weathered 5	Moderately weathered 1	Highly weathered 1	Decomposed 0		
F. EFFECT OF DISCONTINUITY STRIKE AND DIP ORIENTATION IN TUNNELLING									
Strike perpendicular to tunnel axis				Strike parallel to tunnel axis					
Drive with dip-Dip 45-90°	Drive with dip-Dip 20-45°			Dip 45-90°		Dip 20-45°			
Very favourable	Favourable			Very unfavorable		Fair			
Drive against dip-Dip 45-90°	Drive against dip-Dip 20-45°			Dip 0-20°-Irrespective of strike					
Fair	Unfovourable			Fair					

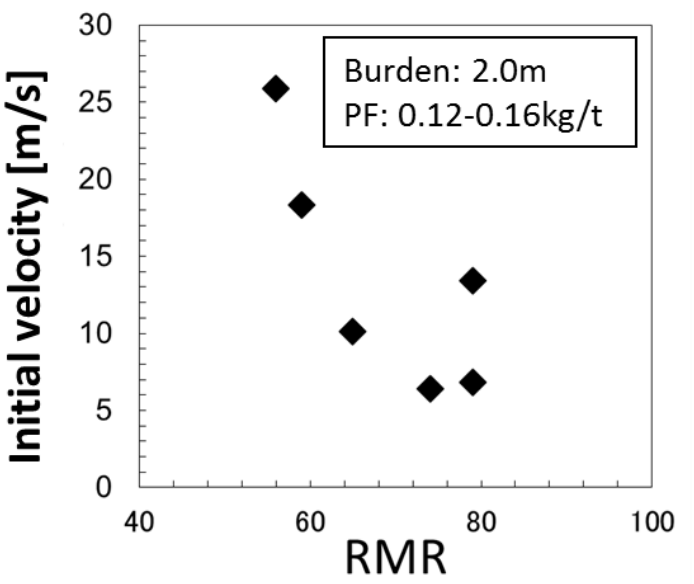

Fig. 4.6 The relationship between RMR and maximum initial velocity of blast-induced fragmented rocks under similar blasting designs

4.4.2. Prediction of Flight Distance of Blast-Induced Fragmented Rock

The prediction equation considering both blasting standard and rock mass conditions are discussed in this section. On a basis of above discussion, the RMR is used for prediction equation as representative value of rock mass conditions. In addition, the results of blasting is influenced by several factors therefore, the degree of each impact on the maximum initial velocity is quantitatively assessed by means of multiple regression analysis for establishing prediction equation of flight distance of fragmented rock. The result of the analysis is listed in Table 4.3. On a basis of this result, a linear regression equation of the maximum initial velocity can be obtained as follow:

$$V_0 = 75.5 \times W - 1.83 \times B - 0.01 \times T_D - 0.09 \times K_{RMR} + 11.2 \qquad (4.1)$$

where V_0 is initial velocity m/s, W is powder factor kg/t, T_D is delay time ms and K_{RMR} is the value of RMR.

Secondly, flight distance of blast-induced fragmented rock is estimated by using equation (1). Assuming that the measured maximum initial velocity is followed by normal distribution, potential maximum initial velocity, V_{max} is calculated by equation (2).

$$V_{max} = \frac{\mu+3\sigma}{\mu} V_0 \qquad (4.2)$$

Where, μ is average initial velocity and σ is its standard deviation. In this study typical hazard analysis is performed in order to evaluate the most dangerous conditions; therefore, 3σ is adopted to equation (2). Based on V_{max} calculated by equation (2), maximum flight distance of blast induced fragmented rock is calculated by equation (3).

$$D = V_{max} \times \cos\theta \times \left(\frac{V_{max}\sin\theta}{g} + \frac{\sqrt{V_{max}\sin\theta^2 + 2 \times H \times g}}{g}\right) \quad (4.3)$$

Where, D is potential maximum flight distance of blast-induced fragmented rock m, θ is flight elevation angle degree °, H is bench height (10 m), and g is acceleration of gravity (9.81 m/s^2) as depicted in Fig. 4.12. The potential maximum distance is calculated with equation (3) in the case of all blasting designs and RMR that is assumed and its results is listed in Table. 4.3. In this test site, 120 m is the limitation of the maximum flight distance, so the conditions over the distance are colored in the Table. The most novel point of this table is that acceptable conditions are different with different rock mass conditions (RMR) even though blasting designs are the same. Note that the limitation of flight distance can be changed by the operating situations. In addition, although 3σ is adopted to calculate the V_{max} assuming the most dangerous case, 2σ or σ can be used in terms of productivity. Based on the above discussion, it can be concluded that the flight distance can be predicted by assessing RMR and then controlled by setting/altering appropriate blasting standard(s) before blasting.

Table 4.3 The result of multiple regression analysis

Multiple correlation coefficient, R		0.47
Multiple determination, R^2		0.22
Standard error		5.74
Number of sample		38
Powder factor	coefficient	75.46
	P-value	0.17
Burden	coefficient	-1.83
	P-value	0.61
Delay time	coefficient	-0.01
	P-value	0.42
RMR	coefficient	-0.09
	P-value	0.38
Intercept	coefficient	11.23
	P-value	0.47

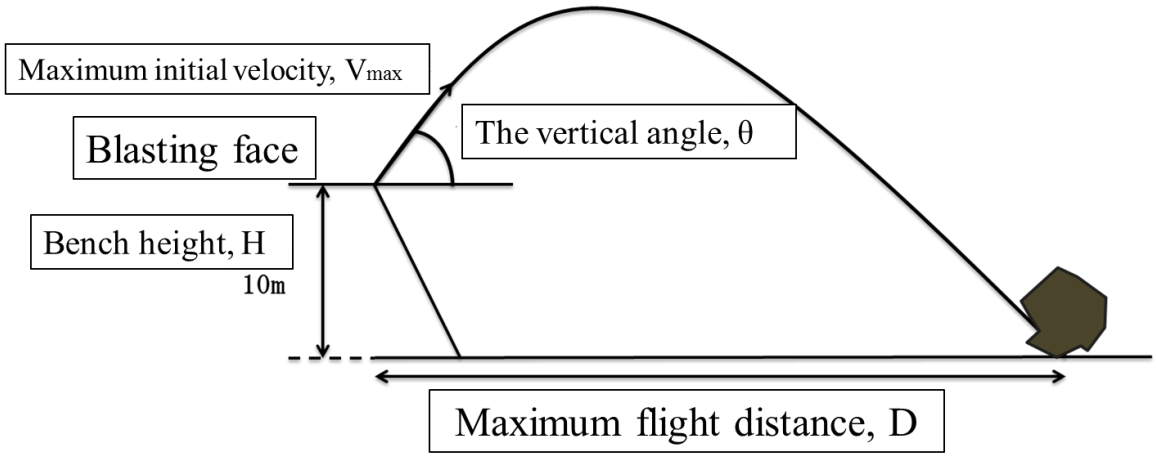

Fig. 4.12 The illustration of parameters for calculating the maximum flight distance

Table. 4.3 The possible maximum flight distance of blast-induced fragmented rocks according to blasting designs and rock mass conditions

Powder factor kg/t	Burden m	Delay time ms	RMR		
			60	70	80
0.12 or more and less than 0.13	1.5	0	143	126	109
		25	138	121	105
		50	133	116	101
		250	97	83	70
	2.0	0	125	109	94
		25	121	105	90
		50	116	100	86
		250	83	70	58
	2.5	0	55	51	48
		25	44	41	38
		50	35	33	30
		250	27	25	23
0.13 or more and less than 0.14	1.5	0	159	140	123
		25	154	135	118
		50	149	131	114
		250	110	95	81
	2.0	0	140	123	106
		25	135	118	102
		50	130	113	98
		250	95	80	68
	2.5	0	122	106	91
		25	118	102	87
		50	113	98	83
		250	80	67	56
0.14 or more and less than 0.15	1.5	0	176	156	138
		25	170	151	133
		50	165	146	128
		250	124	108	92
	2.0	0	156	137	120
		25	151	132	115
		50	145	127	111
		250	107	92	78

	2.5	0	137	120	104
		25	132	115	99
		50	127	111	95
		250	92	78	65
0.15 or more and less than 0.16	1.5	0	194	173	153
		25	188	167	148
		50	182	162	143
		250	139	121	105
	2.0	0	172	153	134
		25	167	147	129
		50	161	142	125
		250	121	105	90
	2.5	0	152	134	117
		25	147	129	112
		50	142	124	108
		250	104	90	76

4.5. Flight Direction of Flight Angle

When the flyrock issue is discussed, not only a flight distance but also a flight direction is an extremely important point of view. Blasting holes are generally arranged in parallel to the blast wall and blast-induced fragmented rocks might fly perpendicular to the bench face if simultaneous firing is performed. However, the result of flight direction is different in each bench face under the same blasting designs conditions as shown in Fig. 4.13. This difference might be considered due to joint system inside rock mass; therefore, the effect of strike of the joint measured by clinometer before the blasting tests on flight angle is discussed in this section.

The parameters for this discussion is depicted in Fig. 4.14. Where, α is gap angle between flight direction and perpendicular line to the bench face and β ($|\beta| < 90°$) is joint angle from the blast wall. The relationship between α and β is shown in Fig. 4.15. From this figure, although there is weak association between them, blast-induced fragmented rock is likely to fly perpendicular to the bench face when β is small. On the other hand, α is tend to be large when β is relatively large. Hence, the effect of joint system in the rock mass on the flight angle is discussed dividing into the case of small joint angle ($0° \leqq \beta \leqq 30°$, $60° < \beta \leqq 90°$) and large joint angle ($30° < \beta \leqq 60°$) assuming that the flight angle follow normal distribution.

Based on the average and standard deviation of flight angle, probability density is

calculated as shown in Fig. 4.16. From this figure, the probability that the rocks fly almost perpendicular to the bench face is approximately 86% in the case of small joint system. On the other hand, α is likely to be over 30° and its probability is approximately 47% in the case of large joint angle. In other words, blast-induced fragmented rocks fly perpendicular to the bench face when the angle of the joint system is approximately 0° or 90°, and flight angle tend to vary widely in the case of large angle of joint system. That is to say, blasting operation should be paid attention to when the angle of joint system inside rock mass, β is from 30° to 60°.

Fig. 4.13 The difference of flight distance of blast-induced fragmented rocks

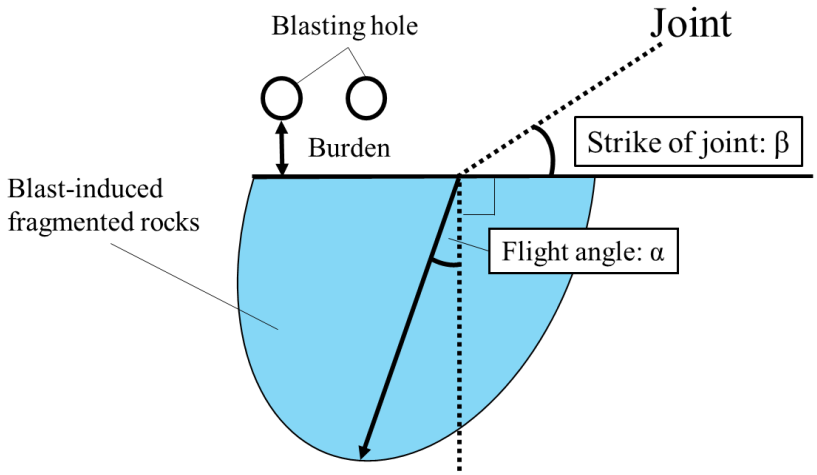

Fig. 4.14 The illustration of each parameter for discussion of flight angle of blast-induced fragmented rock

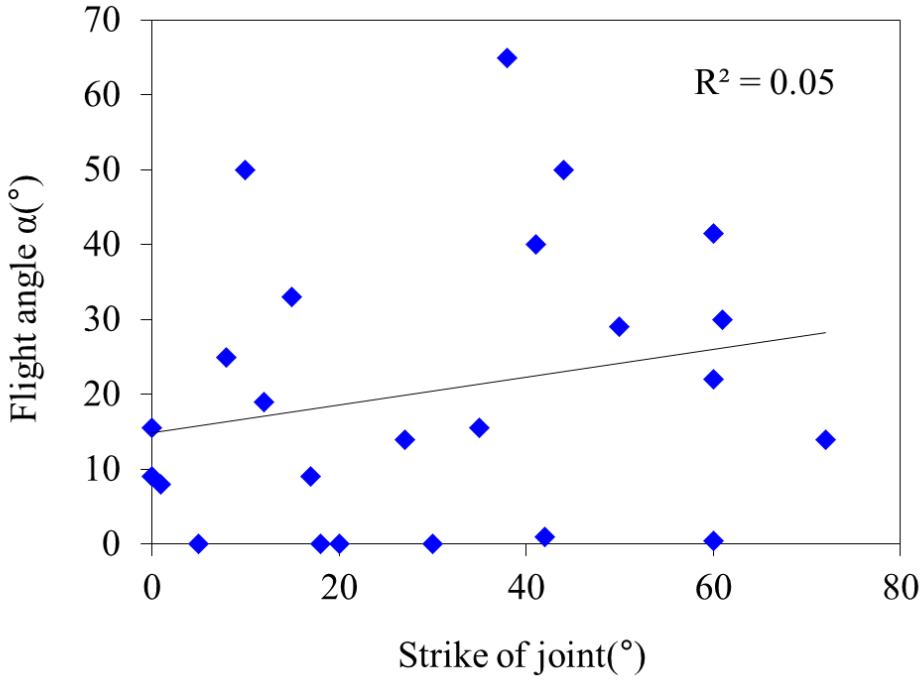

Fig. 4.15 The relationship between strike of joint and flight angle

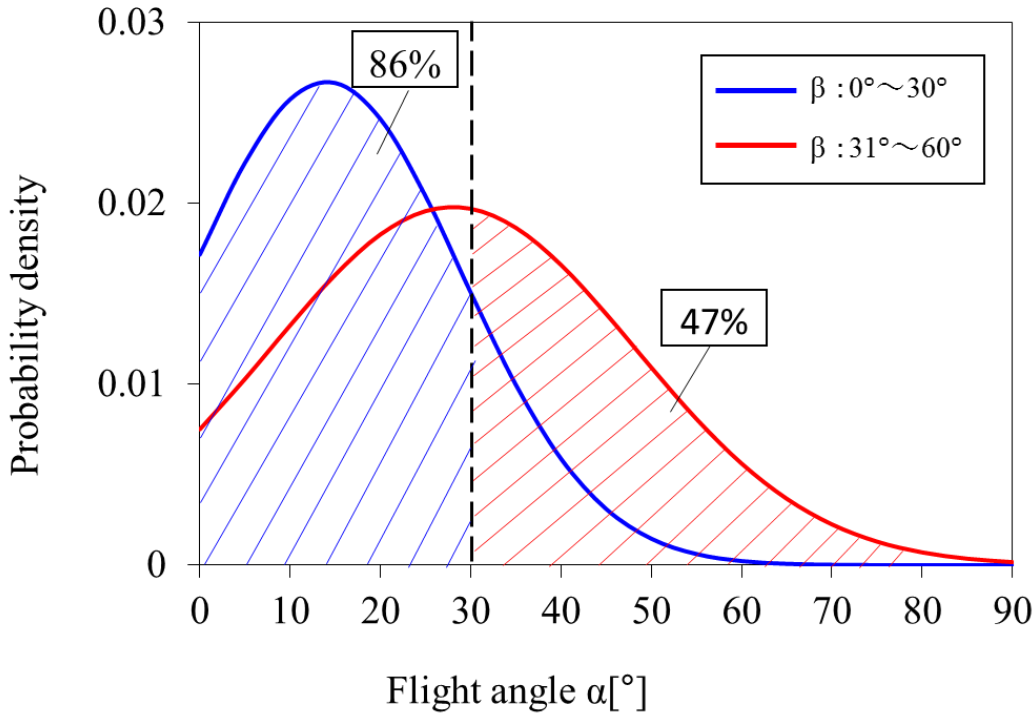

Fig. 4.16 The relationship between strike of joint and flight angle of blast-induced fragmented rock

4.6. Conclusions

In this chapter, a flight characteristic of blast-induced fragmented rock and effect of

rock mass conditions and blasting designs on it is quantitatively discussed by field experiments in operating mine site and the prediction method is established. The results of the discussion are summarized as follows:

1. Blasting designs influence on the maximum initial velocity of blast-induced fragmented rock. The velocity increased with increasing powder factor since the energy of explosive increase. In addition, the velocity is larger in the case of small burden since the distance between free face and blasting source was small and the energy of explosive was easy to contribute to that of flight. When powder factor is less than 0.15 kg/t or burden is more than 2.5 m, the maximum initial velocity is less than 30 m/s and this is one of the index to control the flyrock in this test site.
2. There was, however, weak association between blasting designs and the maximum initial velocity. This was caused by rock mass conditions, such as a strength or crack/discontinuities and especially crack density strongly influence on the maximum initial velocity.
3. As a representative value of rock mass condition, the RMR was applied and the prediction equation for maximum initial velocity based on both blasting designs and rock mass conditions could be successfully obtained by the multiple regression analysis. Moreover, the potential maximum flight distance of blast-induced fragmented rocks was successfully calculated from the equation and the conditions that flyrock is occurred in the test site could be revealed. In other words, the guideline to prevent flyrock accident was established in this study.
4. Flight direction of blast-induced fragmented rock was influenced by joint system inside of the rock mass. The rocks fly perpendicular to the bench face when the angle of the joint system is approximately 0° or 90°, and flight angle tend to vary widely in the case of large angle of joint system due to the influence of it.

References

[1] IME : Glossary of Commercial Explosives Industry Terms. 1st Edition, Institute of Makers of Explosives, 2007.

[2] Shadanhoujin Kayaku Gakkai Happa Senmon Bukai : Genbagijyutsusha no Tameno Happakougaku Handobukku. 1st Eddition, Kyouritsu Shuppan Kabushiki Gaisha, p.465, 2001.

[3] S. Stojadinovic R. Pantovic´ and M. Zikic.: Prediction of Flyrock Trajectories for Forensic Applications Using Ballistic Flight Equations. Int. J. Rock Mech. Rock Eng. 48, pp. 68-73, 2011.

[4] S. Stojadinović, N. Lilić, R. Pantović, M. Žikić, M. Denić, V. Čokorilo, I. Svrkota and D. Petrović : A New Model for Determining Flyrock Drag Coefficient. Int. J.

Rock Mech. Rock Eng. 62, pp. 5383-5396, 2013

[5] M. Monjezi, H. A. Khoshalan and A. Y. Varjani : Prediction of Flyrock and Backbreak in Open Pit Blasting Operation: A Neuro-Genetic Approach. Arab J. Geosci. 5, pp. 441-448, 2012

[6] D. J. Armaghani, M. Hajihassani, E. T. Mohamad, A. Marto, S. A. Noorani : Blasting-Induced Flyrock and Ground Vibration Prediction Through an Expert Artificial Neural Network Based on Particle Swarm Optimization. Arab J. Geosci. 7, pp. 5383–5396, 2014

[7] E. T. Mohamad, D. J. Armaghani, M. Hajihassani, K. Faizi and A. Marto : A Simulation Approach to Predict Blasting-Induced Flyrock and Size of Thrown Rocks. EJGE. 18, pp. 365‑374, 2013

[8] Y. Takahashi, K. Yamaguchi, T. Sasaoka, S. Wahydi and H. Shimada : Effects of Blasting Designs and Rock Mass Conditions on Rock Fragmentation Induced by Blasting in Open Pit Metal Mine. Proc. International Symposium on Earth Science and Technology 2016, 2016

[9] Y. Takahashi, T. Sasaoka, S. Wahydi, H. Shimada, K. Takeuchi and H. Tanaka : Fundamental Study on Behavior of Flyrock in Open-pit Metal Mine. Proc. International Symposium on Earth Science and Technology 2015, 2015.

[10] C. Feng and L. Ze-gong：Energy Distribution of Columnar Explosive Blasting in Rock. EJGE 19, pp.4221-27, 2014

[11] Z. T Bieniawski : Engineering Rock Mass Classifications : a Complete Manual for Engineers and Geologists in Mining, Civil, and Petroleum Engineering. Wiley-Interscience, pp. 40-47, 1989

[12] E. Hoek, P. K. Kaiser and W. F. Bawden : Support of Underground Excavations in Hard Rock.
https://web.mst.edu/~rogersda/umrcourses/ge341/Rock%20Mass%20Rating.pdf

5. CONTROL OF SIZE OF BLAS-INDUCED FRAGMENTED ROCKS IN BENCH BLASTING

5.1. Introduction

In this chapter, the control method of size of blast-induced fragmented rocks is discussed in terms of productivity. Stress wave and crack propagation behavior are described in Chapter 3. It was suggested that the size of blast-induced fragmented rocks could be controlled by altering burden, delay time or hole spacing even though homogeneous conditions. On the other hand, blasting designs in mines are still optimized over months or years by trial and error [(1)]. Hence, continuing from Chapter 4, this chapter described blasting tests with changing blasting pattern under various rock mass conditions to improve blasting effects and establish the guideline for efficient blasting operation in operating mine.

5.1.1. Analysis method of size distribution of blast-induced fragmented rock

Fragmentation assessment was performed by the image analysis on a basis of scaled photograph taken from the muck pile. Two balls with diameter of 24 cm were used as scale in the photograph. The balls were placed in the same vertical line down the fragmented rocks, preferably with one ball near the top of the fragmented rocks and the other near the bottom as shown in Fig. 5.1 [(2)]. The balls should not be placed randomly in the fragmented rocks nor in a horizontal line across them. The camera was held such that the long axis of the photograph is vertical. The photograph was then taken by the camera as perpendicular to the surface of fragmented rocks as possible.

The scaled fragmentation photographs were analyzed by the software known as Split-Desktop developed by Split Engineering as illustrated in Fig. 5.2. The outlines of visible rocks above a certain minimum resolution, 3 mm in diameter on the photograph, were traced by mouse. After the digital image was analyzed, the particle size distribution of fragmented rock was derived as shown in Fig. 5.3. The particle size at 50% of the gain size accumulation curve is defined as Xp50 as a representative value in this research.

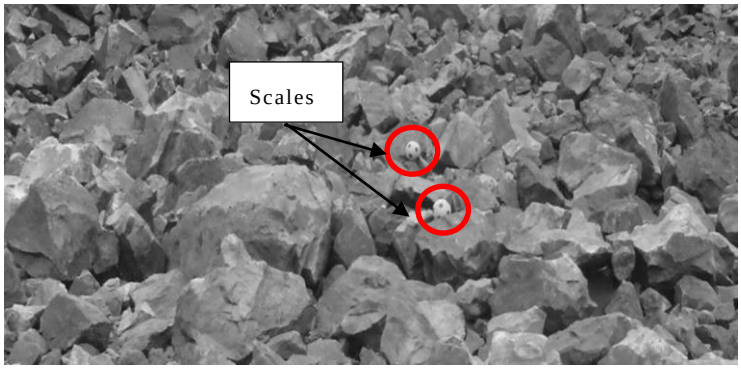

Fig. 5.1 The photograph for image analysis of size distribution of blast-induced fragmented rock

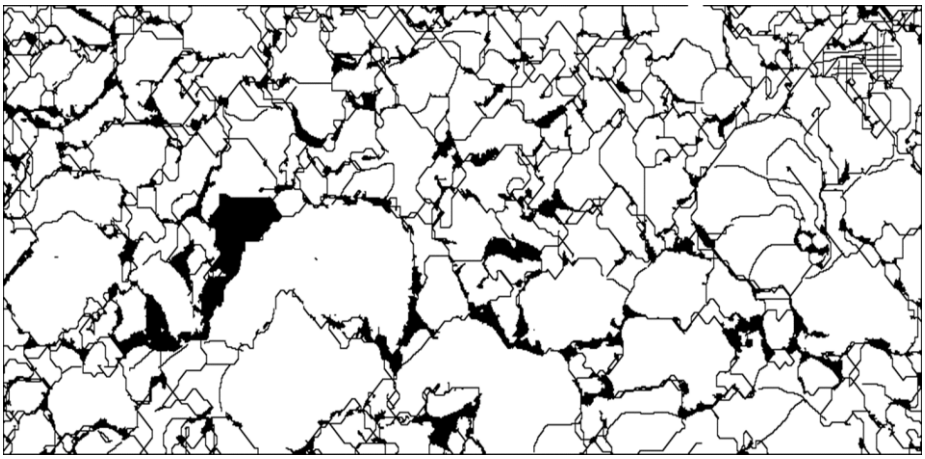

Fig. 5.2 The photograph after image analysis by Split-Desktop

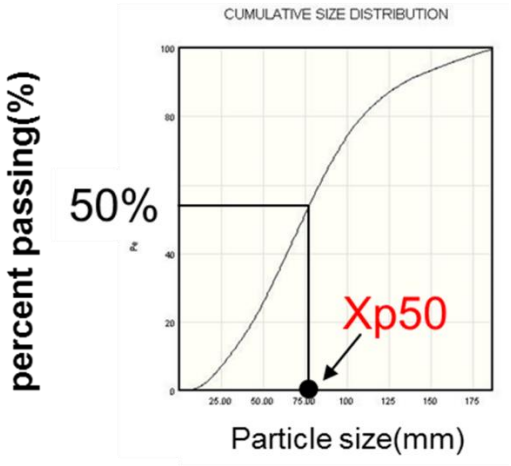

Fig. 5.3 Accumulation curve of blast-induced fragmented rock analyzed by Split-Desktop

5.1.2. Particle size distribution of rock mass before blasting

Same as like crack density introduced in Chapter 4, the face of wall before blasting was taken by digital camera to evaluate crack conditions of the rock mass, and exposed surface of discontinuity of the face of wall was extracted from the picture. Subsequently, as shown in the Fig. 5.4, 10 courses of traverse were set every 2 m at the face of bench face and the cracks crossed to the course of traverse were extracted [3]. The distance from the top of the face to the first crack is X_1, that from the first crack and second one is X_2, that from the $(n-1)^{th}$ and n^{th} ones is Xn [4]. Here, it is assumed that a rock mass is fragmented according to the existing cracks/fractures, the number of rock particles produced by blasting is n and the shape of them is circular. Besides, it is also assumed that the density of rock mass is constant. In this case, the percent passing is represented as $(Xn/L) \times 100$. Where, L is the length of blast hole. The particle size at 50% of the

gain size accumulation curve is defined as Xb50 to discuss the effect of crack conditions in rock mass on particle size of fragmentation. In addition, Xb50-Xp50; the difference of rock blocks before and after blasting was used as an indicator of effect of blasting.

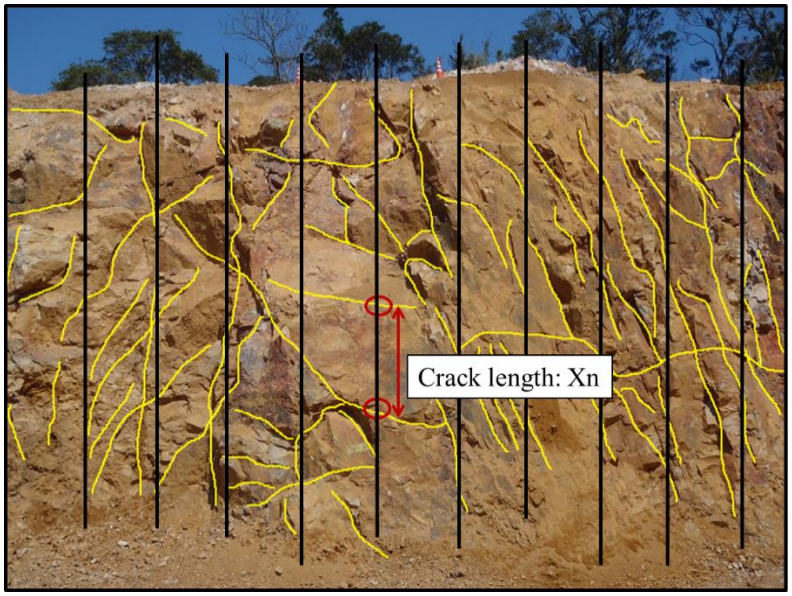

Fig. 5.4 Outline of evaluation method of crack condition of blast wall

5.2. The effect of rock strength and crack on the particle size distribution

Fig. 5.5 shows the relationship between uniaxial compressive strength (UCS) of rocks each face and Xp50. Note that the result of simultaneous blasting is discussed in this section. It is found particle size of fragmentation is large in the case of large strength of rock. It is because the larger strength of rocks, it is require the more large energy. On the other hand, because of huge difference has been demonstrated at Xp50 if the rocks have similar strength, it is clear that particle size of fragmented rock is depend upon not only strength of rock but also other factor(s) except for mechanical properties of rocks. Although Matsui et al. has already pointed out that the size of blast-induced fragmented rock depends upon the blasting designs and mechanical properties of rock [(5)], it can be seen from this figure that the data vary widely and obvious correlation cannot be found.

For this reason, the influence on crack conditions on size of fragmentation is discussed as a next. The relationship of Xb50 and Xp50 is illustrated in Fig. 5.6. As shown in this figure, Xp50 increases with increasing Xb50. In other words, this result suggests that the more number of cracks of rock exists, the smaller particle size of fragmented rock is. Therefore, it can be said that the size of fragmented rock depends upon conditions of cracks. Moreover, the relationship between UCS and the value of (Xb50-Xp50) is reviewed at Fig. 5.7. Here, Xb50 reflects the effect of existing

cracks/fractures on the fragmentation size. As it were, the value of (Xb50-Xp50) reflect the effect of mechanical properties of rock on fragmentation size. That is to say, it was recognized that the higher UCS is, the lower the effect of blasting is. According to the above results, if the effect of crack condition of rock mass on the size of fragmented rock is eliminated, it can be seen clearly that the mechanical properties of rock and blasting standard also affect the size of fragmented rock. Hence, a blast pattern should be altered according to the mechanical properties around bench face of faces in order to improve the effect of blasting at this mine.

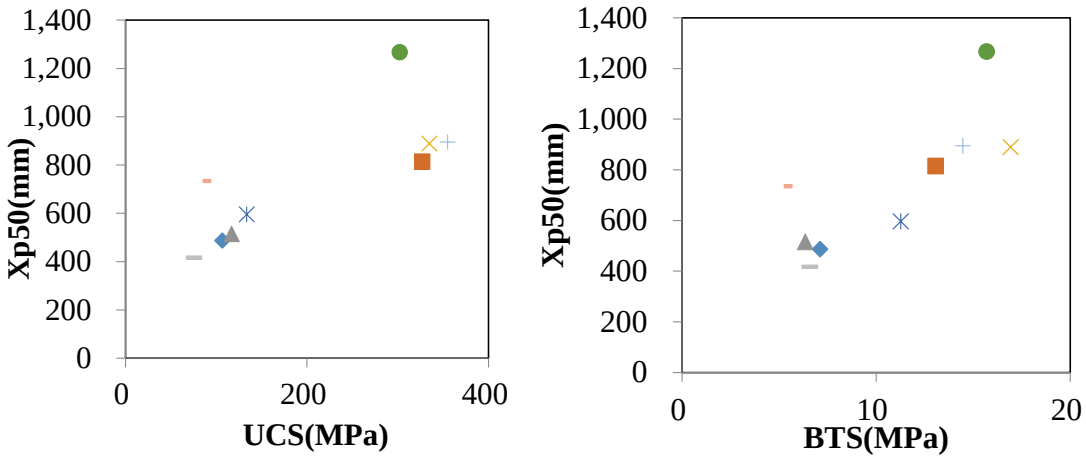

Fig. 5.5 Relationship between strength of rocks around bench faces and Xp50 (a) UCS (b) BTS

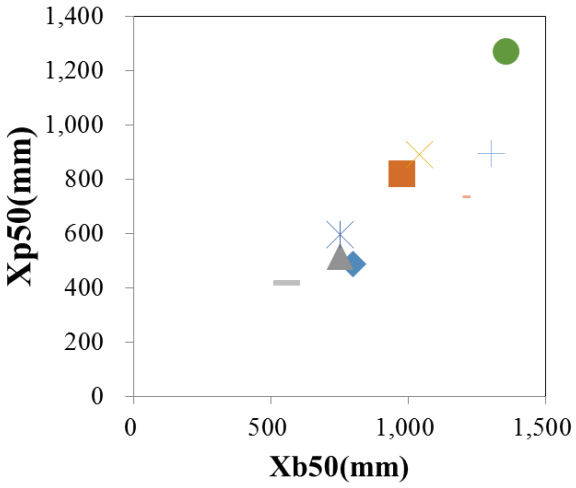

Fig. 5.6 Relationship between Xb50 and Xp50

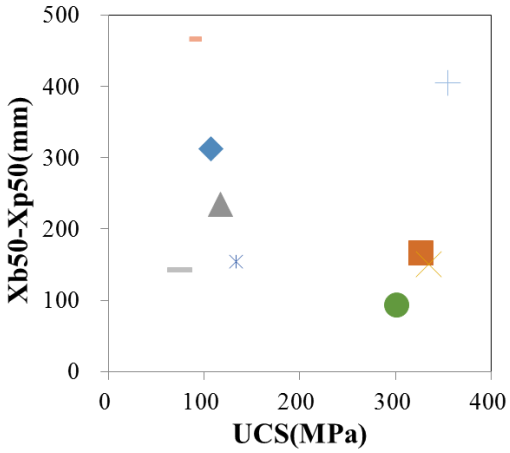

Fig. 5.7 Relationship between UCS and Xb50- Xp50

5.2.1 Improvements of effect of blasting according to change blast pattern

Based on the above results, in order to discuss the method to improve the size of fragmented rock, a blast pattern such as powder factor, burden and hole spacing is changed. The particle size distribution curves of fragmented rock before and after changing each blast pattern are illustrated for comparison of blasting effect. First of all, Fig. 5.8 depicts the particle size distribution curve of fragmented rock at burdens of 2.5 m and 2.0 m, respectively. As shown in these curves, it is clear that particle size of distribution at 2.5 m burden is smaller than that of 2.0 m of burden. This is because an explosive energy is more likely to contribute to the direction of free face by shorting burden. In addition, this result is good accordance with result of experimental and numerical study as described in Chapters 2 and 3.

Secondly, Fig. 5.9 shows the particle size distribution curves of fragmented rocks when a hole spacing is 2.0 m and 1.6 m. From this result, it cannot be recognized a clear difference of the effect of blasting. From the above, effective improvement of at particle size of fragmentation might be difficult by changing hole spacing.

In the third, the effect of a charge volume is discussed. As illustrated in Fig. 5.10, particle size is improved when charging volume is changed from 23.7 kg per blast hole to 26.8 kg per blast hole since the energy contributing the fracture of rock increase. However, it was recognized that the ratio of small particle size less than 250 mm is almost same. On the other hand, the ratio of large fragmented rock could be reduced by reducing burden and hole spacing at the same time. Therefore, it is required that a changing charging volume should be taken care over crushing in terms of loading and carrying in case of increasing charging.

Finally, Fig. 5.11 shows the particle size distribution curves of fragmented rock when burden is 2.5 m and hole spacing is 2.0 m, and the burden is 2.0 m and the hole spacing 1.5 m. In this case, the most major improvement of particle size of fragmented rock can be recognized. It can be because in addition to shorting distance from blast source to

free face, larger amount of explosive per unit volume is used compared with other pattern.

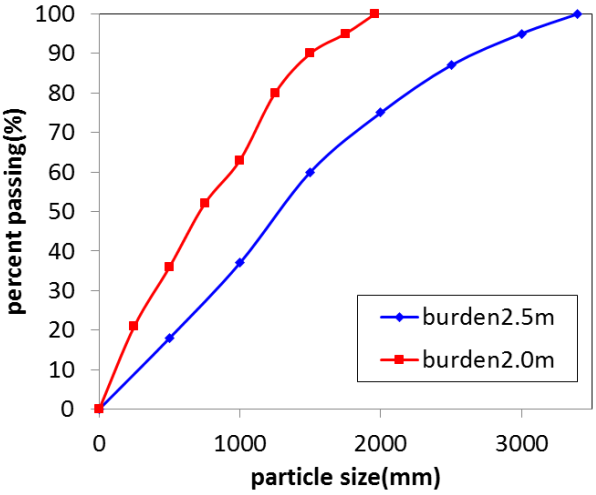

Fig. 5.8 Particle size distribution curve of fragmentation at burden of 2.5 m and 2.0 m

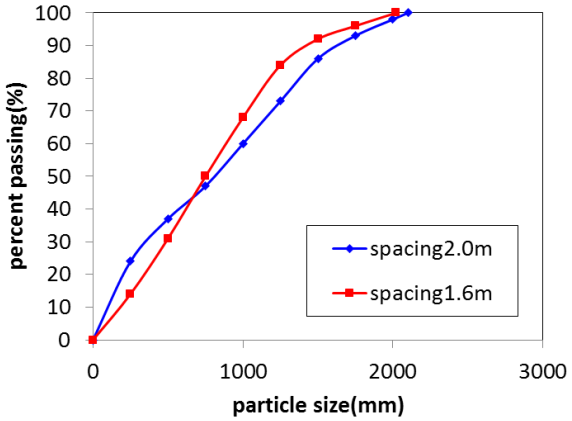

Fig. 5.9 Particle size distribution curves of fragmentation when hole spacing is 2.0 m and 1.6 m

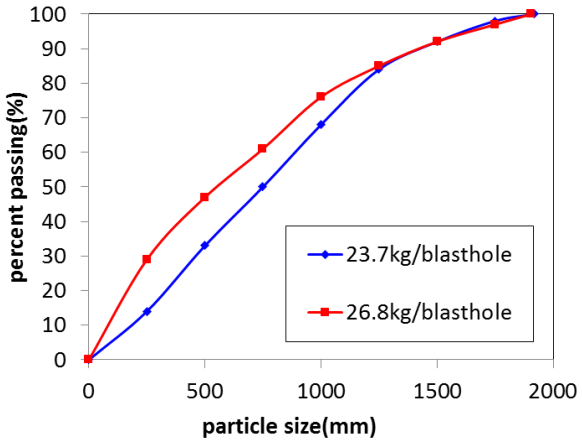

Fig. 5.10 Particle size distribution curves of fragmentation when hole spacing is 2.0 m and 1.6 m

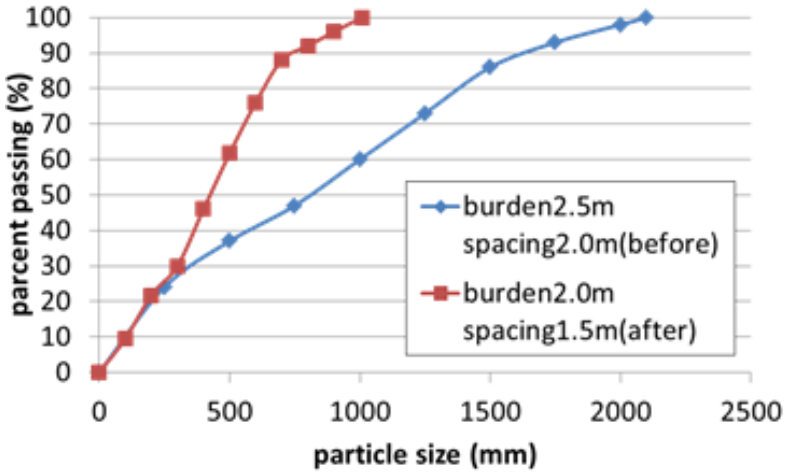

Fig. 5.11 Particle size distribution curves of fragmentation when hole spacing is 2.0 m and 1.6 m

5.2.2. Prediction of particle size of fragmentation

Fig. 5.12 shows that relationship between Xb50 and Xp50 in each blasting pattern described above. In addition, it is also shown the approximation straight line for each blasting pattern. It is found that Xp50 has good accordance with Xb50 and the particle size of fragmented rock is small at faces where blast designs are changed. Therefore, it is possible to predict particle size of fragmentation if crack density (Xb50) can be evaluated in present.

It is recognized that particle size of fragmentation became smaller than that of regular blasting pattern when changing burden and spacing. However, particle size is big and slope of approximation straight line is large compared to changing only burden. As a reason for this, faces of large UCS were roughly discussed changing burden and spacing. It is because if rocks have large UCS, mean particle size becomes large. On the other hand, although R-squared value is 0.68 and this value is relativity lower than other approximation straight line, it can be thought that careful measure is recognized valid for predicting particle size of distribution.

Moreover, it is made also clear that an obvious improvement of particle size could not be obtained compared to the regular blast pattern even though burden and spacing are changed where rock mass has large UCS and a number of cracks. This is because that blasting energy more likely to contribute to generating new cracks than developing present crack in the intact rock. That is to say, it is considered that an effective blasting can be conducted by applying regular blasting pattern at such faces in terms of total volume of crushing rock mass. Accordingly, it is may be presumed that blasting of only changing burden is effective where rock mass has relatively small UCS of rock mass. Moreover, changing both burden and hole spacing is effective way where the face has

large UCS and small number of crack, and regular blasting designs are valid at faces large UCS and growth crack.

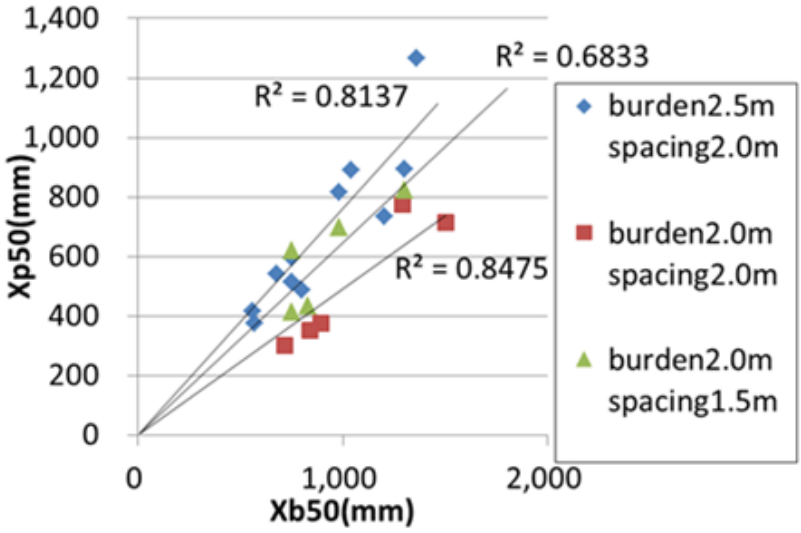

Fig. 5.12 The relationship between Xp50 and Xb50 each blast pattern

5.3 Effect of delay time on size of rock fragmentation

5.3.1 Effect of delay time on distribution of rock fragmentation

Delay blasting is generally conducted in order to control blast-induced ground vibration. In addition, it influence on the fragmented effect since creating new free face. On the other hand, considering the contribution rate of the initial velocity of flyrock shown in Chapter 4, delay time relatively has small impact on flyrock; therefore, the effect if delay time on the size of fragmentation is discussed in this section. Fig 5.13 illustrates the blasting pattern discussed in this section. By using MS electrical detonator, two types of delay time: 25 ms and 50 ms were set in the field experiment. In addition, firing direction was also discussed. One was firing from edge to edge of the blasting hole and the other one was firing from the center to the edges of the holes.

Example photographs of muck pile in each blasting pattern are shown in Fig. 5.14. As shown in these photographs, size distribution of rock fragmentation is different from each blasting pattern. In the case of blasting patterns (A) and (B) in Fig. 5.13, firing from edge to edge of the row, the size of rock fragmentation is obviously different depending bench face. In other words, the size tends to be big around the area of start of firing point and the one is likely to be small around the area of the end of firing point. On the other hand, in the case of blasting patterns (C) and (D) in Fig .5.12, firing from the center to the edges, overall of the size is tends to be homogeneous. Hence, as a next step, the photograph of the muck pile is divided in to 3 parts as shown in Fig. 5.15, the photographs are analyzed by Sprit-Desktop software again. The percent passing of the size of fragmentation of patterns (A) and (C) is shown in Figs 5.16 (a) and (b),

respectively. The results described above are successfully seen in these figures. In case of one direction firing pattern, the size tends to be big around the area of start of firing point since stress wave interference is hard to occur around the area and at the end of firing point, stress wave interference help to reduce the size of rock fragmentation. On the other hand, because stress wave interference equally occurred overall blasting area, resulting in homogenous size distribution.

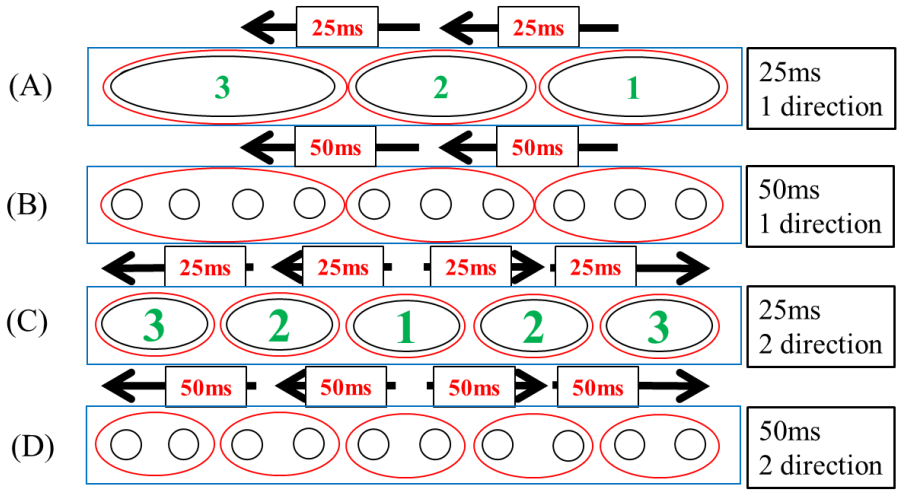

Fig. 5.13 The illustration of blasting pattern

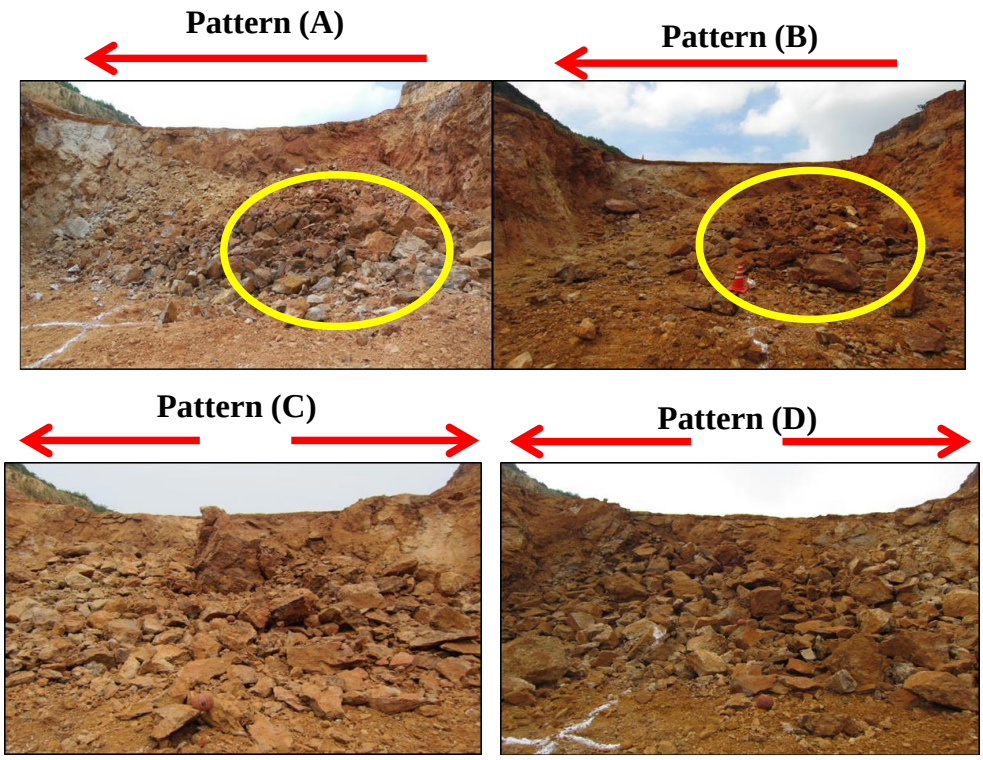

Fig. 5.14 The muck pile after blasting in each blasting pattern

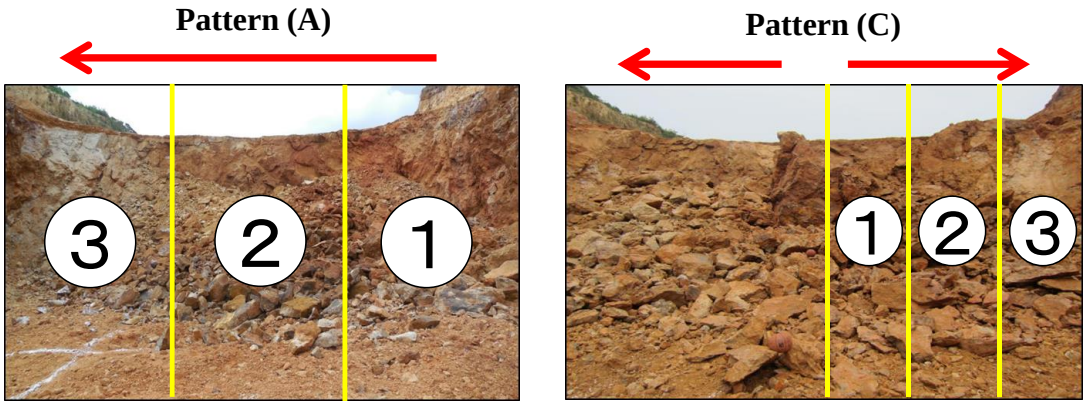

(a) (b)

Fig. 5.15 The divided photographs for discussing the effect of blasting pattern (a) dividing pattern for Pattern (A) and (B) and (b) dividing pattern for Pattern (C) and (D)

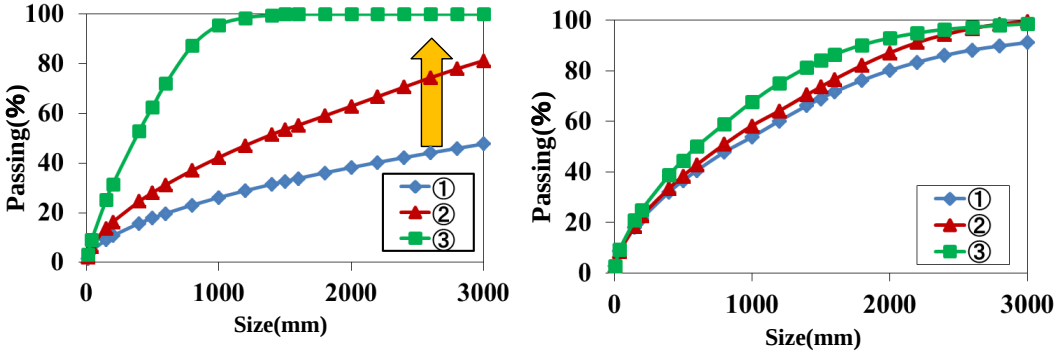

(a) (b)

Fig. 5.16 The accumulation curve obtained from divided photograph (a)the result of Pattern (A) and (b) the result of Pattern (C)

5.3.2 Prediction of the distribution and the size of fragmentation in delay blasting

Based on the discussion described above, the prediction of fragmentation size in delay blasting is established in this section. In order to access the distribution, the homogeneity of the distribution have to be quantitatively evaluated. Therefore, the uniformity coefficient is defined on a basis of uniformity coefficient which is generally used to classify the soil [6] as follow;

$$n = \frac{X_{p60}}{X_{p10}} \tag{5.1}$$

Where, n is uniformity coefficient, Xp60 and Xp10 are the particle size at 60% and 10% of the gain size accumulation curve, respectively. In the field of soil classification, the

range of the size distribution classified as wide when n≧10. On the other hand, the soil is judged as uniform when n is less than 10. Representative distributions and their uniformity coefficient are shown in Figs 5. 17 (a) to (c). By visual observation, the distributions are divided into three rank in this study. The divided rank is listed in Table 5.1. In addition, the result of uniformity coefficient in each firing pattern is shown in Fig. 5.18. Moreover, the averages of uniform coefficient of pattern A, B, C and D are 27.7, 15.1, 5.65 and 7.98. Based on the results, it can be said two directions of firing pattern can make the distribution more uniform. This might because the formation of stress wave interference and free face occur symmetrically in the case of two directions of firing pattern. On the other hand, the behavior of superposition of stress waves is different depending upon the place in the case of one direction of firing pattern, which result in un-uniform size distribution.

Furthermore, the effect of delay time and firing pattern is discussed. The relationship between firing pattern and Xp50 is illustrate in Fig. 5. 19. As can be seen in this figure, Xp50 in the case of 50 ms looks like small. Hence, the average of Xp50 of each firing pattern is calculate. The average Xp50 of pattern A, B, C and D are 961.3 mm, 742.1 mm, 537.6 mm and 500.7 mm. This result suggested that the size of fragmented rock can be reduced by applying 50 ms of delay time in this mine. There might be certain delay time which can be reduce the size of fragmented rock. On the contrary, the average Xp50 of one direction (A and B) and two directions (C and D) of firing pattern are 851.2 mm and 528.3 mm, respectively. Moreover, the average Xp50 of 25 ms (A and C) and 50 ms (B and D) of delay time are 707.0 mm and 661.7 mm, respectively. It can be that although delay time influence on the mean size of fragmented rock, the influence of firing direction is larger than that of delay time. Two direction of delay time has good advantage of both distribution and mean size of fragmented rock. Although the required size is depending upon the operation, two directions of firing pattern is better to apply basically in terms of uniformity and delay time should selected depending upon the operation in order to control the size of fragmented rock.

(a)

(b)

(c)

Fig. 5.17 The representative distribution of fragmented rock in uniformity coefficient (a) 2.1 (b) 15.1 (c) 20.3

Table. 5.1 The rank of distribution in each uniformity coefficient

Rank	Uniformity coefficient
good	0～10
normal	10～20
bad	20～

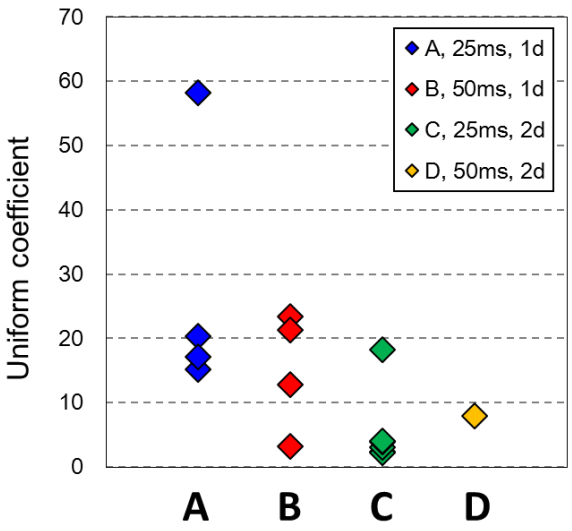

Fig. 5.18 Uniformity coefficient in each firing pattern

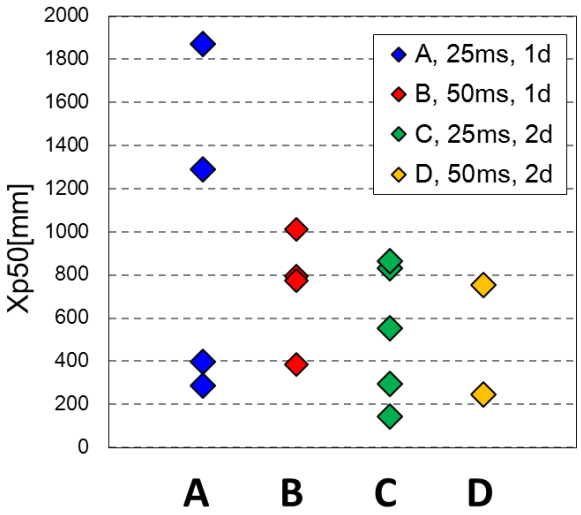

Fig. 5.19 The relationship between firing pattern and Xp50

5.4. Conclusions

In this chapter, control and prediction method of blast-induced fragmented rock considering rock mass conditions were discussed. The results are summarized as follows:

1. Not only blasting designs, but also rock mass conditions strongly influence on the size of blast-induced fragmented rocks. Especially, crack conditions has obvious impact on the size, and the by eliminating the effect of crack condition of rock mass, it can be clearly seen that the mechanical properties of rock and blasting standard affect the size of fragmented rock.
2. As described in Chapter 3, by reducing the burden, the size of blast-induced fragmented rocks can be reduced. In addition, increasing the charge volume has an influence to improve the size of blast-induced fragmented rocks On the other hand, changing the hole spacing does not have an obvious impact on the size of blast-induced fragmented rocks. Moreover, it is also made clear that by considering the crack conditions of blast face, the size of blast-induced fragmented rocks can be estimated be based on the blasting designs.
3. Delay time has an obvious impact on the size and distribution of blast-induced fragmented rocks. Firing direction strongly influence on both the distribution and size of blast-induced fragmented rocks. Homogeneous size of blast-induced fragmented rocks can be obtained by conducting two directions firing pattern and one direction firing pattern make the size distribution heterogeneous. On the other hand, delay time influence on the size of fragmented rocks, but the influence of the firing direction on the size is larger than that of delay time.

References

[1] H. Shimada, K. Matsui, M. Ichinose, T. Sasaoka, S. Kubota : Study on Effect of Blast Vibration on Size of Fragmentation at Limestone Quarry. J. the Mining and Materials Processing Institute of Japan, 122, pp.11-19, 2006 (In Japanese).

[2] Sprit Engineering LLC : Manual of Split-Desktop Software, 2003 http://www.spliteng.com/download/2102/

[3] Y. Takahashi, K. Yamaguchi, T. Sasaoka, S. Wahydi and H. Shimada : Effects of Blasting Designs and Rock Mass Conditions on Rock Fragmentation Induced by Blasting in Open Pit Metal Mine. Proc. International Symposium on Earth Science and Technology 2016, 2016.

[4] T. Sasaoka, Y. Takahashi, W. Sugeng, A. Hamanaka, H. Shimada, K. Matsui1, S. Kubota : Effects of Rock Mass Conditions and Blasting Standard on Fragmentation Size at Limestone Quarries : Open J. of Geology, 5, pp.331-339, 2015.

[5] K. Matsui and H. Shimada : Evaluation of Rock Mass Condition and Effect of Fracture of Rock Mass on Blasting Effect. Sekkaiseki, 330, pp.57-61, 2004 (In Japanese).

[6] Shadanhoujin Jiban Kougakkai : Doshitu Shiken Kihon to Tebiki. 2nd Eddition, Maruzen Shuppan Kabushikigaisha, pp35-36, 2010.

6. CONCLUSIONS

Flyrock is a serious problem induced by blasting in open-pit mine in Japan. Although many counter measures or prediction equations of it has been proposed, the effect of rock mass conditions has not been considered enough. Additionally, not only safe aspect but also productivity have to be considered carefully at the same time for continuous mining operation, which complicate the blasting operation as indicated in Chapter 1. Therefore, in order to establish the guideline for safe and efficient blasting designs, small-scale blasting experiment, numerical simulation and field experiment was carried out in this study.

In Chapter 2, as a first step, fracture mechanism induced by blasting was discusses by conducting small-scale blasting experiment. For the quantitative discussion of crack occurrence or its propagation behavior, the new evaluation method of the two dimensional dynamic strain of brittle material was developed by means of digital image correlation (DIC). By applying the developed measurement system to the experiment, the strain behavior where crack occurred and propagated could be visualized and evaluated quantitatively which have been difficult to measure by conventional method. The results showed that failure could be recognized where strain rate was over a certain value. In this experiment, crack occurred and propagated to the points where strain rate was over 100 1/s. Furthermore, the effect of rock mass strength and blasting designs were also discussed. In regard to the rock mass strength, two types of rock strength were prepared and tested. Strain rate of higher strength material when cracks were generated was larger than that of smaller one. In addition, the number of cracks was larger in the case of large rock mass strength than that of small one even though the charge explosive was same. Besides, by reducing the burden 15%, the criteria value of strain rate increased 25% and the number of cracks increase since the energy of explosive is more likely to contribute to the fracture of rock mass by reducing the distance from the blast source to free face. This result suggested that size of fragmented rock can reduce by decreasing the burden. On the other hand, there were not huge difference of the number of cracks and the criterion value of strain rate when hole spacing enlarging 1.5 times, which indicated the size of fragmented rock increase by increasing hole spacing. Based on the result, it can be said, strain rate is one of the important parameter to evaluate the crack occurrence and propagation behavior and the rock mass condition or blasting designs are strongly influence on strain rate.

In chapter 3, stress wave and crack propagation behavior inside rock mass after detonation were elucidated by means of three dimensional finite element method impact analysis software, AUTDYN-3D. The input parameters were correlated based on the strain-rate obtained in small-scale blasting experiment in chapter 2. The results showed

high compressive pressure waves propagate in concentric circles, reflected at the free face and change into tensile stress waves. Due to the tensile stress waves, tensile failure was generated not immediately after stress waves reflected at the free face, but after reflected tensile stress waves from two blasting holes superposed. The failure zone propagated with spreading the superposed tensile stress waves. Moreover, the position of tensile stress wave superposed moved to near free face by reducing burden length, leading to remarkable failure zone around the free face. This result suggested that the size of fragmented rock can be small to reduce the burden. On the other hand, it was difficult to occur the superposition of tensile stress wave because of enlargement of hole spacing, leading to decreasing of failure zone. Delay time also influenced on the failure generation mechanism inside rock mass due to the change of stress wave propagation behavior. When setting the delay time, the position of superposition of tensile stress wave were changed. Hence the position of failure zone can be controlled by changing delay time. This result suggested that flight direction of blast-induced fragmented rock can be controlled by setting delay time. Besides, in terms of the size of failure zone, huge influence of delay time could not be recognized. It might be indicated that there can be other factor to control the size of blast-induced fragmented rock such as the direction of firing.

In chapter 4, flight characteristic of blast-induced fragmented rocks was demonstrated in order to establish guidelines for preventing and controlling flyrock accidents by conducting field experiment in open-pit mine. On a basis of flight behavior of blast-induced fragmented rock captured by high-speed camera, initial velocity of the rock was analyzed by image analysis. The results showed that not only blasting designs such as powder factor and/or burden but also rock mass conditions such as strength or crack conditions strongly influence on the initial velocity. In addition to quantitative assessments of the flight characteristic, prediction equation for maximum initial velocity considering both blasting designs and rock mass conditions could be successfully obtained by multiple regression analysis. As the results, initial velocity could be expressed by $V = 75.46 \times PF - 1.83 \times B - 0.01 \times T - 0.09 \times K_{RMR} - 11.23$, where V is initial velocity m/s, PF is powder factor kg/t, B is burden m, T is delay time ms and K_{RMR} is Rock Mass Rating (RMR). On a basis of this equation, the maximum flight distance in each blasting designs and RMR could be calculated and the brand-new guidelines for setting blasting designs to prevent flyrock was successfully established. Moreover, in terms of flight direction, it was revealed that strike of the joint system inside rock mass influenced on the flight direction. When the strike was between from 0° to 30° or from 60° to 90°, the fragmented rock tended to fly perpendicular to the bench face. On the other hand, the fragmented rock was likely to fly not perpendicular to the bench face but in various directions due to the influence of joint system when the

strike angle was between 30° and 60° , which will be one of the indicator for preventing flyrock accident.

In chapter 5, finally, control and prediction methods of the size of blast-induced fragmented rocks in operating mine were proposed from the aspect of productivity. Although it is known that the blasting designs and rock mass strength influence theoretically on the size, the results showed that crack conditions also had an obvious impacts on the size of fragmented rock. In other words, it is important to assess the crack conditions before blasting for predicting the size of blast-induced fragmented rocks. Moreover, for the counter measures for large fragmented rock, under the similar rock mass conditions, the size was improved by increasing charge explosive and reducing burden. On the other hand, remarkable improvement of the size could not be obtained by changing hole spacing. This result suggested that improvement of the size can be performed safely and efficiently by altering burden or charge explosive within the range of guideline for controlling flyrock proposed in chapter 4. Additionally, the effect of delay time and firing pattern on the size and distribution were also discussed. The results showed that homogeneous size distribution and small size of blast-induced fragmented rocks could be obtained by conducting two directions (from the center blasting holes to both edges of holes) of firing pattern compared with one direction of firing pattern (from one edge of holes to another edge of holes). Furthermore, in one direction of firing pattern, 50 ms of delay time can make mean size smaller than in the case of 25 ms of delay time. On the contrary, remarkable deference of the size could not be obtained between both delay times. In other words, although control of the size can be performed by setting appropriate delay time, firing pattern is extremely important rather than delay time in terms of control of the size of blast-induced fragmented rock.

In conclusion, the mechanism of rock fracture induced by blasting could be made clear and the guideline for preventing flyrock and large size of blast-induced fragmented rock. The new guideline proposed in this thesis can be applied not only to this mine but also to other open-pit mines by conducting an additional field investigation due to the different field conditions.

Acknowledgment

First of all, I would like to express my special thanks of gratitude to Prof. Hideki Shimada of Department of Earth Resources Engineering, Kyushu University, for supporting my study and giving many advices for experiments as the mentor in the Advanced Graduate Program in Global Strategy for Green Asia, Kyushu University, without which this study could not have been completed. I gratefully acknowledge the support and kind help while working on this research of Dr. Shiro Kubota of National Institution of Advanced Industrial Sciences and Technology, and Associate Prof. Takashi Sasaoka of Department of Earth Resources Engineering, Kyushu University, as the tutor in the Advanced Graduate Program in Global Strategy for Green Asia, Kyushu University.

I would like to express my gratitude and appreciation to Dr. Tei Saburi of National Institution of Advanced Industrial Sciences and Technology, who gave me helpful ideas for this study from many perspectives as the technical advisor in the Advanced Graduate Program in Global Strategy for Green Asia, Kyushu University. This research was also supported by Dr. Ganda Maholiot Simangunsong of Department of Mining Engineering, Institute Technology Bandung, Indonesia, as the overseas mentors in the Advanced Graduate Program in Global Strategy for Green Asia, Kyushu University. I also thank Prof. Hideki Shimada, Associate Prof. Kotaro Yonezu, and Assistant Prof. Toshiaki Tanaka of Department of Earth Resources Engineering, Kyushu University, for kindly supporting the experiments during the laboratory rotation program in the Advanced Graduate Program in Global Strategy for Green Asia, Kyushu University.

I gratefully acknowledge the kind support and advices of Assistant Prof. Akihiro Hamanaka and Assistant Prof. Sugeng Whudi of Department of Earth Resources Engineering, Kyushu University, of Department of Earth Resources Engineering, Kyushu University. The experiments in this study were also conducted with the kind support for assembling the parts of experimental equipment of Mr. Shuichi Fujita of Department of Earth Resources Engineering, Kyushu University. I also would like to show my gratitude to Emeritus Prof. Kikuo Matsui and Dr. Masatomo Ichinose of Center of Urban Infrastructure, Environment and Resources (CUIER), for guiding me to conduct various experiments and to write this thesis.

I would like to express the deepest appreciation to the all staffs Iwado mine for helping me to conduct field experiment, and teaching me the operation in the mine.

I am indebted to Dr. Yuji Ogata and the all the staff in Industrial Safety and Physical Risk Analysis Group of National Institution of Advanced Industrial Sciences and Technology, for helping small-scale blasting experiment.

This research was financially supported by the Advanced Graduate Program in Global Strategy for Green Asia, Kyushu University for visiting the mine sites and obtaining the special equipment for filed investigation and sample analysis, which gave me variety of perspectives to work on this research from many points of view. I also express my sincere thanks to Associate Prof. Hajime Miki for the advices on arranging the schedule of the field investigation in Indonesia and laboratory experiments. I thank to Ms. Miwa Hirashima and Ms. Minako Matsue in the office of the Advanced Graduate Program in Global Strategy for Green Asia, Kyushu University, for kind and helpful advice and support for the visit to the research field.

My deepest appreciation goes to Mr. Kotaro Yamaguchi, Mr. Mitsuki Nishimori, Mr. Hajime Yamauchi, Mr. Takahiro Shiomori, and other members of the Rock Engineering and Mining Machinery Laboratory, Department of Earth Resources Engineering of Kyushu University, for supporting me to conduct experiments for a long time not only in a laboratory but also in the field, also helping many things in my life in Kyushu University.

At the end of this thesis, I would like to show my greatest appreciation again to everything in my life.

March 2019

Yoshiaki Takahashi